ADDIS ABABA UNIVERSITY
SCHOOL OF GRADUATE STUDY
FACULITY OF TECHNOLOGY
DEPARTEMENT OF MECHANICAL ENGINERING
(MECHANICL DESIGN STREAM)

Fracture Analysis of Pressure Vessel under Dynamic Loading and Thermal Effect

By
Mulugeta Habtemariam

Advisor
Dr. Alem Bazezew

June 24, 2009
Addis Ababa, Ethiopia

Fracture Analysis of Pressure Vessel under Dynamic Loading and Thermal Effect

By
Mulugeta Habtemariam

A thesis submitted to the School of Graduate Studies of Addis Ababa University in partial fulfillment of the requirements of the Degree of Masters of Science in Mechanical Engineering (Mechanical Design Stream)

Advisor
Dr. Alem Bazezew

June 24, 2009
Addis Ababa, Ethiopia

ADDIS ABABA UNIVERSITY
SCHOOL OF GRADUATE STUDIES
DEPARTMENT OF MECHANICAL ENGINEERING

Fracture Analysis of Pressure Vessel under Dynamic Loading and Thermal Effect

By
Mulugeta Habtemariam

Approved by Board of Examiners:

Ato Hamsasew Moges Chairperson of Department Graduate Committee (DGC)	Signature	07/07/2009 Date
Dr. Alem Bazezew Advisor	Signature	July 04/09 Date
Dr. Ing. Tamrat Tesfaye Examiner	Signature	4/7-2009 Date

Declaration

I, the under signed, declare that this thesis work is my original work and has not been presented for a degree in any other university, and that all sources of material are duly acknowledged.

Name: Mulugeta Habtemariam
Place: Addis Ababa, Ethiopia
Date of submission: _____
Signature: _____

Title of the thesis:
FRACTURE ANALYSIS OF PRESSURE VESSEL UNDER DYNAMIC LOADING AND THERMAL EFFECT

This thesis has been presented for examination with my approval a university advisor

Dr. Alem Bazezew
Advisor

_____ Signature

July 04/09
Date

Acknowledgment

First, I would like to express my heartfelt appreciation and gratitude to my advisor Dr. Alem Bazezew for his continual encouragement and patient guidance throughout the course of this work. His deep insight into the subject of Fracture Mechanics and its many applications, his infectious enthusiasm, his patience in helping me learn the basics, and his inexhaustible supply of interesting ideas, have all greatly enriched my experience as a graduate student. Besides this, I deeply appreciate his fracture imminent because he strikes interest on me to do my thesis on fracture mechanics.

Many thanks are also extended to all my colleagues and friends especially Ato Tadesse Nega, Ato Hailegnaw Getaneh, Ato Habtamu Tikubet and Ato Birhanu Beshah. Their helpful comments during the research and writing of this thesis are appreciated.

At last, but not least, I would like to take this opportunity to thank my brothers, my mother and my friends for all their help and understanding. Without them encouragement, love and support, this work would never have been accomplished.

Table of Contents

List of Figures

List of Tables

Abstract

Pressure vessel system has an extremely broad range of application, from simple storage vessels to complicated reactor pressure vessels. The causes of failure in pressure vessels are mainly related to fracture. To avoid appalling failure, it is important to study their fracture characteristics at the design stage and even during operation for maintenance process. The thesis work has investigated the fracture behavior of pressure vessels under dynamic loading.

The pressure vessel is modeled for longitudinal, circumferential and edge cracks for thin and thick walled pressure vessels. The solution to the equation of motion is obtained by transient analysis and finite element method employing a twenty-node brick element.

The model is developed and analyzed using ANSYS. The study includes dynamic fracture analyses for longitudinal, circumferential and edge cracks, to obtain dynamic stress intensity factor. Also included are the stress and deflection analysis as time response. The validity of the results obtained from the research is verified by comparing with results obtained for numerical static analysis with analytical solution and previously published by other researchers, and good agreement is obtained.

Key words:

Pressure Vessel, Crack, Dynamic Loading, Dynamic Fracture Analysis, Thermal Shock, Stress Wave, Quasi-static Stress Intensity Factor, Dynamic Stress Intensity Factor

Chapter One

1 Background and Literature Review

1.1 Back ground and Overview

1.1.1 Introduction

Pressure vessel systems have contributed large to high standard of living existing to day [17]. In order to enhance the standards, the design technology becomes sophisticated. These complexities of design technology, however, have brought catastrophic failures [34].

A pressure vessel is a leak proof container that is designed to hold gases or liquids at a pressure different from the ambient pressure [31, 17]. It can be any shape and range from beverage bottles to complicated ones encountered in engineering construction [31, 17, and 30]. In the latter high pressure, extreme temperatures and severity of functional performance requirements pose exacting design problems [31].

Pressure vessel systems have an extremely broad range of application, from simple storage vessels to complicated reactor pressure vessels. It is possible to say that pressure vessels are the most widely spread component within different industrial sectors. In fact, there is no factory without pressure vessel: steam boilers, tankers, autoclaves, collectors, heat exchanger pipes are a few examples to mention. More specifically, pressure vessels represent fundamental components in sectors of enormous industrials importance such as the nuclear reactor vessel, oil refineries and petrochemicals plants, habitat of spaceship, habitat of submarine including pneumatic reservoir & hydraulic reservoir under pressure, storage vessels for liquefied gases such as ammonia, chlorine propane, butane etc.

The structure of pressure vessels can theoretically be almost any shape. Usually a shape mode of sections of cylinders, spheres, cones are employed. So most of the pressure vessels are cylindrical in shapes with spherical, semi elliptical heads or end capes at each

end [31, 17, and 30]. Pressure vessels are designed and analyzed using thick walled, or thin walled cylinder theory [30, 31, 12, and 13].

A pressure vessel must overcome various loads on it that causes internal stress to the material. The loads can be internal and/or external pressure, temperature, weight of the vessel and it's contents, superimposed loads (such as mounted equipments, baffle, support reactions), wind load, earthquake load, impact load (such as colliding with other object or sudden altering of pressure/temperature or process of chemical reactions), blast/explosion loading etc [17,19,9].

All the above loads are allocated either as static or dynamic load impact, blast/explosion, earthquake, mounted equipment that can cause vibration, and wind loads create dynamic loading on pressure vessel. However, these dynamic loadings occur rarely. This thesis treats the behavior of pressure vessels due to dynamic loading caused by impact/suddenly applied load.

1.1.2 Pressure Vessel Design Approach

Most of the pressure vessel system earlier mentioned have great potential pressurized force stored within them, and when this potential energy is released, there is devastating effect to life and property [17, 31,19]. Due to this, design of pressure vessel needs careful design considerations. The preliminary/elementary design approach (stress and deflection analysis) is not enough for the current sophisticated technology. In order to minimize catastrophic failure the modern design approach/criteria have been growing. The former design approach has been studied deeply for a century and a number of research papers have been presented. On the other hand, the latter approach has been studied in the late 1960's and since. The modern study of fracture analysis approach also has been growing with new fracture mechanics development since 1980. However, the study has mainly focused on quasi-static fracture mechanics approach including thermal loading problems in pressure vessels. The dynamic fracture analyses of pressure vessels have not been studied at great depth.

1.1.3 The Effect of Dynamic Loading on the Fractured Pressure Vessels

Before discussing about the effect of dynamic loading on the cracked body, it is important to have a clue about fracture. Fracture mechanics is concerned with the quantitative description of the mechanical state of a deformable body containing a crack or cracks, with a view toward characterizing of and measuring the resistance of materials to crack growth. The fracture analysis of a cracked body can be analyzed either as quasi-static fracture or as dynamic fracture condition depending on the type of load condition. The analysis of cracked systems concerning quasi-static situations in which the kinetic energy is relatively insignificant compared with the other energy terms and can be omitted. In this case, the crack is assumed either to be stationary or to grow in a controlled stable manner, and the applied loads varied quite slowly. In dynamic fracture situation, either time dependent material properties or inertia effects due to suddenly applied loading or, rapid propagation of crack may be taken as causes of for the time dependent behavior of fracture. Sometimes all the three situations may happen at the same time to cause dynamic fracture. Dynamic analysis of crack problems indicates that stresses and displacements caused by dynamic loading can differ greatly from those associated with the corresponding static loading. This result may be explained by the intersection of the elastic waves with the crack faces and other characteristic boundaries of the body. Therefore, when a dynamic load is applied to a body, the stress waves travel to the boundary of a deformable body. Similarly, when a dynamic load is applied on a body containing a crack or cracks, the stress waves travel to the crack surface and boundary. This implies that dynamic loading: impact, earthquake and blast/explosion increases the stress at the tip of the crack, whether the crack is stationary or growing [29, 32, 33, 34, 37, 38, and 39].

1.1.4 Fracture Treatment on the Cracked Deformable Body

Fracture analysis of a cracked deformable body is treated by determining the fracture parameters [34, 32]. These parameters are different according to the material properties. For elastic materials stress intensity factor and energy release rate are the main

parameters, where as for the elastoplastic materials the J–integral and CTOD (crack tip opening displacement) are more appropriate parameters [34, 32, and 30].

1.2 Literature Review

The wide application of pressure vessels has been an incentive for conducting various researchers from different aspects to fulfill the growth of industry all over the world. As the science and technology permits researchers had focused on the preliminary or classical design approaches such as stress analysis and deflection, and many papers had been published to present results obtained. Since the late sixties, there has been great interest in fracture analysis of pressure vessel. Therefore, including review of quasi-static analysis, and dynamic loading conditions is of paramount importance

Fracture analysis of pressure vessel was started in late 1960's. This indicates that quasi – static fracture studies had been started before modern fracture mechanics was compiled in the current form in 1980's. National Aeronautics Space Administration (NASA) contributed a number of technical and memorandum paper notes concerning quasi static fracture analysis pressure vessels for their aeronautics application.

At NASA Lewis research center Anderson and Sullivan in 1965 [1] investigated that the strength of pressure vessels (having longitudinal through crack) depends on or related to the geometry of the cylinder, crack length, material yield strength, fracture toughness and pressure bulging factor at the tip of the crack.

After three years, at the same research center Sullivan and Pierce in 1968 [2] studied the effect of cylinder radius on the bulge coefficient of cracked pressure vessel. The result of their investigation was that the bulging coefficient remains constant for different radii of pressurized cylinder with through crack.

In the same research center Orange, Sullivan and Calfo in1971 [12] studied fracture of thin sections having through and part through cracks. Their research investigation was

supported by an experiment. More specifically their studies focused on the applicability of plane strain fracture mechanics theory for problems of surface cracks in thin metal sections. Their result was that the fracture behavior of thin sections containing surface cracks might be strongly influenced by the ratio of the crack tip plastic zone size to the "ligament depth"[1].

In 1976, at NASA Langley research center, Newman [3] studied the correction of the theoretical fraction criterion with the experimental data for surface and through cracked cylindrical pressure vessels. The fracture criterion was found to correlate the failure stress within $\pm$ 10% correction for flat plate (having through crack and through edge crack) and cylindrical pressure vessels containing through crack.

Prause, in 1977, [4] reviewed dynamic modeling of pressure vessels. In his paper, the dynamic response of structure / pressure vessel was predicted from a mathematical model. His review showed the equation of motion that described the dynamic response of the model was expressed in matrix form as

$[M]\{\ddot{u}\} + [C]\{\dot{u}\} + [K]\{u\} = \{F\}$ for which $[M]$, $[C]$ and $[K]$ are mass, damping and stiffness matrixes respectively; and $\{u\}$ and $\{F\}$ are the displacement and force vectors respectively.

Raju and Newman [20] studied the stress intensity factor for cracks in cylindrical pressure vessels. They presented that the stress intensity factors influence coefficient for a wide range of semi elliptical surface cracks on the outside and inside of the cylinder. They used four stress distributions, uniform, linear, quadratic and cubic, to determine the crack behavior. These stresses are caused by internal pressure and thermal shock.

[1] by 'ligament depth' is meant thickness minus crack depth

Surface cracks of pressure vessels were studied by of Nishioka and Alturi [21] in 1982. They analyzed surface flaw in pressure vessels using three-dimensional alternating methods. They determined the magnification of the internal pressure loading and a polynomial influence function for the polynomial crack surface loading.

Bass, Bryan, Bryson and Merkle [22] studied the semi elliptical surface crack in an experimental test vessel under elastic plastic condition using finite element method under application of energy release rate techniques to part through crack of the vessel.

Jung and Kanninen [23] studied dynamic crack propagation and arrest in a nuclear pressure vessel. The dynamic loading condition of their study was thermal shock. Finally, they investigated that the dynamic effects of the crack behavior is larger than the static case.

Lee and Raymund [24] studied the stress intensity factor of internal longitudinal semi-circular surface flaws of a cylinder. Non dimensional magnification factor was derived from separate loading which is almost similar to that of Raju [20],the applied stress distribution were constant, linear, quadratic and cubic crack surface pressure.

Haroun [25] examined the application of momentum balance method for evaluation of hydrodynamic pressure in a seismically excited rectangular tank.

At NASA Langley research center Young, Rose and Strainers [5] conducted a research to determine the curvature correction factors or "bulging factors"[2]. It was a geometrically non linear finite element parametric study to determine the bulging factor for increased stresses due to curvature for longitudinal and circumferential cracks in unstiffened pressured cylindrical shells. The study included the shell radius, the shell wall thickness and the crack length. The result was normalized by the stress intensity

[2] which is the ratio of the Stress intensity factor at the tip of a longitudinal crack to the Stress intensity factor for the same crack in a flat panel

factor flat plates and “bulging factor” used in the design to represent the effects of shell curvature on the stress intensity factor.

Kiciak, Glinka and Burns [16] calculated stress intensity factors and crack tip opening displacement. In their paper, they used a method of generalized weight function to calculate stress intensity factor and/or crack opening displacement for cracks subjected to complex stress fields.

Valougeorgis, Papaspyrou, and Karamanos [28] developed a mathematical model for sloshing effects in half-full horizontal cylindrical vessels, under external excitation in the direction of the longitudinal vessel axis. Hydrodynamic pressures and forces were calculated for harmonic excitation and for a real seismic motion event. Finally, the equivalence between the half-full horizontal cylinder and an equivalent rectangle was demonstrated

Chao and Shepherd in 2003 [6] studied the fracture response of externally flawed cylindrical shells to internal gaseous detonation loading. They performed experiments to observe the fracture behavior of thin wall and initially- flawed aluminum tubes to internal gaseous detonation. They observed different kinds of crack propagation for various loading amplitudes and flaw/crack sizes.

Chao and Shepherd, 2004 [7] made comparison of fracture response for cracked tubes under internal static and detonation loadings. They used an experiment on thin walled and pre cracked aluminum 6061-76 tubes for statically (with oil, nitrogen) and dynamically with gaseous detonations traveling at 2.4 km/s.

Rodriguez – Caste llanos et al [15] studied crack effects on the propagation of elastic waves in a plate and tubular sections. They analyzed the dynamic stress intensity factor for both plate and tubular sections. The dependence of dynamic stress intensity factor values of the three stress waves such as dilatational, transversal and Raleigh waves with time history were seen.

In 2005, Goncalves et al [10] studied the non-linear dynamic behavior of shallow cylindrical shells under axial loading. They used qualitatively accurate low dimensional model for their studies. Finally, they investigated that stability analysis which only considers the steady state and neglects the global transient behavior, may be seriously non-conservative.

Roy Xu and Ping Wang [27] studied dynamic fracture analysis of failure mode along weakened interfaces in elastic solids. They obtained stress intensity factors of the kinked cracks as a function of kinking angle and crack speeds by using fixed dynamic stress intensity factors and the non singular stresses of the included cracks.

In 2006, Leishear [26] studied the stress created due to shock inside the cylinder. He presented the vibration equations and compared it with experimental work. In this work, at shock velocities of liquid or gas, the maximum hoop stress is related to a vibration equation for a suddenly applied load.

Ngo et al [18], in 2007, reviewed the effects of explosion on structures. They explained the nature of explosion and the mechanisms of blast waves in free air. They also introduced different methods to estimate blast loads and structural response.

Health and Executive Paper in 2007 [9] reviewed the dynamic responses of pressure vessels and tanks subjected to dynamic loading. This explained the cause of strong vibrations on pressure vessels such as earthquake, blast and specially ship impact on the offshore. It also included the three hydrodynamic components such as convective or sloshing, rigid impulsive and flexible impulsive components that are created due to strong vibrations. In its part II study, numerical results were described for the given dynamic responses of pressure vessels and tanks.

P. Hosseini-Tehrani [41] did fracture analysis under thermo elastic assumption. The paper discuses fracture analysis of edge crack using coupled effect by using boundary

element method. He determined the non-dimensional dynamic stress intensity factor that is created due to thermal shock.

1.3 Objective of the Thesis

The objective of this thesis is to determine the dynamic fracture parameters of pressure vessels made of an elastic material. Dynamic stress intensity factor and dynamic energy release rate are the two parameters of fracture for the dynamic loaded elastic material pressure vessel. To obtain these parametric results the finite element analysis [FEA] is used. Finite element method [FEM] is used to find quantitative and qualitative analysis of stress intensity factor, stress distribution, and deformed shape under load. Thus, detailed modeling and specialized knowledge of FEM theory is indispensable to perform these analyses with high accuracy [34, 35].

More specifically, this paper intends to analyze dynamic stress intensity factor for longitudinal stationary through crack of thin walled pressure vessel due to suddenly applied pressure, and edge crack of thick walled pressure vessel caused by thermal shock. In addition to this, circumferential through crack is analyzed to compare the results of longitudinal through crack behavior. The analysis investigates the characteristics of the dynamic stress intensity factor for three different crack lengths. The investigation also includes crack tip stress, strain and displacement as a function of time.

To achieve the above results, the study includes quasi-static fracture analysis (in comparison), and modal and harmonic/frequency/ analysis (as an input) is dealt with. The thesis also gets ahead of thorough analytical and finite element mathematical modeling to show how the numerical analysis has done using ANSYS.

1.4 Problem Definition and Scope of Research

Based on the background (literature review) in section 1.2, it has been deemed desirable to obtain the fracture parameter of cracked pressure vessel and dynamic analysis of pressure vessel. The focus of the dynamic fracture analysis will be to study coupled (thermo elasticity for thick walled pressure vessel) and uncoupled (without thermal

analysis for thin walled pressure vessel) systems. Therefore, the aim of this research is to obtain the dynamic fracture parameter and its characteristics when the size of the stationary crack increases. This paper also will show how fracture and crack (from our references) analysis are interpreted.

1.5 Organization of the Thesis

The first chapter of the thesis deals with different aspects of the research. It discusses outlined background and previous research works carried in the field and gave the necessary background to proceed throughout the thesis. The second chapter deals with the basic concepts of dynamic fracture, the causes of dynamic loading and analytical fracture computation. It also discusses elasticity and thermo elasticity problems to show analytical stress wave equation. In the third chapter, finite element mathematical descrtization for structural and heat problems are discussed. The forth chapter presents geometrical modeling and descrtization of the model using ANSYS, and the analysis procedure is presented. Chapter five covers all the numerical results and discussion of results obtained in the thesis. Finally, chapter six gives a conclusion to the thesis, its contribution and possible future research directions.

Chapter two

2 Basics of Dynamic Fracture Mechanics

2.1 Introduction

Facture mechanics is concerned with the qualitative description of the mechanical state of a deformable body containing a crack or cracks with a view toward characterizing and measuring the resistance of materials to crack growth [32]. It is a relatively new area of solid mechanics research, with its foundation laid in the late 20th century. Already it has broad application in systems ranging in size from micrometer length scales (thin films) up to kilometer length scales (earthquake fault lines)

Dynamic fracture mechanics is the sub-field of fracture mechanics concerned with fracture phenomena for which the role of material inertia becomes significant and/or material behavior becomes time dependent material behavior. Inertial effects can be raised from rapidly applied loading on a cracked body or due to rapid crack propagation in the vicinity of crack tip or both effects happen at the same time [32, 34].

Dynamic fracture may happen, when either one of the above causes occur or when all (the time dependent of material behavior, rapidly applied loading and crack growing) happen at the same time. If all causes happen, there is great sophistication in analysis. In the case of rapid loading, the influence of loads is transferred to the crack by means of stress waves [32]. These stress waves propagate through the materials and reflect off free surfaces such as boundaries and the crack plane/ surfaces. Reflected stress waves influence the local crack tip stress and strain fields which, in turn affect the fracture behavior [34, 32]

To determine whether or not a crack will advance due to the stress wave loading, it is necessary to determine the transient driving force acting on the crack faces. In the case of rapid crack propagation, material particles on opposite crack faces displace with respect to each other once the crack edged has passed [32].

The first dynamic fracture was proposed by Mott considering the kinetic energy of growing speed which causes inertial effect on a deformable body. This was analyzed by stress wave in the elastic cracked body [32, 38, and 19].

Before analytical computation is started the terms which describe/ or characterize dynamic fracture should be defined.

1. *Stationary crack*: This means that the crack length is constant and crack tips remain permanently fixed [15]
2. *Time dependent materials*: The mechanical properties of the materials depend markedly on the time for which the applied loading is maintained in the solid. For example in most metals both the yield and ultimate strength increases with the rate of loading [38]
3. *Growing crack*: This means that the length of the crack increases with time. The speed of the crack may be constant or variable. This occurs when the driving force for crack extension exceeds the material resistance and the structure becomes unstable [34].

As mentioned earlier either the three above points as a whole or each one of them may be affected by rapidly loading /impact or impulsive/ on the cracked body. The last two directly can cause dynamic fracture but the first is considered when rapidly applied loading arise.

When the nonlinear material behavior or time independence behavior is neglected, the version becomes elastodynamic fracture mechanics. Elastodynamic analysis of crack problems indicates that stresses and displacements caused by dynamic loading can differ greatly from those associated with the corresponding static loading. The result may be explained by the intersection of elastic stress waves with the crack faces and the corresponding boundaries of the body [38]. Due to this; dynamic loading gives rise to high stress levels near cracks [38]. A single excellent source regarding dynamic fracture is Freund [32]

2.2 Causes of Dynamic loading

The sources of dynamic loading of pressure vessels as mentioned earlier are either external loads or internal loads. The external loads are direct impact with another body, impact of mounting pumps, earthquake, blast, and wind and so on. The internal sources are impact/suddenly altering of pressure, impact of temperature (thermal shock/sudden alternating of temperature), chemical reactions etc. All these loads create response on the structure.

The response of the pressure vessel is evaluated using FEM whether it is internal or external rapid loading is represented as a transient load. The equation governing response is:

$$\{F\} = [M]\left\{\ddot{u}\right\} + [C]\left\{\dot{u}\right\} + [K]\{u\} \tag{2.1}$$

$\{F\}$ load vector

$[M]$ Mass matrix

$[C]$ Damping matrix

$[K]$ Stiffness matrix

$\{\ddot{u}\}$ Acceleration vector

$\{\dot{u}\}$ Speed vector

$\{u\}$ Displacement vector

Here the inertia effects are more significant at short times and are minimal after sufficiently long times.

2.2.1 Impact /Suddenly Applied Load

Impact load happens when one body is explicitly colliding with other objects or may be due to sudden/random change in temperature or pressure. This sudden change in temperature is referred as thermal shock. Thus, thermal shock creates inertial effect on the cracked body because of rapid temperature change within very short period usually small enough to that of the first natural frequency. Similarly, dynamic pressure is created

due to shock wave of fluid or by sudden discharging and sudden shock creation due to pumping in fluid.

2.2.2 Blast Loading

A blast wave in fluid dynamics is the pressure and flow resulting from the deposition of a large amount of energy in a small and higher localized volume. The flow field can be approximated as a lead shock wave, followed by a 'self-similar' subsonic flow field. When blast arises near the cracked pressure vessel, the pressure wave crates dynamic load.

2.2.3 Earthquake

Earthquake is the sudden movement of the earth caused by the abrupt release of accumulated strain along a fault in the interior. The released energy passes through the earth as seismic waves (low-frequency sound waves), which cause the shaking of structures on the surface of the earth. Seismic waves continue to travel through the earth after the fault motion has stopped. The wave transfers from the ground to the pressure vessel and creates vibration. The vibration causes dynamic fracture effects on a cracked pressure vessel.

2.3 Fracture Parameters and Stress Intensity Factor

Fracture is characterized mostly by three or four parameters. For elastic materials crack is parameterized by stress intensity factor and energy release rate. Similarly, for elasto-plastic materials it is parameterized by the J-counter integral and crack tip opening displacement [34]. In ANSYS, cracks are parameterized by stress intensity factor, energy, release rate or J- counter integral. Therefore cracks are modeled by the above three parameters due to the types of loading and materials that cracks experience.

2.3.1 Stress Intensity Factor

Stress intensity factor is a measure of the stress-field intensity near the tip of an ideal crack in a linear elastic material. Stress intensity factor, K_I, is used in fracture mechanics to more accurately predict the stress state ("stress intensity") near the tip of a crack

caused by a remote load or residual stresses. It is a theoretical construction applicable to a homogeneous elastic material, and is useful for providing a failure criterion for brittle materials. The fracture parameter of ductile materials is examined using J-integral or crack tip opening displacement.

The magnitude of K_I depends on sample geometry, the size and location of the crack, and the magnitude and the model distribution of loads on the material. A number of methods have been used for the determination of stress intensity factors. They may be classified as

1. Theoretical (Wastergaard semi-inverse method and method of complex potentials).
2. Numerical (Green's function, weight functions, boundary collocation, alternating method, integral transforms, continuous dislocations and finite elements methods).
3. Experimental (photo elasticity, moiré, holography, caustics, and combinations of these methods).

Theoretical methods are generally restricted to plates of infinite extent with simple geometrical configurations of cracks and boundary conditions. For situations that are more complicated, one must resort to numerical or experimental methods.

2.3.2 Dynamic Stress Intensity Factor

Quasi-static crack conditions are obtained when loading is sufficiently slow that stresses throughout the body are in equilibrium and the crack tip is stationary or at most moving very slowly. In dynamics, loading is characterized by stress waves, or the crack tip is moving fast enough to invoke inertial/rate effects near the crack tip, or both.

$$K_{Id} = K_{Id}\left(P(t), a(t), t\right) \text{ for stationary crack} \tag{2.2}$$

$$K_{Id} = K_{Id}\left(P(t), a(t), \dot{a}(t), t\right) \text{ for grawing crack} \tag{2.3}$$

where $P(t)$ =generalized load

$a(t)$ =half crack length

$\dot{a}(t)$ = speed of crack growing,

t=time

K_{Id} =dynamic intensity factor

The cause of stress waves rapidly applied load is modeled by *P(t)* which is equivalent to the body response of dynamic loading. Then *P(t)* is created due to suddenly/rapidly applied loading.

2.3.3 Modes of Fracture

In the Mode l, tensile forces load the body such that the crack surfaces are pulled apart in the y direction. The deformations are then symmetric with respect to the planes perpendicular to the y-axis and the z-axis. This mode can be described by hammering of a work piece-using wedge to split in to two.

Figure 2.1 Mode I Opening or splitting

In the mode II or sliding mode, the body is loaded by shear force parallel to the crack surfaces, which slide over each other in the x directions are then symmetric with respect to the plane perpendicular to the z-axis and skew symmetric with respect to the plane perpendicular to the y-axis. Turning of round shaft using lath cutter can demonstrate mode II.

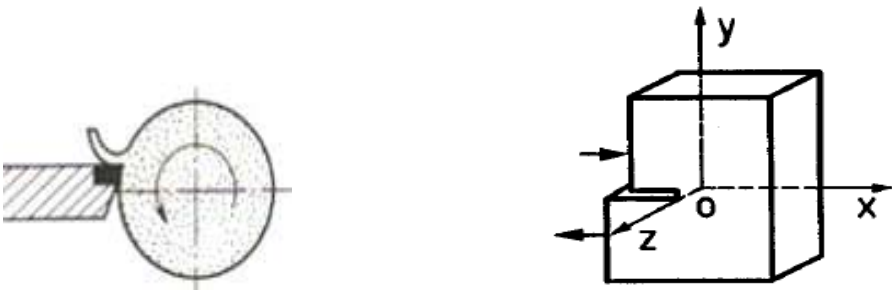

Figure 2.2 Mode II Shearing or sliding

In mode III or tearing mode, the body is loaded by shear forces parallel to the crack surfaces and the crack surfaces slide over each other in the z direction the deformations are then skew symmetric with respect to the plane perpendicular to the z and y-axes. Tearing of a paper with a scissors can describe this mode.

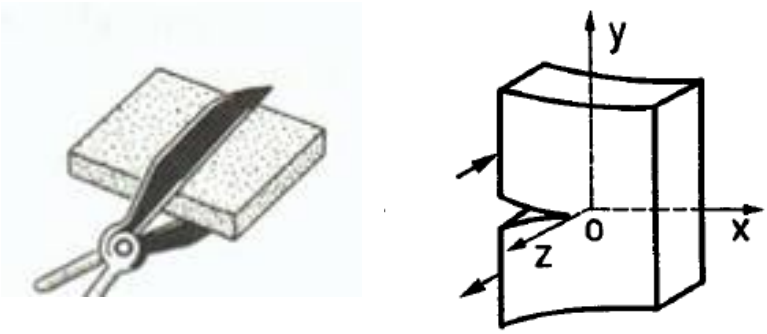

Figure 2.3 Mode III Tearing

2.3.4 Singular Stress and Displacement Fields using Analytical Method

The study of stress and displacement fields near the crack tip is very important, because these fields govern the fracture process that takes place at the crack tip. In this section we shall make a thorough study of the stresses and displacements near the crack tip.

2.3.4.1 Crack Tip Stress

Anderson shows the demonstration of Williams that the universal nature of the $1/\sqrt{r}$ singularity for elastic crack problems, although Ingles, Westergaard, and Sneddon had earlier obtained this result in specific configurations. The demonstration begins by

considering stresses at the corner of a plate with various boundary conditions and included angles: a crack is special cases where the included angle of the plate corner is 2π and the surfaces are traction free Figure 2.4.

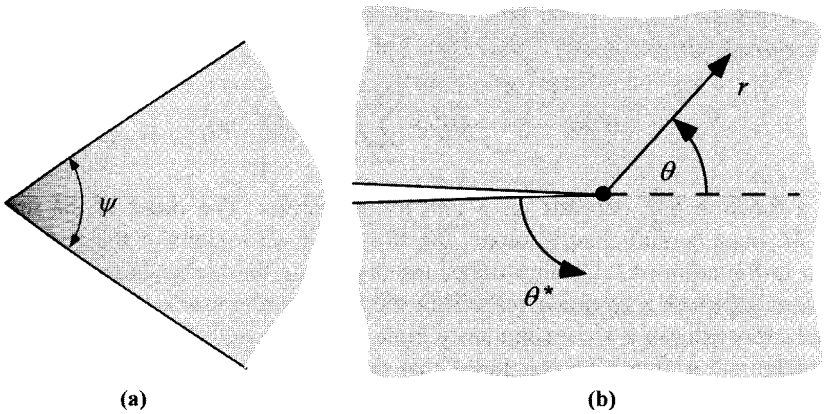

Figure 2.4 Plate corner configuration

Figure 2.4a shows about a plate corner which is formed when the included angle ψ and figure 2.4b shows special case of a sharp crack when ψ=2π. For the configuration shown in figure 2.4b, Anderson used William's postulate the following stress function:

$$\Phi = r^{\lambda+1}[c_1 \sin(\lambda+1)\theta^* + c_2 \cos(\lambda+1)\theta^* + c_3 \sin(\lambda-1)\theta^* + c_4 \cos(\lambda-1)\theta^*] \quad (2.4)$$

$$\Phi = r^{\lambda+1}\,\Phi(\theta^*, \lambda) \quad (2.5)$$

where c_1, c_2, c_3 and c_4 are constants, θ^* is defined in figure (2.4a).

Invoking polar airy stress function equations [34] give the following expressions for the stresses:

$$\sigma_{rr} = r^{\lambda-1}\left[F^*(\theta^*) + (\lambda+1)F(\theta^*)\right] \quad (2.6)$$

$$\sigma_{\theta\theta} = r^{\lambda-1}\left[\lambda(\lambda+1)F(\theta^*)\right] \quad (2.7)$$

$$\tau_{r\theta} = r^{\lambda-1}\left[-\lambda F'(\theta^*)\right] \quad (2.8)$$

where the primes denote derivatives with respect to θ^*, σ_{rr}= crack tip stress in the r direction, $\sigma_{\theta\theta}$ = crack tip stress in the θ direction $\sigma_{r\theta}$ = crack tip shear stress

Anderson also showed that equation (2.5) implies that the displacements near the crack tip of the body vary with r^{λ}. In order for displacements to be finite in all regions of the body, λ must be greater than zero. If the crack faces are traction free,

$$\sigma_{\theta\theta}(0) = \sigma_{\theta\theta}(2\pi) = \tau_{r\theta}(0) = \tau_{r\theta} = (2\pi) = 0 \tag{2.9}$$

This implies the following boundary conditions:

$$F(0) = F(2\pi) = F'(0) = F'(2\pi) = 0 \tag{2.10}$$

Assuming the constants in equation (2.5) are nonzero in the most general case, the boundary conditions can be satisfied only when $\sin(2\pi\lambda) = 0$ thus,

$$\lambda = \frac{n}{2}, \text{ Where n=1, 2, 3}$$

There are an infinite number of λ values that satisfy the boundary condition: the most general conditions to a crack problem, therefore, is a polynomial of the form

$$\Phi = \sum_{n=1}^{N} \left(r^{\frac{n}{2}+1} F\left(\theta^*, \frac{n}{2} \right) \right) \tag{2.11}$$

And the stresses are given by

$$\sigma_{ij} = \frac{\Gamma_{ij}\left(\theta^*, -\frac{1}{2} \right)}{\sqrt{r}} + \sum \left(r^{m/2} \Gamma_{ij}(\theta^*, m) \right) \tag{2.12}$$

where Γ is a function that depends of F and its derivative and(i,j= r, θ)

The order of the stress function polynomial, *m* must be sufficient to model the stresses in all regions of the body. When $r \to 0$, the first term in equation (2.12) approaches infinity, while the higher-order terms remain finite (when m=0) or approach zero (for m>0). Thus, the higher-order terms are negligible close to the crack-tip, and stress exhibits a $1/\sqrt{r}$ singularity.

A further evaluation of equation (2.5) and equation (2.6)-(2.8) with the appropriate boundary conditions reveals the precise nature of the function Γ. Here equation (2.5) contains four, as yet unspecified, constants; by applying equation (2.10) for a given value of n on equation (2.9), it is possible to eliminate two of these constants (c_1 and c_2), resulting in.

$$\Phi(r,\theta) = r^{n/2+1}\left\{c_3\left[\sin\left(\frac{n}{2}-1\right)\theta^* - \frac{n-2}{n+2}\sin\left(\frac{n}{2}+1\right)\theta^*\right] + c_4\left[\cos\left(\frac{n}{2}-1\right)\theta - coc\left(\frac{n}{2}+1\right)\theta\right]\right\} \tag{2.13}$$

For crack problem, it is more convenient to express the stress function in terms of θ, the angle from the symmetry plane, figure (2.4). Substituting θ, $\theta = \theta^* - \pi$ into equation (2.13) yields, after some algebra, the following stress function for the first few values of *n*

$$\Phi(r,\theta) = r^{3/2}\left(s_1\left[-\cos\frac{\theta}{2} - \frac{1}{3}\cos\frac{3\theta}{2}\right] + t_1\left[-\sin\frac{\theta}{2} - \sin\frac{3\theta}{2}\right]\right) + s_2 r^2\left[1-\cos 2\theta\right] + O(r^{5/2)} + ... \tag{2.14}$$

where s_i and t_i are constants to be defined

The stresses are given by

$$\sigma_{rr} = \frac{1}{4\sqrt{r}}\left\{s_1\left[-5\cos\frac{\theta}{2} + \cos\frac{3\theta}{2}\right] + t_1\left[-5\sin\frac{\theta}{2} + 3\sin\frac{3\theta}{2}\right]\right\} + 4s_2\cos^2\theta + O(r^{1/2}) + ... \tag{2.15}$$

$$\sigma_{\theta\theta} = \frac{1}{4\sqrt{r}}\left\{s_1\left[-3\cos\frac{\theta}{2} - \cos\frac{3\theta}{2}\right] + t_1\left[-3\sin\frac{\theta}{2} - 3\sin\frac{3\theta}{2}\right]\right\} + 4s_2\sin^2\theta + O(r^{1/2}) + ... \tag{2.16}$$

$$\tau_{r\theta} = \frac{1}{4\sqrt{r}}\left\{s_1\left[-\sin\frac{\theta}{2} - \sin\frac{3\theta}{2}\right] + t_1\left[\cos\frac{\theta}{2} + 3\cos\frac{3\theta}{2}\right]\right\} - 2s_2\sin 2\theta + O(r^{1/2}) + ... \tag{2.17}$$

The constants s_i in the stress function equation (2.14) is multiplied by cosine terms while the t_i is multiplied by sine terms. Thus, the stress function contains symmetric and antisymmetric components, with respect to θ=0. When the loading is symmetric about θ=0, t_i=0, while s_i= 0 for the special case of pure antisymmetric loading. Thus symmetric loading include pure bending and pure tension. In both cases, principal stress is normal to the crack plane. Therefore, symmetric loading corresponds to mode I; antisymmetric loading is produced by in-plane shear on the crack faces and corresponds to mode II.

It is convenient in most cases to treat the symmetric and antisymmetric stresses separately. The constants s_i and t_i can be replaced by the mode I and modes II stress intensity factors, respectively;

$$s_1 = -\frac{K_I}{\sqrt{2\pi}} \tag{2.18}$$

$$t_1 = \frac{K_{II}}{\sqrt{2\pi}} \tag{2.19}$$

The crack-tip stress fields for symmetric [mode I] loading, assuming the higher-order terms are negligible] are given by

$$\sigma_{rr} = \frac{K_I}{\sqrt{2\pi r}}\left[\frac{5}{4}\cos\left(\frac{\theta}{2}\right) - \frac{1}{4}\cos\left(\frac{3\theta}{2}\right)\right] \tag{2.20}$$

$$\sigma_{\theta\theta} = \frac{K_I}{\sqrt{2\pi r}}\left[\frac{3}{4}\cos\left(\frac{\theta}{2}\right) + \frac{1}{4}\cos\left(\frac{3\theta}{2}\right)\right] \tag{2.21}$$

$$\tau_{r\theta} = \frac{K_I}{\sqrt{2\pi r}}\left[\frac{1}{4}\sin\left(\frac{\theta}{2}\right) + \frac{1}{4}\sin\left(\frac{3\theta}{2}\right)\right] \tag{2.22}$$

The stress intensity factor defines the amplitude of the crack-tip singularity; all the stress and strain components at points near the crack tip increase in proportion to K_I, provided the crack is stationary.

When suddenly applied loading applies the cracked body remote to the crack, the stress wave travels to the crack faces and crack tips affects the behavior of the stress around the crack tip. The applied load travels through elastic body with heavy time step function, H(t). Thus the suddenly applied loading, P(t) is a product of applied stress (σ^*) by heavy time step function.

$$P(t) = \sigma^* \times H(t) \tag{2.23}$$

Then, the dynamic stresses at the crack tip becomes [27, 32]

$$\sigma_{ij} = \frac{K_I(t)}{\sqrt{2\pi r}}\sum_{ij}(\theta) + \textit{higher order terms} \tag{2.24}$$

where $\Sigma_{ij}(\theta)$ angular orientation function and (i,j=r, θ)

$$\sigma_{rr}(t) = \frac{K_I(t)}{\sqrt{2\pi r}}\left[\frac{5}{4}\cos\left(\frac{\theta}{2}\right) - \frac{1}{4}\cos\left(\frac{3\theta}{2}\right)\right] \tag{2.25}$$

$$\sigma_{\theta\theta}(t) = \frac{K_I(t)}{\sqrt{2\pi r}}\left[\frac{3}{4}\cos\left(\frac{\theta}{2}\right) + \frac{1}{4}\cos\left(\frac{3\theta}{2}\right)\right] \tag{2.26}$$

$$\tau_{r\theta}(t) = \frac{K_I(t)}{\sqrt{2\pi r}}\left[\frac{1}{4}\sin\left(\frac{\theta}{2}\right) + \frac{1}{4}\sin\left(\frac{3\theta}{2}\right)\right] \tag{2.27}$$

The formula to calculate crack tip stresses using cartesian coordinate

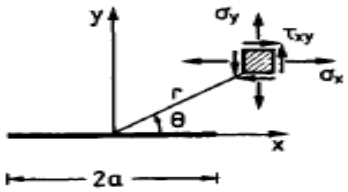

Figure 2.5 crack tip representation

$$\sigma_x = \frac{K_I}{\sqrt{2\pi r}}\cos\left(\frac{\theta}{2}\right)\left[1 - \sin\left(\frac{\theta}{2}\right)\sin\left(\frac{3\theta}{2}\right)\right] \tag{2.28}$$

$$\sigma_y = \frac{K_I}{\sqrt{2\pi r}}\cos\left(\frac{\theta}{2}\right)\left[1 + \sin\left(\frac{\theta}{2}\right)\sin\left(\frac{3\theta}{2}\right)\right] \tag{2.29}$$

$$\tau_{xy} = \frac{K_I}{\sqrt{2\pi r}}\cos\left(\frac{\theta}{2}\right)\left[\sin\left(\frac{\theta}{2}\right)\cos\left(\frac{3\theta}{2}\right)\right] \tag{2.30}$$

The dynamic crack stress equation for cartesian coordinate system

$$\sigma_x(t) = \frac{K_I(t)}{\sqrt{2\pi r}}\cos\left(\frac{\theta}{2}\right)\left[1 - \sin\left(\frac{\theta}{2}\right)\sin\left(\frac{3\theta}{2}\right)\right] \tag{2.31}$$

$$\sigma_y(t) = \frac{K_I(t)}{\sqrt{2\pi r}}\cos\left(\frac{\theta}{2}\right)\left[1 + \sin\left(\frac{\theta}{2}\right)\sin\left(\frac{3\theta}{2}\right)\right] \tag{2.32}$$

$$\tau_{xy}(t) = \frac{K_I(t)}{\sqrt{2\pi r}}\cos\left(\frac{\theta}{2}\right)\left[\sin\left(\frac{\theta}{2}\right)\cos\left(\frac{3\theta}{2}\right)\right] \tag{2.33}$$

2.3.4.2 Crack tip displacement

When the load is applied, the crack tip displacement is evaluated using cartesian coordinate system as follows

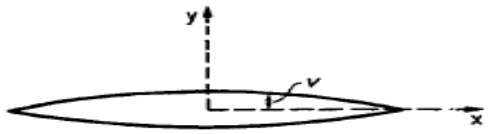

Figure 2.6 Crack tip displacement representation

$$u = \frac{K_I}{2G}\sqrt{\frac{r}{2\pi}}\cos\frac{\theta}{2}\left(\kappa - \cos\theta\right) \tag{2.34}$$

$$v = \frac{K_I}{2G}\sqrt{\frac{r}{2\pi}}\sin\frac{\theta}{2}\left(\kappa - \cos\theta\right) \tag{2.35}$$

G = Coulomb-Mohr fracture criterion constant

k=3-4v for plain strain and (3-v)/ (1-v) for plain stress

Dynamic equation of crack tip displacement using Cartesian coordinate system

$$u(t) = \frac{K_I(t)}{2G}\sqrt{\frac{r}{2\pi}}\cos\frac{\theta}{2}\left(\kappa - \cos\theta\right) \tag{2.36}$$

$$v(t) = \frac{K_I(t)}{2G}\sqrt{\frac{r}{2\pi}}\sin\frac{\theta}{2}\left(\kappa - \cos\theta\right) \tag{2.37}$$

Crack tip displacement using cylindrical coordinate system

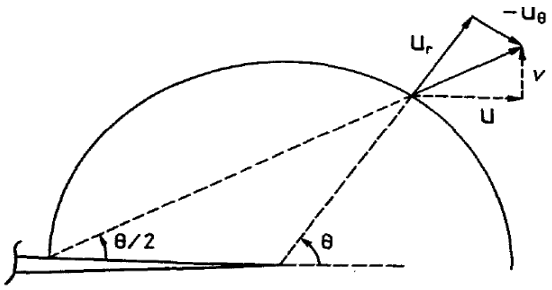

Figure 2.7 crack tip displacement in cylindrical coordinate system

$$u_r = \frac{K_I}{4G}\sqrt{\frac{r}{2\pi}}\left[(2k-1)\cos\frac{\theta}{2} - \cos\frac{3\theta}{2}\right] \tag{2.38}$$

$$u_\theta = \frac{K_I}{4G}\sqrt{\frac{r}{2\pi}}\left[(-1-2k)\sin\frac{\theta}{2} + \sin\frac{3\theta}{2}\right] \tag{2.39}$$

Dynamic equation of crack tip displacement in cylindrical coordinate system

$$u_r(t) = \frac{K_I(t)}{4G}\sqrt{\frac{r}{2\pi}}\left[(2k-1)\cos\frac{\theta}{2} - \cos\frac{3\theta}{2}\right] \tag{2.40}$$

$$u_\theta(t) = \frac{K_I(t)}{4G}\sqrt{\frac{r}{2\pi}}\left[(-1-2k)\sin\frac{\theta}{2} + \sin\frac{3\theta}{2}\right] \tag{2.41}$$

2.4 Analytical Elasto-dynamic or Stress Wave Analysis

2.4.1 Elasticity

2.4.1.1 Elasticity Equation using Cartesian Coordinate System

The fundamental set of field equations governing the motion of a homogenous and isotropic elastic body consists of the strain displacement relation for small strain

$$\varepsilon = \frac{1}{2}(\nabla u + u\nabla) \quad or \quad \varepsilon_{ij} = \frac{1}{2}(u_{j,i} + u_{i,j}) \tag{2.42}$$

The governing momentum balance equation is

$$\nabla.\sigma + \rho f = \rho \ddot{u} \quad or \quad \sigma_{ij,i} + \rho f_j = \rho \ddot{u}_j \tag{2.43}$$

where (i,j,k=1,2,3)

And linear stress strain relation

$$\sigma_{ij} = \lambda \delta_{ij} \varepsilon_{kk} + 2\mu \varepsilon_{ij}$$
$$where \quad \sigma = stress, \quad \varepsilon = strain \quad and \delta_{ij} = cronec\,\ker delta \tag{2.44}$$

where λ and μ are the positive lame constants, *f* is body force, *u* displacement and ∇ is operator

The field equations are to be satisfied through out a region of space occupied by the elastic solid in its initial undeformed configuration. No distinction is made between the deformed and undeformed configuration in the linear theory.

If the momentum equation is written in terms of displacement *u* by substituting by first from equation (2.44) and then from equation (2.42) Navier's equation of motion

$$(\lambda + \mu)\nabla(\nabla.u) + \mu\nabla^2 u + \rho f = \rho \ddot{u} \tag{2.45}$$

is obtained in light of the vector identity

$$\nabla \times (\nabla \times u) = \nabla(\nabla.u) - \nabla^2 u \tag{2.46}$$

equation 2.45 can be written as

$$c_d^2 \nabla(\nabla.u) - c_s^2 \nabla \times ((\nabla \times u)) + f = \ddot{u} \tag{2.47}$$

$$where \quad c_d = \sqrt{\frac{\lambda + 2\mu}{\rho}} = \sqrt{\frac{(1-\nu)E}{(1-2\nu)(1+\nu)\rho}} \tag{2.48}$$

$$c_s = \sqrt{\frac{\mu}{\rho}} = \sqrt{\frac{E}{(1+\nu)2\rho}} \tag{2.49}$$

$$and \quad \lambda = \frac{\nu E}{(1-2\nu)(1+\nu)}, \qquad \mu = \frac{E}{2(1+\nu)}$$

When the equation of motion (2.45) along x, y and z direction using displacement is represented as:

$$(\lambda + \mu)\frac{\partial e}{\partial x} + \delta\nabla^2 u + F_X = \rho\frac{\partial^2 u}{\partial t^2} \tag{2.45a}$$

$$(\lambda + \mu)\frac{\partial e}{\partial y} + \delta\nabla^2 v + F_Y = \rho\frac{\partial^2 v}{\partial t^2} \tag{2.45b}$$

$$(\lambda+\mu)\frac{\partial e}{\partial z}+\delta\nabla^2 w+F_Z=\rho\frac{\partial^2 w}{\partial t^2} \tag{2.45c}$$

where $\nabla^2=\frac{\partial^2}{\partial x^2}+\frac{\partial^2}{\partial y^2}+\frac{\partial^2}{\partial z^2}$

e =volume expansion

F_x, F_y, F_z =(ρ*f*) are body forces

And the equation of motion using stress function along each coordinate system is

$$\frac{\partial\sigma_{xx}}{\partial x}+\frac{\partial\sigma_{xy}}{\partial y}+\frac{\partial\sigma_{xz}}{\partial z}+F_x=\rho\ddot{u}_x \tag{2.45a'}$$

$$\frac{\partial\sigma_{xy}}{\partial x}+\frac{\partial\sigma_{yy}}{\partial y}+\frac{\partial\sigma_{yz}}{\partial z}+F_y=\rho\ddot{u}_y \tag{2.45b'}$$

$$\frac{\partial\sigma_{xz}}{\partial x}+\frac{\partial\sigma_{yz}}{\partial y}+\frac{\partial\sigma_{zz}}{\partial z}+F_z=\rho\ddot{u}_z \tag{2.45c'}$$

2.4.1.2 Equation of Elasticity using Cylindrical Coordinate System

Navier's displacement equation of motion

$$(\lambda+2\mu)\frac{\partial I_e}{\partial r}-2\mu\left(\frac{1}{r}\frac{\partial w_z}{\partial\theta}-\frac{\partial w_\theta}{\partial z}\right)+F_r=\rho\frac{\partial^2 u_r}{\partial^2 t} \tag{2.45a''}$$

$$(\lambda+2\mu)\frac{\partial I_e}{r\partial\theta}-2\mu\left(\frac{1}{r}\frac{\partial w_r}{\partial z}-\frac{\partial w_z}{\partial r}\right)+F_\theta=\rho\frac{\partial^2 u_\theta}{\partial^2 t} \tag{2.45b''}$$

$$(\lambda+2\mu)\frac{\partial I_e}{\partial z}-2\mu\left(\frac{\partial(rw_\theta)}{\partial r}-\frac{\partial w_r}{\partial\theta}\right)+F_z=\rho\frac{\partial^2 u_z}{\partial^2 t} \tag{2.45c''}$$

where

$$I_e=e_{ii}=\nabla.u=\frac{1}{r}\frac{\partial(ru_r)}{\partial r}+\frac{1}{r}\frac{\partial u_\theta}{\partial\theta}-\frac{\partial u_z}{\partial z}$$

$$2w_r=\frac{1}{r}\frac{\partial u_z}{\partial\theta}-\frac{\partial u_\theta}{\partial z}$$

$$2w_\theta=\frac{1}{r}\frac{\partial u_r}{\partial z}-\frac{\partial u_z}{\partial r}$$

$$2w_z=\frac{1}{r}\frac{\partial(ru_r)}{\partial r}+\frac{1}{r}\frac{\partial u_r}{\partial\theta}$$

F_r, F_θ, and F_z are body forces, but in all cases the body forces are assumed to be zero

Equation of motion using stress function

$$\frac{\partial \sigma_{rr}}{\partial r}+\frac{\partial \sigma_{r\theta}}{r\partial \theta}+\frac{\partial \sigma_{rz}}{\partial z}+\frac{\partial \sigma_{rr}-\partial \sigma_{\theta\theta}}{r}=\rho \ddot{u}_r \tag{2.45a'''}$$

$$\frac{\partial \sigma_{r\theta}}{\partial r}+\frac{\partial \sigma_{\theta\theta}}{r\partial \theta}+\frac{\partial \sigma_{\theta z}}{\partial z}+\frac{2\partial \sigma_{r\theta}}{r}=\rho \ddot{u}_\theta \tag{2.45b'''}$$

$$\frac{\partial \sigma_{rz}}{\partial r}+\frac{\partial \sigma_{\theta z}}{r\partial \theta}+\frac{\partial \sigma_{zz}}{\partial z}+\frac{\partial \sigma_{rz}}{r}=\rho \ddot{u}_z \tag{2.45c'''}$$

2.4.2 Thermo Elasticity

Thermal stresses are stresses in a structure caused by changes in the structure's temperature distribution, stresses due to constraints of thermal expansion or contraction, non-uniform temperature distributions or inhomogeneous thermal expansion properties. They are self-stresses, and are self-equilibrating if there are no external constraints, or if the reactions at external constraints vanish. When the temperature is suddenly changed, it creates thermal shock. If this thermal shock duration is small enough compared to the first natural frequency, inertial effects happen and the solution is found through the coupled field. For homogeneous isotropic material the coupled thermo elastic governing equation without body force is given by Navier-Lame-stoke [44].

$$\frac{E}{2(1+\sigma)}\nabla^2 u+\frac{E}{2(1+\sigma)(1-2\sigma)}\nabla(\nabla.u)-\frac{E\alpha}{3(1-2\sigma)}\nabla T=m\frac{\partial^2 u}{\partial t^2} \tag{2.50}$$

$$\rho c_v \frac{\partial T}{\partial t}=k\nabla^2 T-\frac{E\alpha T}{(1-2\sigma)}\frac{\partial}{\partial t}\nabla.u \tag{2.51}$$

where T is temperature, α is thermal expansion, m is mass and σ applied stress

Chapter Three

3 Finite Element Analysis

3.1 Introduction

Numerical modeling of fracture mechanics is an indispensable tool, since relatively practical problems have closed form analytical solution. A variety of numerical techniques has been applied to problems in solid mechanics including finite difference method, finite element method and boundary integral methods have been applied almost exclusively. The vast majority of analysis of cracked bodies used finite elements although the boundary integral method may be useful in limited circumstances. In this paper finite element analysis is used to calculate the fracture parameter of pressure vessels. The mathematical modeling of finite element method is derived for structural, thermal and thermo-elasticity equation in the following three sections.

3.2 Finite Element Descritization

In finite element analysis of cracked problems, two formations of elements require. The first one is to mesh the whole body with regular elements except the crack tip and secondly to form singular elements at the crack tip. 20-node brick elements are more appropriate to analyze the characteristics of a crack. This is due to the behavior of the element to be formed into wedge type of singular elements at the crack tip. The following figure shows the isoperimetric representations of the element and its nodal configuration.

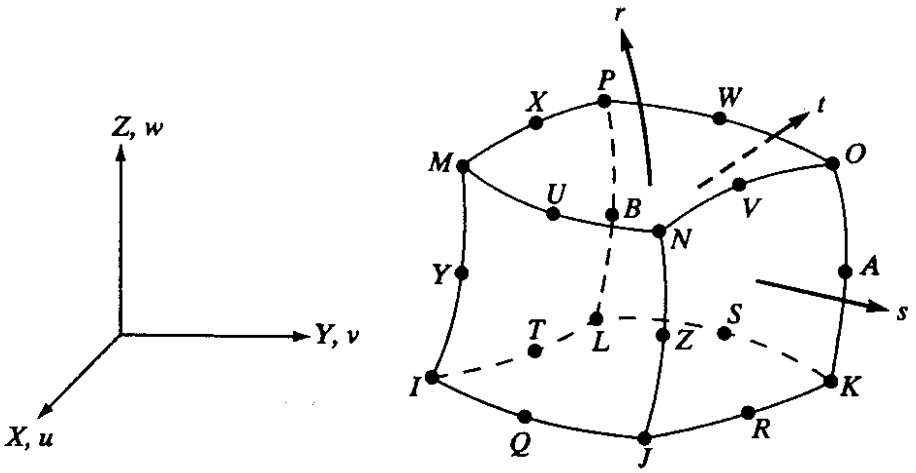

Figure 3.1 20- node brick element

$$u = \frac{1}{8}(u_I(1-s)(1-t)(1-r)(-s-t-r-2) + u_J(1+s)(1-t)(1-r)(s-t-r-2) +$$
$$u_K(1+s)(1+t)(1-r)(s+t-r-2) + u_L(1-s)(1+t)(1-r)(-s+t-r-2) +$$
$$u_M(1-s)(1-t)(1+r)(-s-t+r-2) + u_N(1+s)(1-t)(1+r)(s-t+r-2) +$$
$$u_O(1+s)(1+t)(1+r)(s+t+r-2) + u_P(1-s)(1+t)(1+r)(-s+t+r-2)) +$$
$$\frac{1}{4}(u_Q(1-s^2)(1-t)(1-r) + u_R(1+s)(1-t^2)(1-r) + u_S(1-s^2)(1+t)(1-r) + u_T(1-s)(1-t^2)(1-r) +$$
$$u_U(1-s^2)(1-t)(1+r) + u_V(1+s)(1-t^2)(1+r) + u_W(1-s^2)(1+t)(1+r) + u_X(1-s)(1-t^2)(1+r) +$$
$$u_Y(1-s)(1-t)(1-r^2) + u_Z(1+s)(1-t)(1-r^2) + u_Z(1+s)(1-t)(1-r^2) + u_A(1+s)(1+t)(1-r^2))$$
$$v = \frac{1}{8}v_I(1-s)(ana\log ous\ to\ u)$$
$$w = \frac{1}{8}w_I(1-s)(ana\log ous\ to\ u)$$
$$T = \frac{1}{8}T_I(1-s)(ana\log ous\ to\ u)$$

(3.1)

Where *u v* and *w* are global displacements and $u_{I\ to\ A}$, $v_{I\ to\ A}$ and $w_{I\ to\ A}$ are nodal displacements of the isoperimetric element

T is temperature and $T_{I\ to\ A}$ *is* nodal temperatures

3.2.1 Derivation of Structural Matrix for Finite Element Analysis

The principle of virtual work states that a virtual (very small) change of the internal strain energy must be offset by an identical change in external work due to the applied loads [42, 43]

$$\delta U = \delta V \tag{3.2}$$

where: U = strain energy (internal work) = $U_1 + U_2$

V = external work = $V_1 + V_2 + V_3$

U_1 = *energy of the volume*

U_2= *energy due to area*

V_1 = *work over the volume*

V_2 = *work due to pressure force*

V_3 = *work due to nodal force*

δ = virtual operator

The virtual strain energy over the volume is [42, 43]:

$$\delta U = \int_{vol} [\delta\varepsilon]\{\sigma\} d(vol) \tag{3.3}$$

where :[δε]= virtual strain

$\{\sigma\}$ = stress vector

[D]= material property matrix

vol = volume of element

we know that mechanical strain from constitutive equation is given by

$$\{\sigma\} = [D](\{\varepsilon\} - \{\varepsilon^{th}\}) \tag{3.4}$$

$\{\varepsilon^{th}\}$=thermal strain vector

$\{\varepsilon\}$ = strain vector

Continuing the derivation for linear materials, equations (3.3) and (3.4) are combined to give

$$\delta U_1 = \int_{vol} (\{\delta\varepsilon\}[D]\{\varepsilon\} - [\delta\varepsilon][D]\{\varepsilon^{th}\}) d(vol) \tag{3.5}$$

The strains are related to the nodal displacements by

$$\{\varepsilon\} = [B]\{u\} \quad and \quad [\delta\varepsilon] = [\delta u][B]^T \tag{3.6}$$

where: [*B*] = strain-displacement matrix, based on the element shape functions

$\{u\}$ = nodal displacement vector

[δu]= virtual displacement

$$\delta U_1 = [\delta u]\int_{vol} [B]^T [D][B] d(vol)\{u\} - [\delta u]\int_{vol} [B]^T \{D\}\{\varepsilon^{th}\} d(vol) \tag{3.7}$$

Another form of virtual energy is when a surface move against a distributed resistance, as in a foundation stiffness (energy at the surfaces)

$$\delta U_2 = \int_{area_f} [\delta w_n]\{\sigma\} d(area_f) \tag{3.8}$$

where: $[\delta w_n]$ = motion normal to the surface

$\{\sigma\}$ = stress carried by the surface

$area_f$ = area of the distributed resistance

The point-wise normal displacement is related to the nodal displacements by:

$$\{w_n\} = [N_n]\{u\} \quad and \quad [\delta w_n] = [\delta u][N_n]^T \tag{3.9}$$

where: $[N_n]$ = matrix of shape functions for normal motions at the surface

The stress, $\{\sigma\}$, is

$$\{\sigma\} = k_f \{w_n\} \tag{3.10}$$

where: kf the foundation stiffness in units of force per length per unit area

Combining equations (3.8), (3.9) and (3.10), and assuming that k_f is constant over the area

$$\delta U_2 = [\delta u] k_f \int_{area_f} [N_n]^T [N_n] d(area_f) \{u\} \tag{3.11}$$

Next the virtual work is considered

$$\delta V_1 = -\int_{vol} [\delta W] \frac{\{F^a\}}{vol} d(vol) \tag{3.12}$$

where: $\{W\}$ = vector of displacements of a general point

$\{F^a\}$ = acceleration (D' Alembert) force vector

According to Newton's second law

$$\frac{\{F^a\}}{(vol)} = \rho \frac{\partial^2}{\partial t^2}\{W\} \tag{3.13}$$

where: ρ = density, t = time

The displacements within the element are related to the nodal displacements by

$$\{W\} = [N]\{u\} \quad and \quad [\delta W] = [\delta u][N]^T \tag{3.14}$$

where [N] = matrix of shape functions.

Combining equation (3.12), (3.13), and (3.14); and assuming that ρ is constant over the volume

$$\delta V_1 = -[\delta u]\rho \int_{\text{vol}} [N]^{\text{T}}[N]\text{d}(\text{vol})\frac{\partial^2}{\partial t^2}\{u\} \tag{3.15}$$

Virtual work due to the pressure force vector formulation

$$\delta V_2 = \int_{area_p} [\delta w_n]\{P\}d(area_p) \tag{3.16}$$

where: $\{P\}$ = the applied pressure vector

$area_p$ = area over which pressure acts

$$\delta V_2 = [\delta u] \int_{area_p} [N_n]^T \{P\}d(area_p) \tag{3.17}$$

Unless otherwise noted, pressures are applied to the outside surface of each element and are normal to curved surfaces.

Virtual work due to nodal forces applied to the element can be given by:

$$\delta V_3 = [\delta u]\{F_e^{nd}\} \tag{3.18}$$

where: $\{F_e^{nd}\}$ nodal force applied to the element

Finally, equation (3.2), (3.7), (3.11), (3.15), (3.17), and (3.18) may be combined to give

$$[\delta u]\int_{vol}[B]^T[D][B]d(vol)\{u\}-[\delta u]\int_{vol}[B]^T[D]\{\varepsilon^{th}\}d(vol)+[\delta u]k_f\int_{area_f}[N_n]^T[N_n]d(area_f)\{u\}$$
$$=-[\delta u]\rho\int_{\text{vol}}[N]^{\mathrm{T}}[N]\mathrm{d}(\text{vol})\frac{\partial^2}{\partial t^2}\{u\}+[\delta u]\int_{area_p}[N_n]^T\{P\}d(area_p)+[\delta u]\{F_e^{nd}\} \tag{3.19}$$

Here the $[\delta u]$ vector is a set of arbitrary virtual displacements common in all of the above terms, the condition required to satisfy equation (3.19) reduces

$$[M_e]\left\{\ddot{u}\right\}+([K_e]+[K_e^{ef}])\{u\}=\{F_e^{th}\}+\{F_e^{pr}\}+\{F_e^{nd}\} \tag{3.20}$$

where: $[K_e]=\int_{vol}[B]^T[D][B]d(vol)$=element stiffness matrix

$[K_e^{ef}]=k_f\int_{area_f}[N_n]^T[N_n]d(area_f)$=element foundation stiffness matrix

$\{F_e^{th}\}=\int_{vol}[B]^T[D]\{\varepsilon^{th}\}d(vol)$=element thermal load vector

$[M_e]=\rho\int_{\text{vol}}[N]^{\mathrm{T}}[N]\mathrm{d}(\text{vol})$= element mass matrix

$\left\{\ddot{u}\right\}=\frac{\partial^2}{\partial t^2}\{u\}$ =acceleration vector

$\{F_e^{pr}\}=\int_{area_p}[N_n]^T\{P\}d(area_p)$=element pressure vector

$\{F_e^{nd}\}$= nodal force vector

3.2.2 Derivation of Thermal Matrix for Finite Element Analysis

The first law of thermodynamics states that thermal energy is conserved. Specializing this to a differential control volume

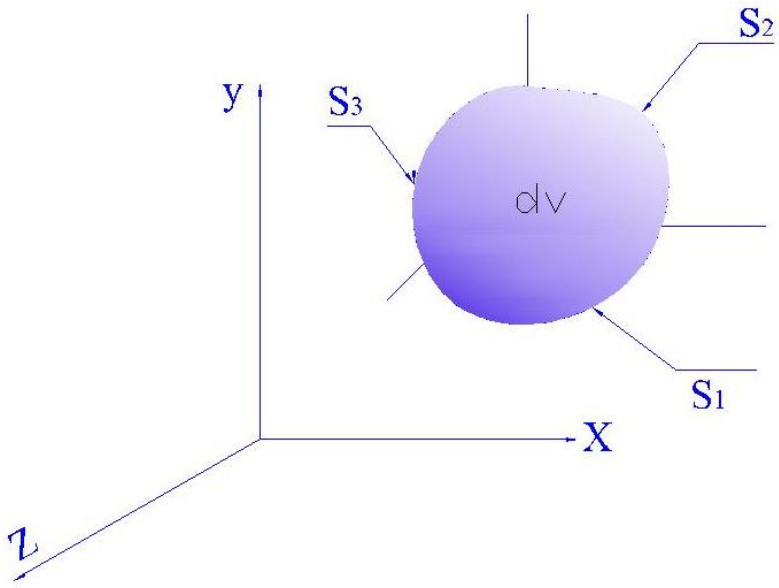

Figure 3.2 20- node brick element

$$\rho c\left(\frac{\partial T}{\partial t}\right)+\{L\}^{T}\{q\}=\tilde{q} \tag{3.21}$$

where: ρ = density

c = specific heat

T = temperature

t = time

$\{L\}$=vector operator

$\{q\}$ = heat flux vector

$\tilde{q}$ =heat generation rate per unit volume

Next, Fourier's law is used to relate the heat flux vector to the thermal gradients

$$\{q\}=-[K_c]\{L\}T \tag{3.22}$$

where: $[K_c] = \begin{bmatrix} k_{xx} & 0 & 0 \\ 0 & k_{yy} & 0 \\ 0 & 0 & k_{zz} \end{bmatrix}$

k_{xx}, k_{yy}, k_{zz} = conductivity in the element x, y, and z directions, respectively

Combining equation (3.21) and (3.22)

$$\rho c \frac{\partial T}{\partial t} = \{L\}^T \left([K_c] \{L\} T \right) + \tilde{q} \tag{3.23}$$

Expanding equation 3.22 to its more familiar form

$$\rho c \frac{\partial T}{\partial t} = \frac{\partial}{\partial x}\left(k_x \frac{\partial T}{\partial x} \right) + \frac{\partial}{\partial y}\left(k_y \frac{\partial T}{\partial y} \right) + \frac{\partial}{\partial z}\left(k_z \frac{\partial T}{\partial z} \right) + \tilde{q} \tag{3.24}$$

Three types of boundary conditions are considered. It is presumed that these cover the entire element.

1. Specified temperatures acting over surface S_1:

$$T(x, y, z, t) = T_s \tag{3.25}$$

where T^* is the specified surface temperature

2. Specified heat flow acting over surface S_2:

$$\{q\}^T \{\eta\} = -q_s \tag{3.26}$$

where: $\{\eta\}$ = unit outward normal vector

q_s = specified heat flow rate per unit area

3. Specified convection surfaces acting over surface S_3 (Newton's law of cooling):

$$\{q\}^T \{\eta\} = h(T_s - T_b) \tag{3.27}$$

where: h= convective heat transfer coefficient

T_b= bulk temperature of the adjacent fluid

T_S = temperature at the surface of the model

Combining equation 3.22 with 3.26 and 3.27

$$\{\eta\}^T [K_c]\{L\}T = q_s \tag{3.28}$$

$$\{\eta\}^T [K_c]\{L\}T = h_f (T_B - T) \tag{3.29}$$

Pre multiplying equation 3.23 by a virtual change in temperature, integrating over the volume of the element, and combining with equation 3.28 and equation 3.29 with some manipulation yields

$$\int_{vol}\left(\rho c \delta T \frac{\partial T}{\partial t} + \{L\}^T \delta T([K_c]\{L\}T)\right)d(vol) = \int_{S_2} \delta T q_s d(S_2) + \int_{S_3} \delta T h(T_B - T) d(S_3) + \int_{vol} \delta T \tilde{q} d(vol) \tag{3.30}$$

where: δT = an allowable virtual temperature

The variable T is allowed to vary in both space and time. This dependency is separated as:

$$[N(x,y,z)]\{T_e(t)\} = T(x,y,z,t) \tag{3.31}$$

where: $T(x,y,z,t)$ = temperature of each element

$[N]$ = temperature interpolation matrix

$\{T_e(t)\}$ = nodal temperature vector of element

Thus, the time derivatives of equation (3.31) may be written as:

$$[N]\{\dot{T}_e(t)\} = [N]\frac{\partial T}{\partial t} = \dot{T} \tag{3.32}$$

δT has the same form as T:

$$[N]\{\delta T_e\} = \delta T \Rightarrow \{\delta T_e\}^T [N]^T = \delta T \tag{3.33}$$

The combination $\{L\}\ T$ is written as

$$\{L\}T = [B]^T \{T_e(t)\} \tag{3.34}$$

where: $[B]$ is temperature gradient interpolation matrix

Now, the variational statement of equation (3.30) can be combined with equation (3.31) through (3.34) to yield:

$$\int_{vol} \rho c\{\delta T_e\}^T [N]^T [N]\left\{\dot{T}_e\right\} d(vol) + \int_{vol} \{\delta T_e\}^T [B]^T [K_c][B]\{T_e\} d(vol) + \int_{S_2} \{\delta T\}^T [N]^T \tilde{q}\, d(S_2)$$
$$+ \int_{S_3} \{\delta T_e\}^T h[N]^T (T_B - [N]\{T_e\}) d(S_3) + \int_{vol} \{\delta T_e\}^T [N]^T \tilde{q}\, d(vol)$$

(3.35)

Terms are defined in heat flow fundamentals. ρ is assumed to remain constant over the volume of the element. On the other hand, c and $\tilde{q}$ may vary over the element. Finally, $\{T_e\}$, $\{\dot{T}_e\}$, and $\{\delta T_e\}$ are nodal quantities and do not vary over the element, so that they also may be removed from the integral. Now, since all quantities are seen to be pre multiplied by the arbitrary vector $\{\delta T_e\}$, this term may be dropped from the resulting equation. Thus, equation (3.35) may be reduced to:

$$\rho \int_{vol} c[N]^T [N] d(vol)\left\{\dot{T}_e\right\} + \int_{vol} [B]^T [D][B] d(vol)\{T_e\} = \int_{S_2} [N]^T \tilde{q}\, d(S_2)$$
$$+ \int_{S_3} h[N]^T T_B d(S_3) - \int_{S_3} h[N]^T [N]\{T_e\} d(S_3) + \int_{vol} \tilde{q}[N]^T d(vol)$$

(3.36)

equation 3.36 may be written as

$$\left[C_e^t\right]\left\{\dot{T}_e\right\} + \left(\left[K_e^{tb}\right] + \left[K_e^{tc}\right]\right)\{T_e\} = \left\{Q_e^f\right\} + \left\{Q_e^c\right\} + \left\{Q_e^g\right\} \qquad (3.37)$$

where: $\left[C_e^t\right] = \rho \int_{vol} c[N]^T [N] d(vol)$ =thermal damping matrix

$\left[K_e^{tb}\right] = \int_{vol} [B]^T [D][B] d(vol)$ =element diffusion conductivity matrix

$\left[K_e^{tc}\right] = \int_{S_3} h[N]^T [N] d(S_3)$ =element convection matrix

$$\{Q_e\} = \int_{S_2} [N]^T \tilde{q} d(S_2)$$ =element mass flux vector

$$\{Q_e^c\} = \int_{S_3} h[N]^T T_B d(S_3)$$ = element convection surface heat flow matrix

$$\{Q_e^g\} = \int_{vol} \tilde{q}[N]^T d(vol)$$=element heat generation load

3.2.3 Thermo Elasticity

The coupled thermo elastic constitutive equations

$$\{\varepsilon\} = [D]^{-1}\{\sigma\} + \{\alpha\}\Delta T \tag{3.38}$$

$$S = \{\alpha\}^T\{\sigma\} + \frac{\rho C_p}{T_o}\Delta T \tag{3.39}$$

where: $\{\varepsilon\}$ = total strain vector

S = entropy density

$\{\sigma\}$ = stress vector

$\Delta T = T - T_{ref}$

T = current temperature

T_0 = absolute reference temperature

T_{ref}= reference temperature

$[D]$ = elastic stiffness matrix

$\{\alpha\}$ = vector of coefficients of thermal expansion

ρ = density

C_p = specific heat at constant stress or pressure

Using $\{\varepsilon\}$ and ΔT as independent variables, and replacing the entropy density S in equation (3.38) by heat density Q using the second law of thermodynamics for a reversible change

$$Q = T_o S \tag{3.40}$$

$$\{\sigma\} = [D]\{\varepsilon\} - \{\alpha\}\Delta T \tag{3.41}$$

$$Q = T_o \{\beta\}^T \{\varepsilon\} + \rho C_v \Delta T \tag{3.42}$$

where: {β} = vector of thermo elastic coefficients = [D] {α}

$$C_v = C_p - \frac{T_o}{\rho}\{\alpha\}^T \{\beta\} \tag{3.43}$$

Substituting Q from equation (3.40) into the heat flow equation (3.21) produces

$$\frac{\partial Q}{\partial t} = T_o \{\beta\}^T \frac{\partial\{\varepsilon\}}{\partial t} + \rho C_v \frac{\partial(\Delta T)}{\partial t} - [K]\nabla^2 T \tag{3.44}$$

Using the variational principle to stress equation of motion and heat flow equation coupled by thermo elastic constitutive equations produces the following matrix equation [42, 44]

$$\begin{bmatrix} [M] & [0] \\ [0] & [0] \end{bmatrix} \begin{Bmatrix} \{\ddot{u}\} \\ \{\ddot{T}\} \end{Bmatrix} + \begin{bmatrix} [0] & [0] \\ [C^{tu}] & [C^t] \end{bmatrix} \begin{Bmatrix} \{\dot{u}\} \\ \{\dot{T}\} \end{Bmatrix} + \begin{bmatrix} [K] & [K^{ut}] \\ [0] & [K^t] \end{bmatrix} \begin{Bmatrix} \{u\} \\ \{T\} \end{Bmatrix} = \begin{Bmatrix} \{F\} \\ \{Q\} \end{Bmatrix} \tag{3.45}$$

Where: [K] = element stiffness matrix

{F} = sum of the element nodal force

[M] = element mass matrix

[C_t] = element specific heat matrix

[K_t] = element diffusion conductivity matrix

{Q} = sum of the element heat generation load and element convection surface heat flow vectors

[C_{tu}] = element thermo elastic damping matrix

$$[K^{ut}] = -\int_{vol} [B]^T \{\beta(\nabla)[N]\} d(vol)$$

3.3 Transient Dynamic Analysis

Transient dynamic analysis is a technique used to determine the dynamic response of a structure under time-dependent loads. In this context, when the loads are rapidly applied to the cracked body, the inertial effects must be taken into account, so that the response of the system is measured in a “short-term period of time”. In this case of rapid loading, the influence of the loads is transferred to the crack by means of stress waves through the body [32]. Therefore, by using this technique, the displacements, strains, stresses and dynamic stress intensity factor can be determined as a time function.

As earlier mentioned, the basic equation of motion solved by a transient dynamic analysis is given by equation (3.45) in general for coupled analysis. The first term of equation (3.43) is used for transient analysis with thermal effect, and the second term for thermal analysis only.

Equation (3.45) can be evaluated using different time integration methods. This thesis uses Newmark time integration method because of its appropriate approach for implicit analysis and the re recommended method in ANSYS.

Chapter Four

4 Geometrical Modeling and Numerical Analysis Using ANSYS

4.1 Introduction

ANSYS is general-purpose finite element analysis (FEA) software package. Finite Element Analysis is a numerical method of constructing a complex system into very small pieces called elements. The software implements equations that govern the behavior of these elements and solves them all; creating a comprehensive explanation of how the system acts as a whole. These results then can be presented in tabulated or graphical forms. This type of analysis is typically used for the design and optimization of a system for too complex to analyze by hand. Systems that may fit into this category are too complex due to their geometry, scale, or governing equations. The product offers a complete set of elements behavior, material models and equation solvers for a wide range of engineering problems. In addition, ANSYS mechanical offers thermal analysis and coupled-physics capabilities involving acoustic, piezoelectric, thermal–structural and thermal–electric analysis

Basic steps in finite element method

Like solving any problem analytically, we need to define (1) the solution domain, (2) the physical model, (3) boundary conditions and (4) the physical properties. Then we solve the problem and present the results. In numerical methods, the main difference is an extra step called mesh generation. This step divides the complex model into small elements that become solvable in an otherwise too complex situation. The procedures that have to be carried out are:

Building Geometry: Constructing of three-dimensional representation of the object to be modeled and tested using the work plane coordinates system within ANSYS.

Defining of Material Properties: Now that the part exists, define a library of the necessary materials that compose the object (or project) being modeled. This includes thermal and mechanical properties.

Generating Mesh: At this point ANSYS understands the makeup of the parts which defines how the modeled system should be broken down into finite pieces

Applying Loads: Once the system is fully designed, the last task is to burden the system with constraints, such as physical loadings or boundary conditions

Reading the Solution: This is the difficult step, because ANSYS needs understanding within, what state (steady state, transient), the problem must be solved.

Presentation of the Results: After the solution has been obtained, there are many ways to present ANSYS' results such as tables, graphs, and contour plots.

4.2 Geometrical Modeling

Three-dimensional regions that define mechanical parts are often solved using solid/brick elements when simpler models are not available, sometimes when the development of a simpler model involves an excessive commitment of engineering time, or if one needs explicit solutions for a problem. Therefore, appropriate modeling is required to have accurate solution and to save time. Figure 4.2 shows the full modeling and the implicit location of the crack.

Since the pressure vessel is symmetrical, it is possible to take one eighth of the actual object at the crack region to attain accurate results and economical time. Figure 4.3 shows the $1/8^{th}$ model for 20mm through crack length. In this paper five different kinds of modeling are done.

a) Full crack model: It is to show dynamic stress wave traveling from the suddenly applying area to the crack region. Longitudinal through crack (28mm) is modeled which includes one forth of the actual pressure vessel model.
b) Half symmetrical longitudinal through crack model: This model contains three different crack lengths (20mm, 24mm and 28mm) to show the effect of the crack length on a cracked pressure vessel.

c) Half symmetrical circumferential through crack model: this model contains 20mm crack length to compare the results obtained from longitudinal crack with the circumferential.

d) Circumferential edge crack: 11.45mm edge crack is modeled. The use of this model is to show the thermal shock effect on cracked pressure vessel.

The most important region in a fracture model is the region around the edge of the crack. We refer to the edge of the crack as a crack tip in a 2-D model and crack front in a 3-D model as is illustrated below

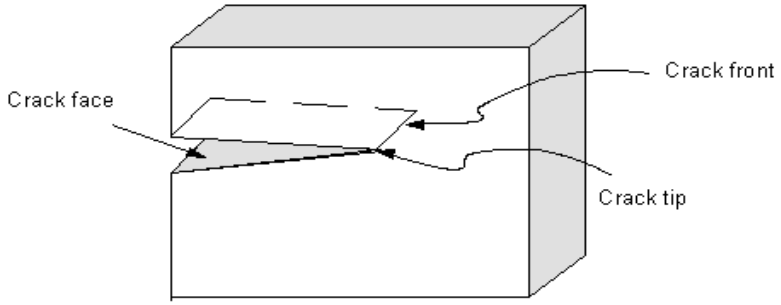

Figure 4.1 crack tips and crack front of a 3-D crack model

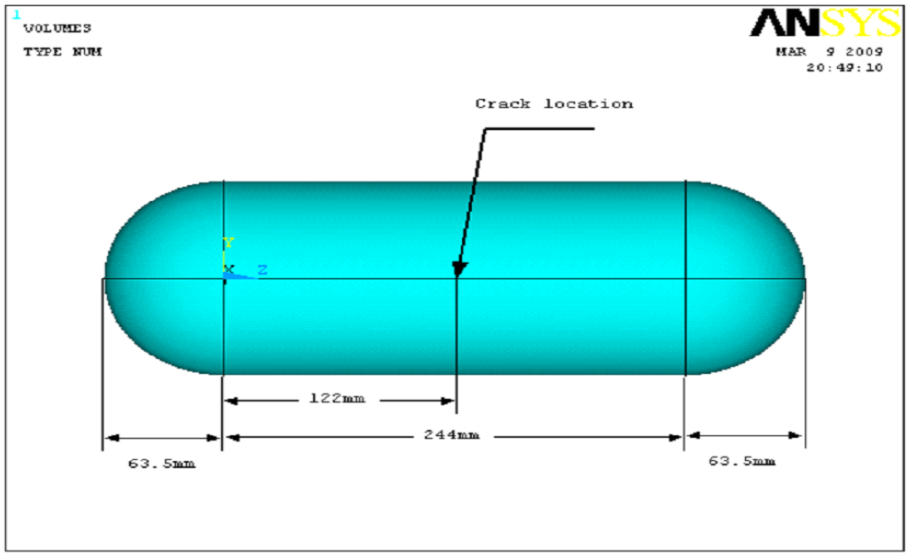

Figure 4.2 Crack location of a three dimensional pressure vessel model

4.3 Finite Element Discretization of a Model

In the finite element method, the structure of interest is sub-divided in to discrete shapes called elements. The most common element types include one dimensional beam, two dimensional elements, or three dimensional bricks or tetrahedrons.

The big problem in fracture analysis is the modeling of crack tip. In order to analyze the fracture parameter the crack tip elements should be quarter point (1/4) singular elements. In 3-D fracture elements using ANSYS, the recommended element type is SOLID95, the 20-node brick element. This may be replaced by SOLID90 for thermal analysis and SOLID226 for coupled case. As shown in figure 4.3, the first rows of elements around the crack front are singular elements. The element is wedge-shaped, with the KLPO face collapsed into the line KO.

Generating a 3-D fracture model is considerably more difficult than a 2-D model. The command is not available, and it is necessary to make sure that the crack front is along edge KO (in section 3.2) of the elements. Either we should create the singular elements manually, or we use another method. In this thesis, mesh200 elements are used to obtain 3-D singular elements mesh.

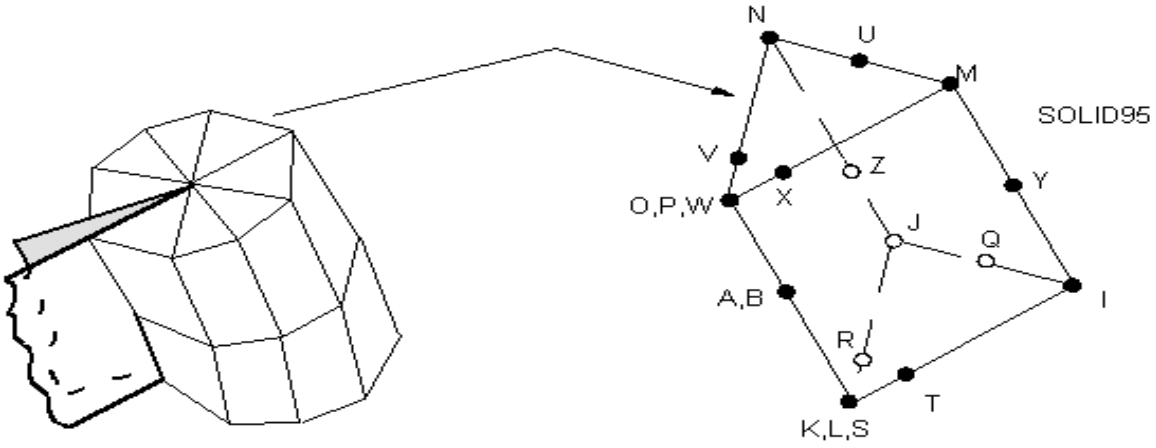

Figure 4.3 Singular elements

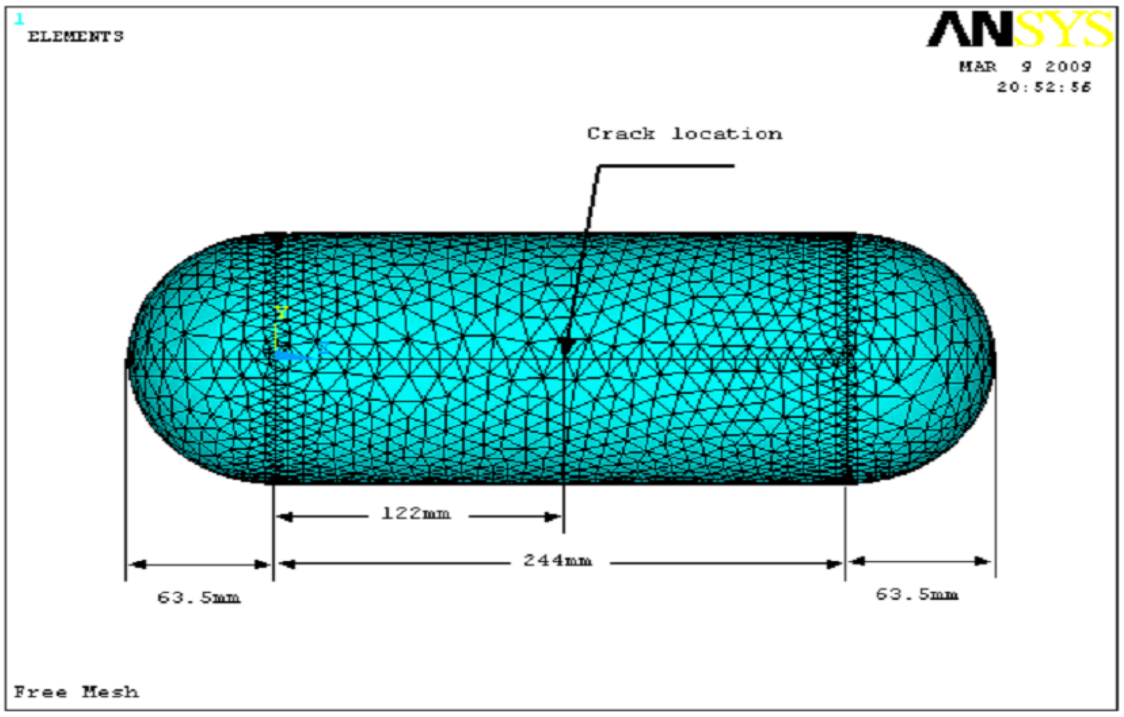

Figure 4.4 full free meshed model

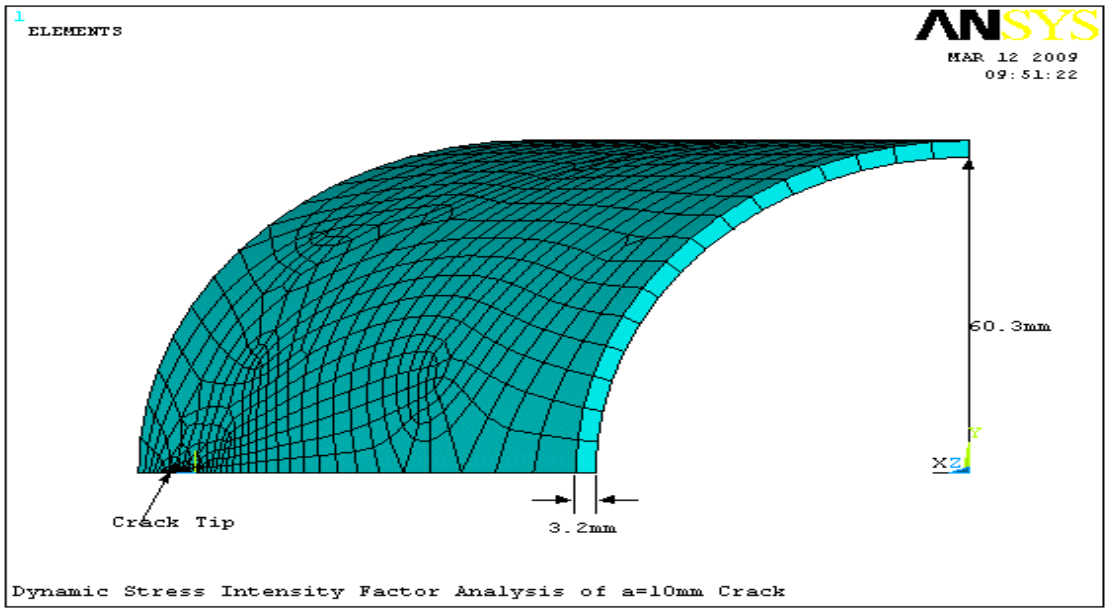

Figure 4.5a pictorial view of the meshed model for longitudinal

The full and one eight of the model is sown by figure 4.4, 4.5 and 4.6 respectively. Each of the model shows the dimensions of the object and crack locations.

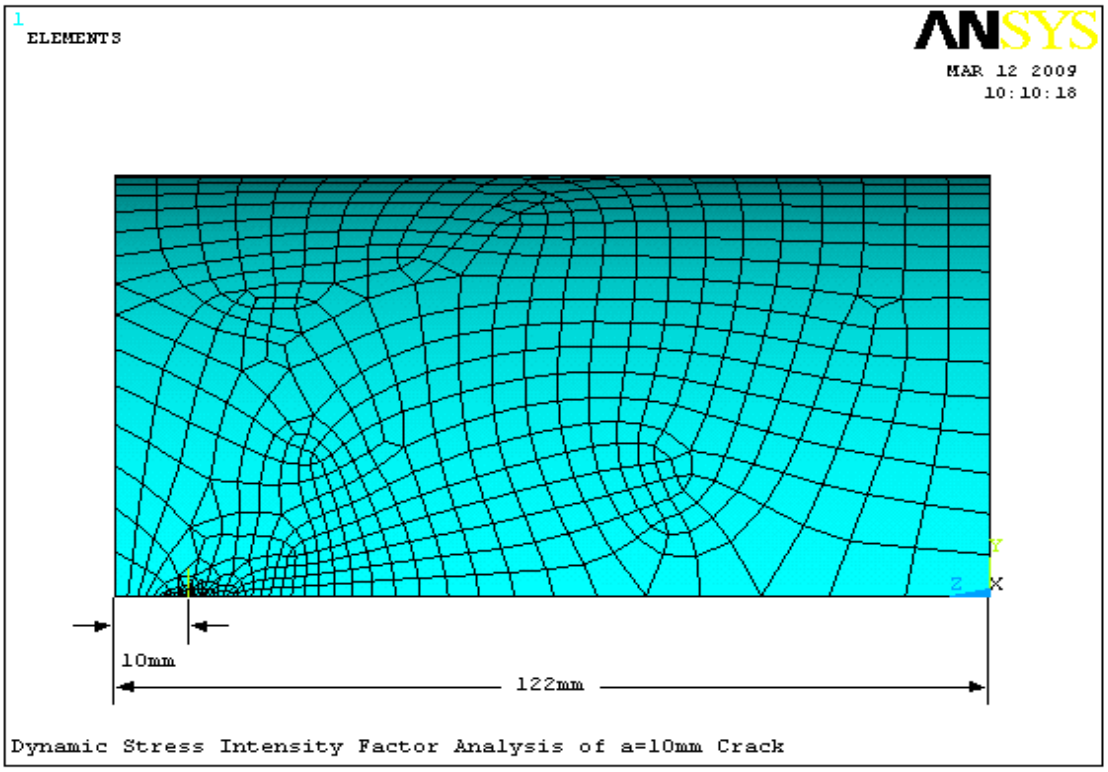

Figure 4.5b longitudinal dimensions of the symmetrical meshed model and half crack length for 20mm crack**.**

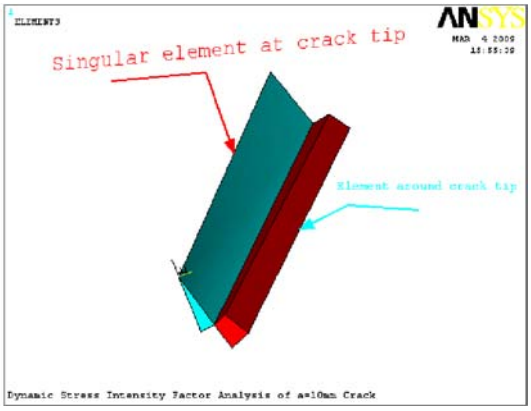

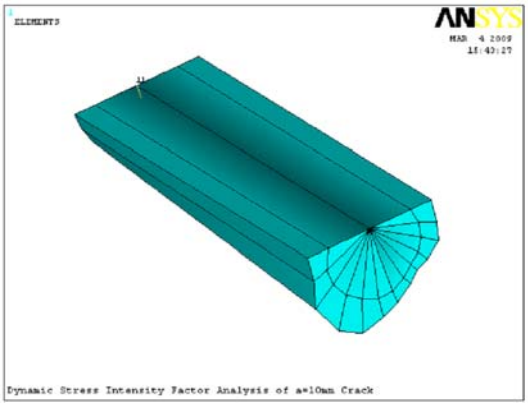

Figure 4.6 singular elements at crack tip

Modeling of circumferential through crack, the crack ordination of figure5, is taken on the surface of x-y plane. All the dimensions are the same to that of longitudinal crack.

For thermal shock analysis, infinite strip is taken from 2.061 inside diameter and 0.229m thickness. The dimensions infinite strip is 0.229m width by 0 .485m length. Since the loading system is symmetrical, 0.229m by 0.229 m is from figure 4.7 to analyze half of the infinite strip.

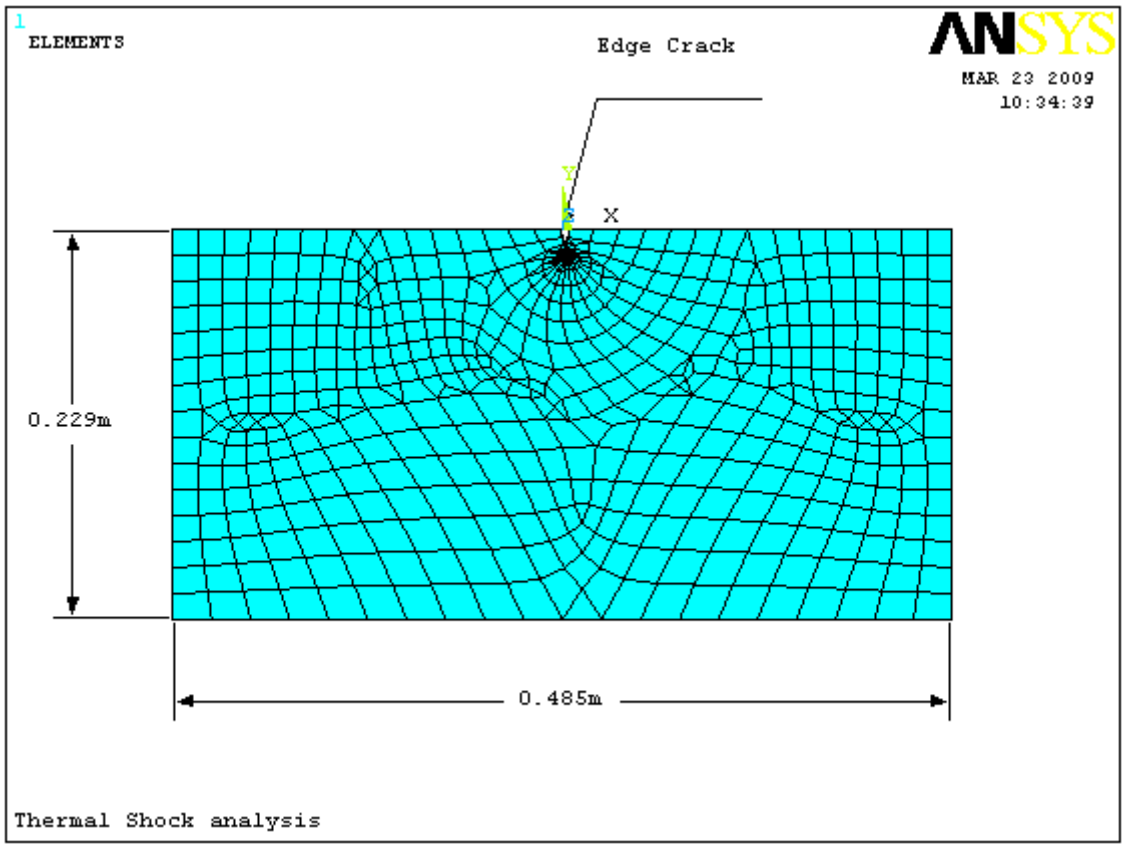

Figure 4.7 Infinite strip for thermal shock analysis

4.4 Numerical Analysis

4.4.1 Boundary and Loading Conditions

As already mentioned in section 4.2, of different kinds of crack length and orientations are analyzed.

a) Three types of analysis, of 20, 24 and 28 mm through crack using 1/8 symmetrical model, are done. Static analysis at normal pressure (2.2Mpa), static analysis at maximum pressure (5.1Mpa) and dynamic analysis at suddenly applied loading are analyzed. The symmetrical model has 60.3 mm inside diameter and 3.2 mm thickness as shown in figure 4.5. Symmetrical boundary conditions are applied on the area y=0 (x-z plane) and on the area z = 122mm from the origin (x-y plane) as shown in figure 4.5. The uniform hoop stress is applied on area x=0 (z-y plane) and uniform pressure on the inside area of the vessel.

b) For the same geometrical dimension in (a), having length of 20mm circumferential crack, static and dynamic analysis are done. Since this has circumferential through crack, symmetrical boundary conditions are applied on the area z=122mm(x-y plane) and y=0(x-z) plane, and the uniform axial stress is applied on area z=0(x-y) plane. The uniform pressure is applied on the inside area.

c) The same geometrical dimensions and crack orientation in (a) but a full crack having 28 mm with 1/4 vessel model is done.

d) Coupled thermal shock analysis for Longitudinal and circumferential edge crack for inside radius of 2.061m and thickness 0.229m is done. Here the thermal shock (uniform temperature 303K and suddenly cooled to 273K) is created on the inside surface of the model. It is assumed that the outside surface is insulated. But the infinite strip is taken for this analysis. A 0 .229 by 0.229m model is done for 0.01145m edge crack. The analysis is done by applying symmetry boundary condition.

4.4.2 Dynamic Analysis

The accuracy of the transient dynamic solution depends on the integration time step: the smaller the time step, the higher the accuracy. A time step that is too large will introduce

error that affects the response of the higher modes (and hence the overall response). A time step that is too small wastes computer resources. The time step should be small enough to resolve the motion (response) of the structure. Since the dynamic response of a structure can be thought of as a combination of modes, the time step should be able to resolve the highest mode that contributes to the response. For the Newmark time integration scheme, it has been found that using approximately twenty points per cycle of the highest frequency of interest results in a reasonably accurate solution. That is, if *f* is the frequency (in cycles/time), the integration time step (ITS) is given by ITS = 1/(20*f*). However, time step can be determined manually, frequency analysis is required to compare the appropriate time integration step found analytically using numerical analysis.

4.4.3 Reading Fracture Parameters from ANSYS

Once the analysis is completed, we can use POST1, the general postprocessor, to calculate fracture parameters. As mentioned earlier, typical fracture parameters of interest is a stress intensity factor. For static stress results, it is possible to use POST1 and POST2 for time history stress and displacement reading.

Material properties of aluminum alloy (1 and 2) and steel (3) used for static, dynamic (uncoupled) and dynamic (coupled) analysis

S.No.	E(modulus of elasticity) Mpa	Poisson ratio	Density(kg/m^3)	Longitudinal speed(m/s)	Specific heat(J/kgK)	Fracture toughness (Mpam$^{1/2}$)	Thermal conductivity(W/mK)	Type of analysis
1	7e11	0.3	2700		-	36	-	static
2	7e11	0.3	2700		-	36	-	Dynamic(uncoupled)
3	2.1e11	0.3	7800	5100	465	50	54	Dynamic(coupled)

Table 4.1 Material properties

Chapter Five

5 Results and Discussion

5.1 Static Analysis at Normal Operating and Maximum Pressure

5.1.1 Von Misses Stress Distribution for Longitudinal Cracks Tip

This section discusses the quasi-static fracture analysis of pressure vessel to show the background of the fracture behavior and for normalization of dynamic fracture analysis. Figure 5.1 to figure 5.3 show how the von Misses stress distribution around the crack tip at normal operating and maximum pressure. The maximum pressure is assumed to be created by suddenly applied loading which will be referred in dynamic analysis of section 5.3. Figure 5.1a and 5.1b show the stress distribution around crack tip for a=10mm crack at normal and maximum pressure.

Crack length and parameters	At normal pressure	At maximum pressure
For a=10mm crack		
Stress Intensity Factor Manual ($pa(m)^{1/2}$)	1.12E+07	2.43E+07
Stress Intensity Factor ANSYS($pa(m)^{1/2}$	1.13E+07	2.59E+07
Deviation	8.66E-03	5.93E-02
Percentage (%)	0.866%	5.93%
For a=12mm crack		
Stress Intensity Factor Manual($pa(m)^{1/2}$)	1.26E+07	2.74E+07
Stress Intensity Factor ANSYS($pa(m)^{1/2}$)	1.35E+07	2.94E+07
Deviation	6.62E-02	6.62E-02
Percentage (%)	6.62%	6.62%
For a=14mm crack		
Stress Intensity Factor Manual($pa(m)^{1/2}$)	1.47E+07	2.95E+07
Stress Intensity Factor ANSYS($pa(m)^{1/2}$)	1.57E+07	3.15E+07
Deviation	6.29E-02	6.29E-02
Percentage (%)	6.29%	6.29%

Table 5.1 Analytical and numerical stress intensity factor results

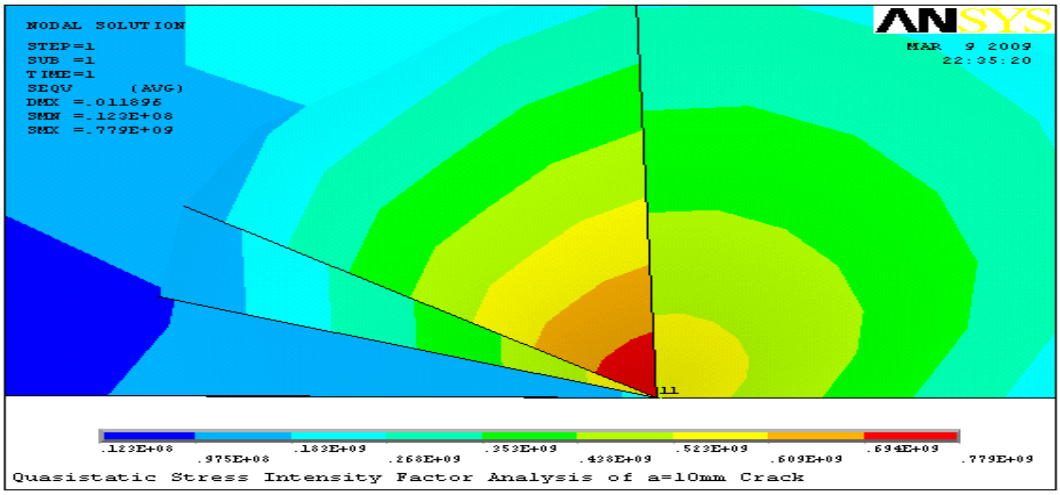

a) At normal pressure

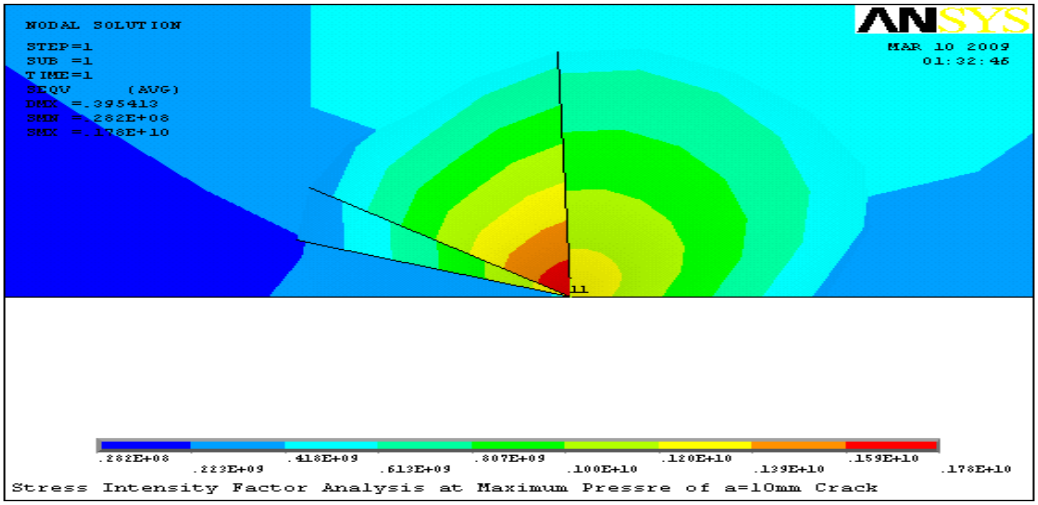

b) At maximum pressure

Figure 5.1 Von Misses results at normal and maximum pressure for a=10mm

In each case, from figures 5.1 – 5.3 the magnitude of the stress distribution of (b) is much greater than that of (a). This is due to the magnitude of the pressure applied. We can refer that as the pressure increases with the same crack length, the magnitude of the stress as well as stress intensity factor increases.

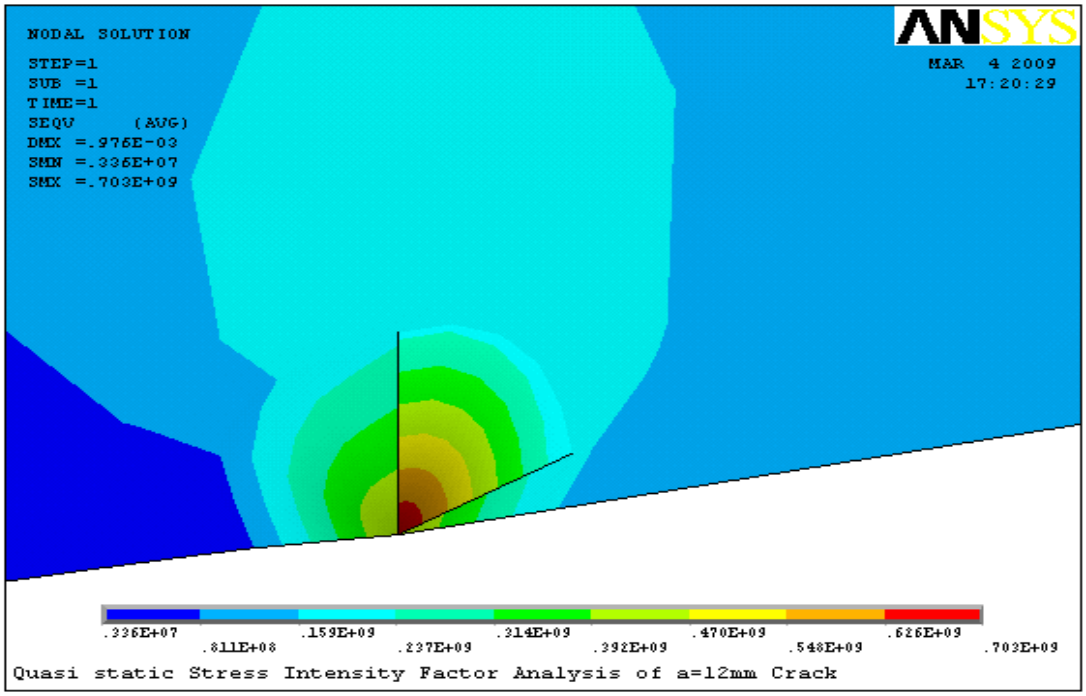

a) At normal pressure

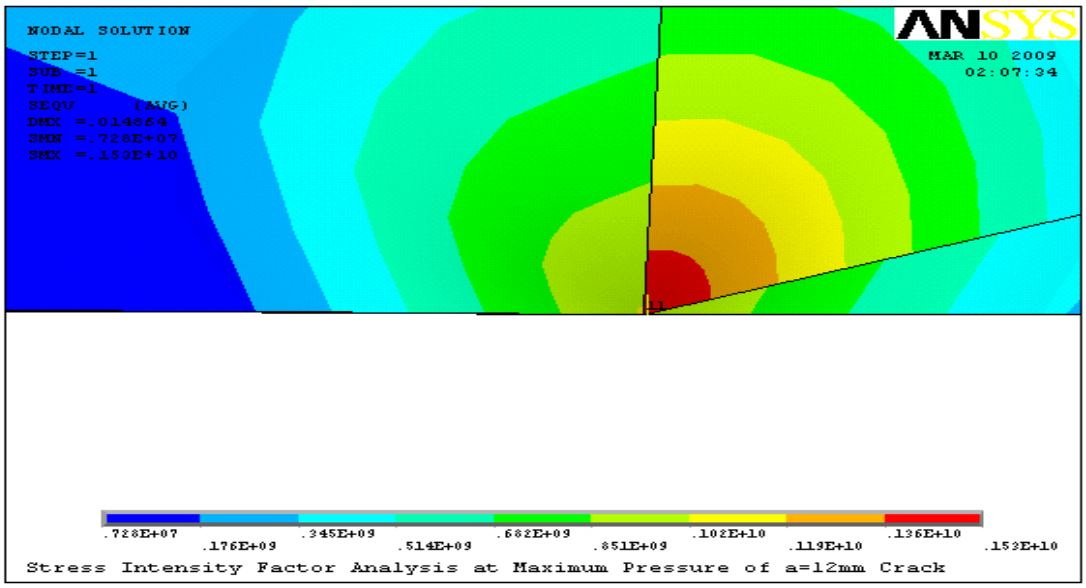

b) At maximum pressure

Figure 5.2 Von Misses results at normal and maximum pressure for a=12mm

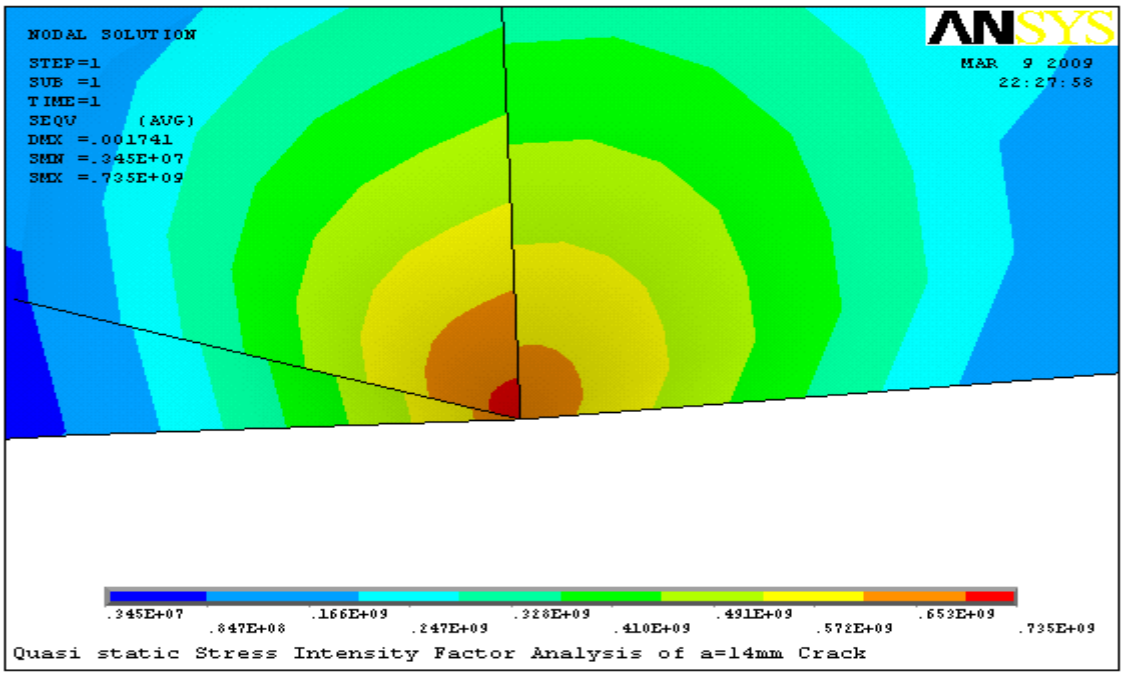

a) At normal pressure

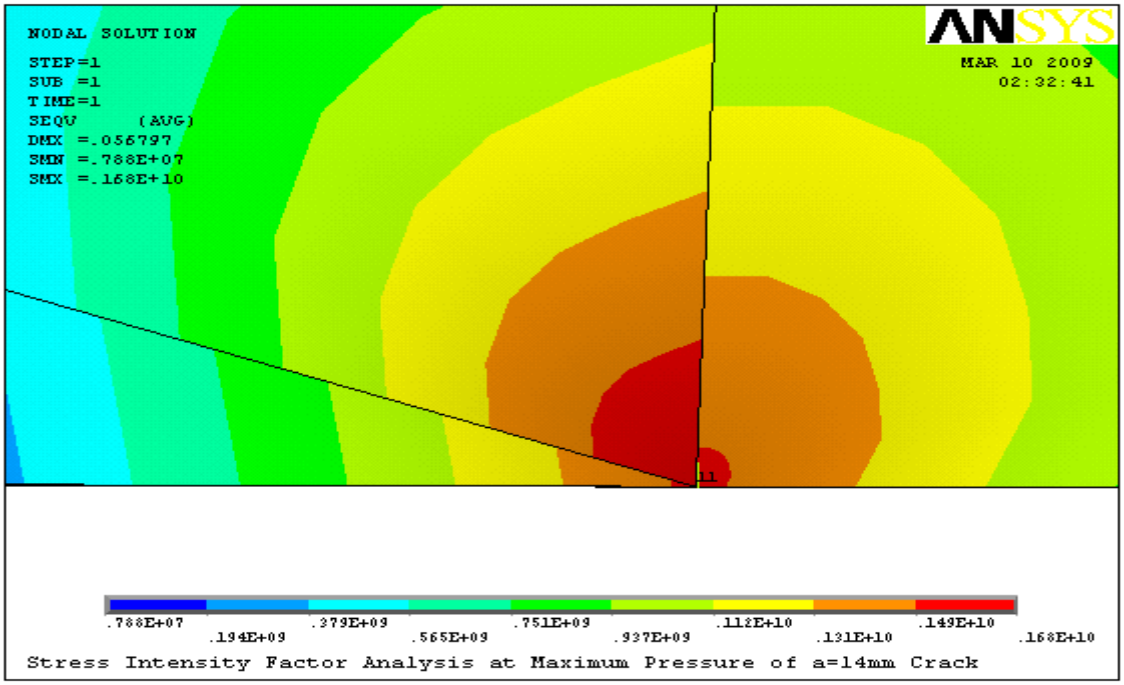

b) At maximum pressure

Figure 5.3 Von Misses results at normal and maximum pressure for a=14mm

5.1.2 Stress Singularity at the Crack Tip for Longitudinal Crack

Figures 5.4 to figure 5.6 tell us how the von Misses stress decreases as it moves outward from the crack tip with any radius r or/ path distance from the crack tip. At crack tip maximum stress is obtained as expected, and decreases to zero as it goes far from the crack tip. This completely agrees with the previous literature and the fracture theory as a whole.

Quasi-static stress intensity factor is calculated using POST1 (ANSYS results' command) from ANSYS. The result obtained from ANSYS is compared with analytical value, the results completely agree with its analytical value as shown in table 5.1 with small-expected percentage error. In section, 5.1.1 table 5.1 also describes how the analytical value at normal pressure and at maximum pressure agrees with the numerical value.

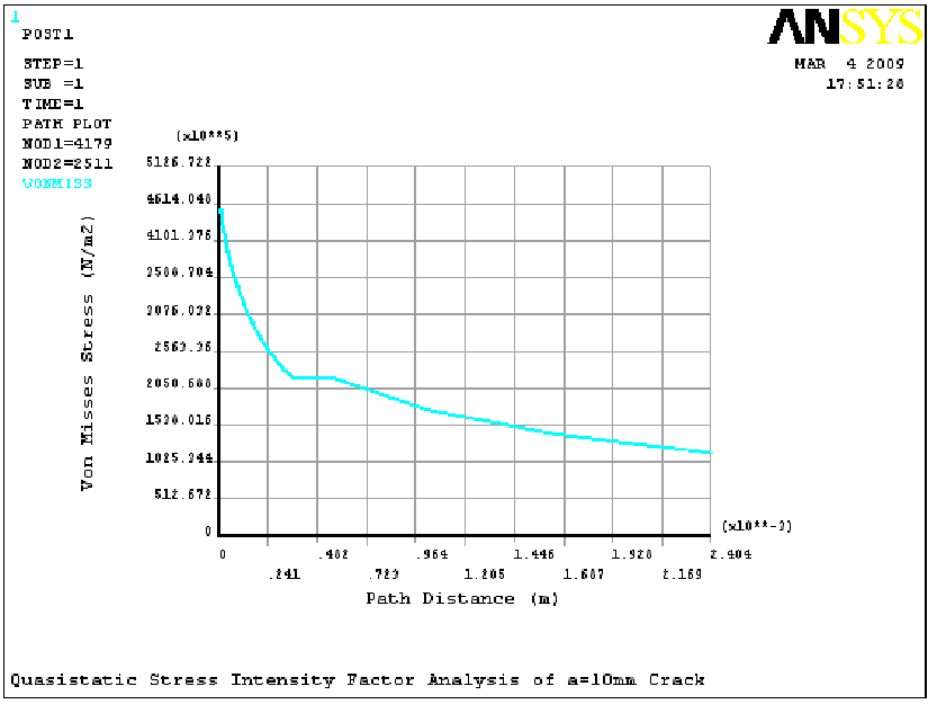

Figure 5.4 Von Misses results at distance from crack tip for a=10mm

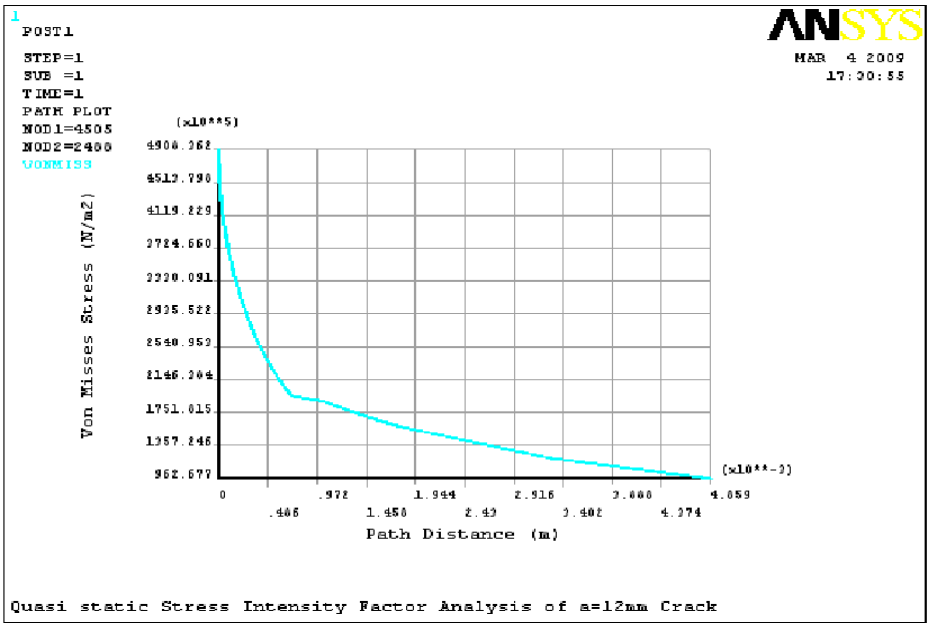

Figure 5.5 Von Misses results at distance from crack tip for a=12mm

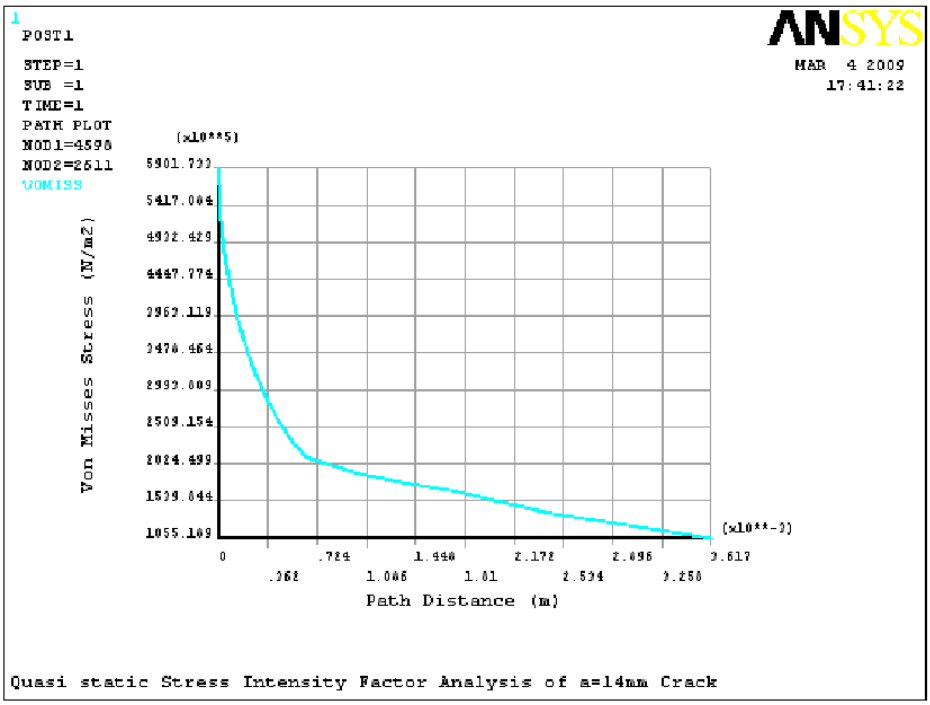

Figure 5.6 Von Misses results at distance from crack tip for a=14mm

5.1.3 Von Misses Stress Distribution for Circumferential Cracks around Tip

The aim of the circumferential through crack analysis is to show and compare the stress distribution and stress intensity factor with longitudinal crack having the same crack length and vessel geometry. The maximum value of the von Misses stress for circumferential crack orientation is less than from the value of longitudinal crack stress values at the crack tip. This shows that when the crack orientation is changed from longitudinal to circumferential, the value of the stress decreases.

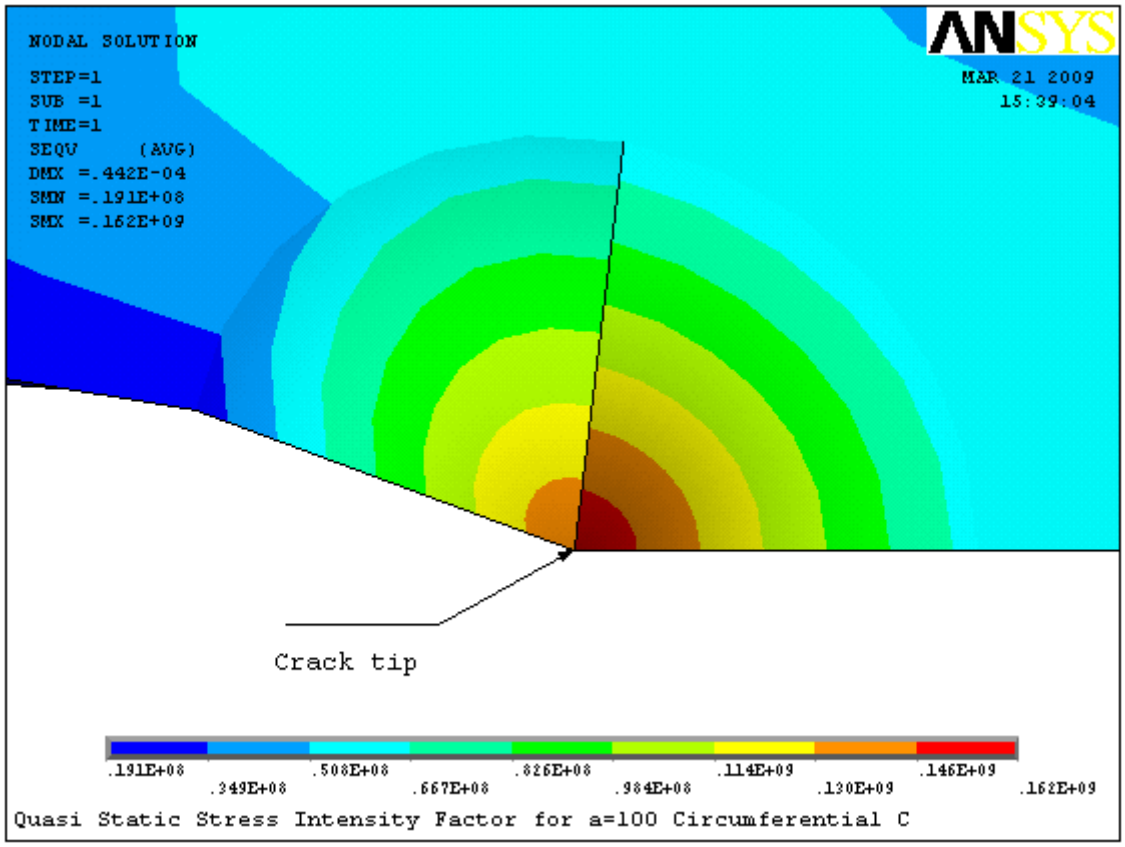

Figure 5.7 Von Misses stress distribution at the crack tip

The static stress intensity factor from the ANSYS is obtained 4.86E+06. As previously done, the ANSYS value is compared with the analytical value. The calculated value is found 4.50E+06. The percentage error is 7.3%. This percentage error is found because of the rough mesh to minimize the memory size of the computer. From longitudinal and

circumferential fracture analysis, the value of longitudinal stress intensity factor is almost double of the circumferential crack.

5.2 Stress Wave Demonstration for 28mm Through Crack 1/4 model

The result shows how the stress wave travels, strikes the traction free of the crack face, and reflects back to the body. This reflected wave travels to the crack tip and create high stress concentration on the crack front. The stress concentration is due to the reflection and travel waves collision at the tip. In addition, they create high magnitude of stress. Figure 5.7 shows the stress wave on the solid body at one microsecond.

The longitudinal stress wave starts traveling here. The magnitude of the stress at red region is very high. Similarly, figure 5.8 shows the stress wave location after 6 microseconds from the suddenly applied load.

Before the longitudinal stress wave reaches at the crack face, the shear wave arrives and creates stress interaction at the crack tip. In similar manner, figure 10 and figure 11 show the wave phenomenon at 11 and 26 microseconds, respectively. The figures show that starting from 11microseconds and then onwards the stress creates tensile stress on the crack faces. This process continuous until the stress wave reaches maximum at the tip of the crack. Figure 5.12 shows how the shape of the von Misses stresses at the crack tip when the whole stress wave reaches. It also shows how the distance between cracks faces apart each other by this tension process. At last, figure 5.15 shows what the crack faces looks like and the crack front due to this stress waves.
As already mentioned before, this analysis is done to show how the dynamic stress wave travels and creates stress intensity at the crack tip. This analysis verifies the stress wave interaction at the crack faces and the way in which the dynamic stress intensity factor is created.

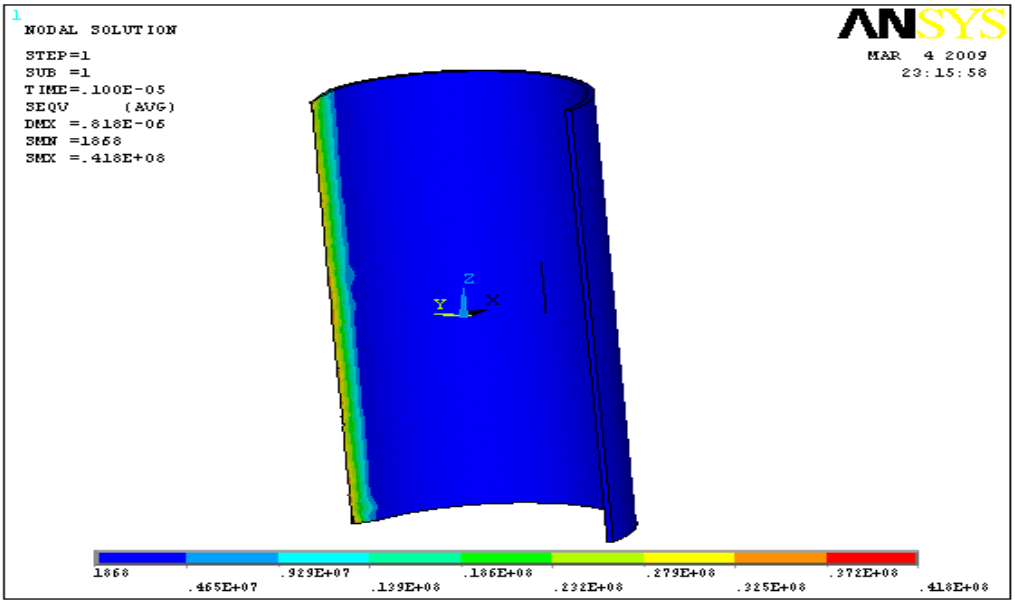

Figure 5.8 Von Misses stress at 1µs

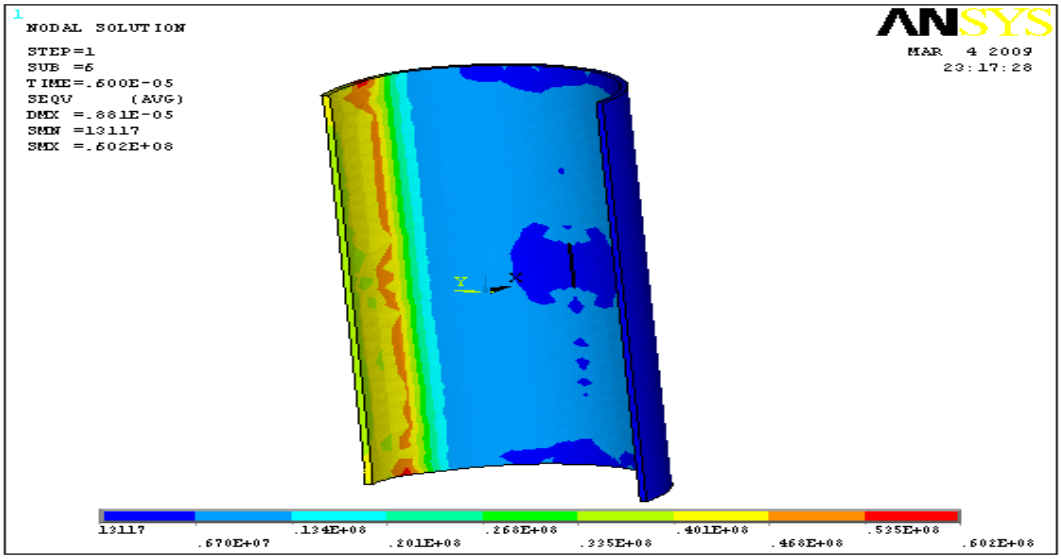

Figure 5.9 Von Misses stress at 6µs

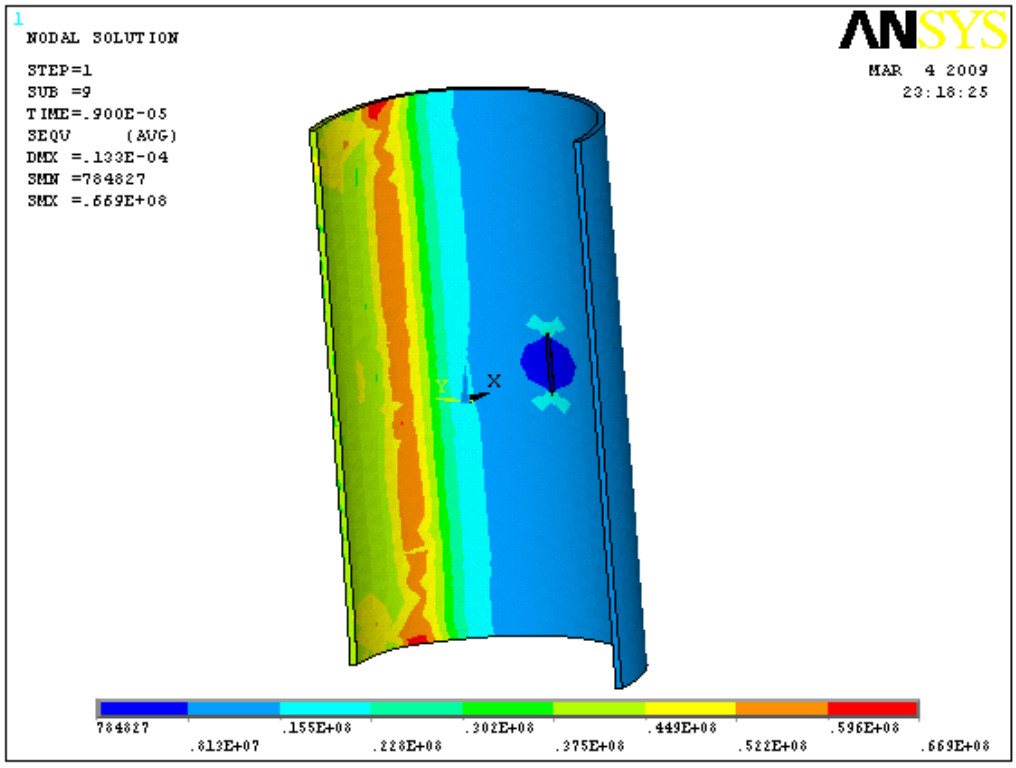

Figure5.10 Von Misses stress at 9μs

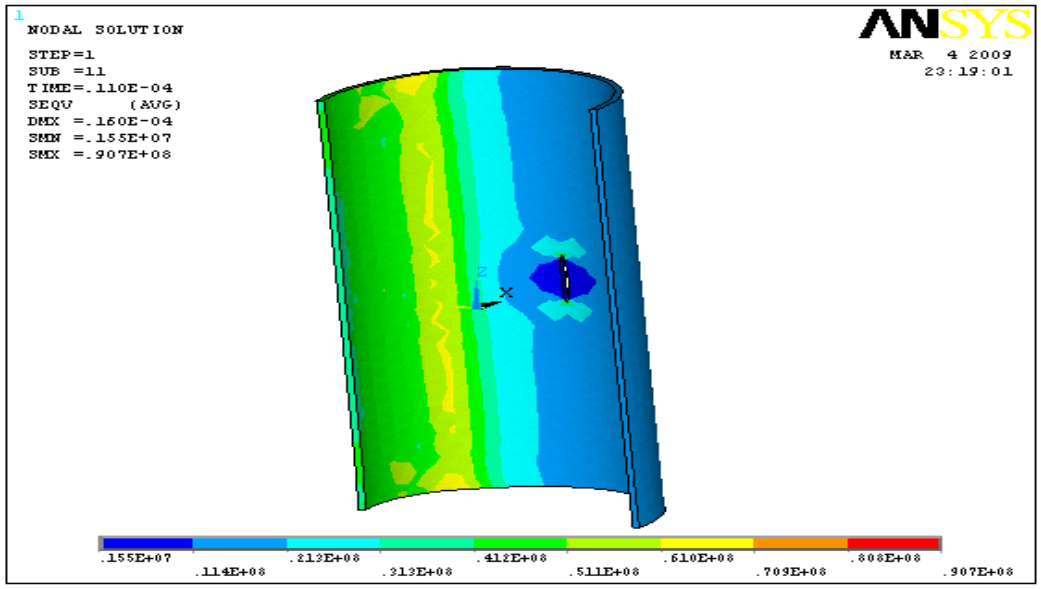

Figure 5.11 Von Misses stress at 11μs

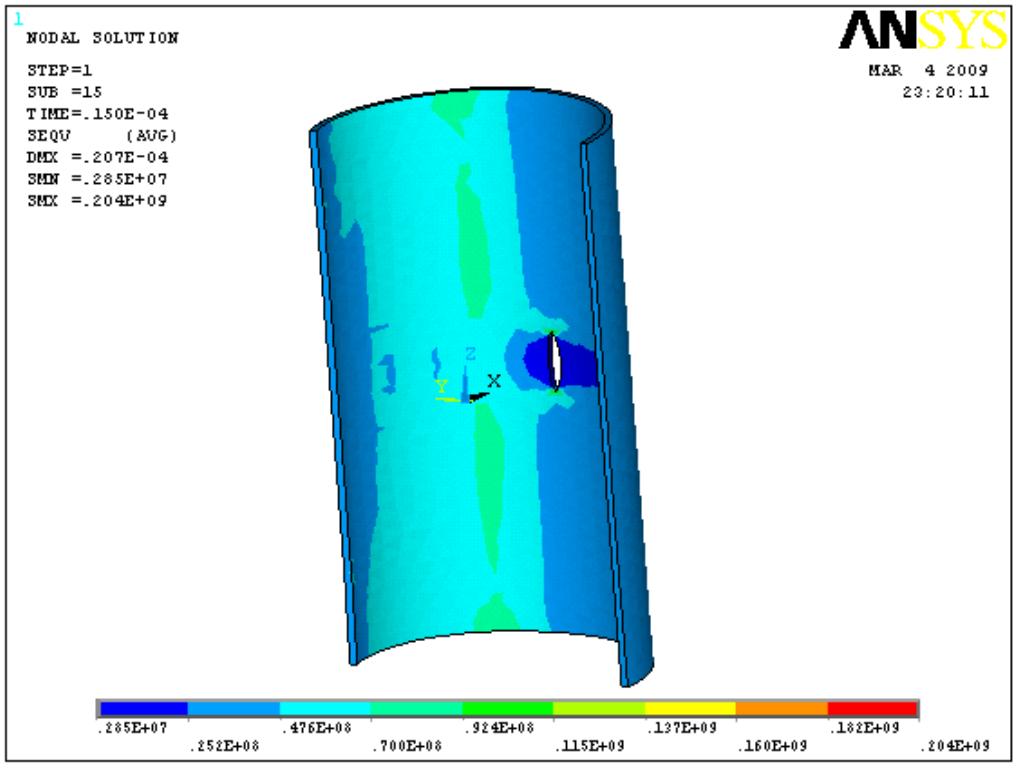

Figure 5.12 Von Misses stress at 15μs

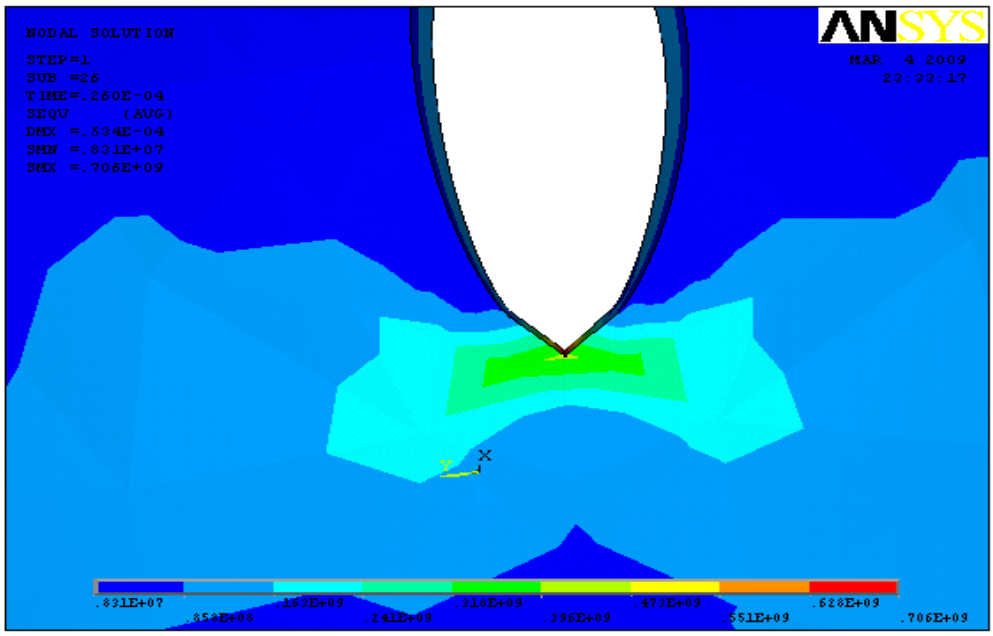

Figure 5.13Von Misses stress at 26μs

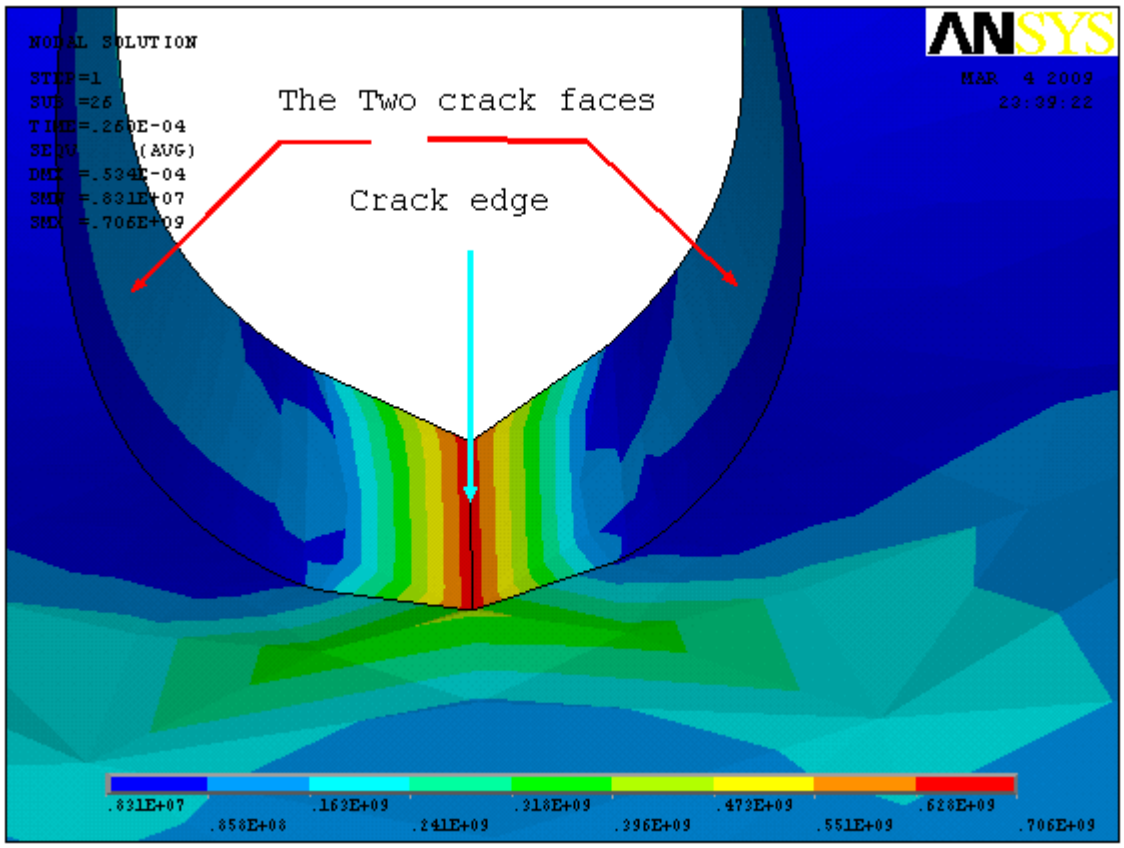

Figure 5.14 Von Misses stress at 26μs

5.3 Stress Distribution and Dynamic Stress Intensity Factor for different crack lengths

5.3.1 Stress, Displacement and Strain for Longitudinal Crack

As described in the literature and background of the thesis, the parameter used to obtain here is the dynamic stress intensity factor. The previous sections describe stress wave and static analysis. Section 5.1 and 5.2 are used for comparison and helps how dynamic stress intensity factor can be created. This section discusses the results of von Misses stress, displacement and strain time history. More broadly, the fracture parameter, dynamic stress intensity factor, is discussed.

From figure 5.14 to figure 5.16, the dynamic von Misses stress verses time is shown for a=10, 12 and 14mm crack lengths. For a=10mm the von Misses is maximum at 28 microsecond. This shows that the maximum dynamic stress intensity factor occurs on the crack tip at this time. Similar conditions are obtained for a=12 and 14mm crack lengths.

The dynamic Von Misses at the crack tip decreases from the first load cycle as the time increases. This agrees with theoretical background that maximum stress is obtained in the quarter of the period after suddenly applied loading occurs. Figure 5.17 validate the theoretical background. Figure 5.18 shows the displacement at the crack tip and at random point away from the tip verses time graph. It shows the maximum displacement at the crack tip and decrease as it goes far from the crack tip. In similar manner von Misses strain showed in figure 19 how the strain looks like with time.

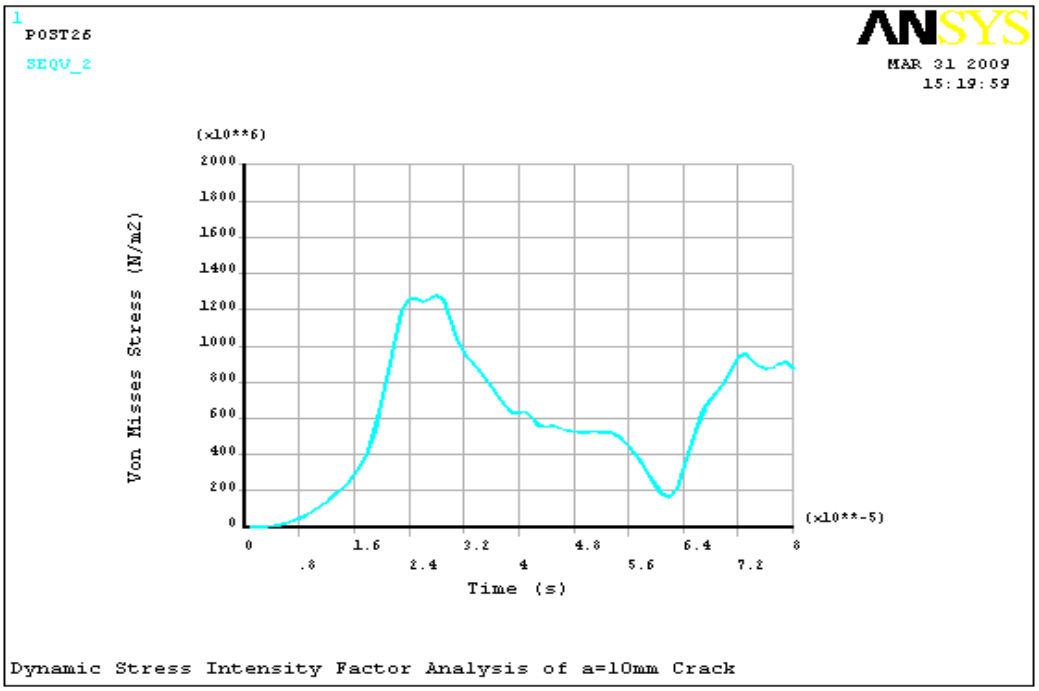

Figure 5.15 Dynamic von Misses stress time history graph for a=10mm

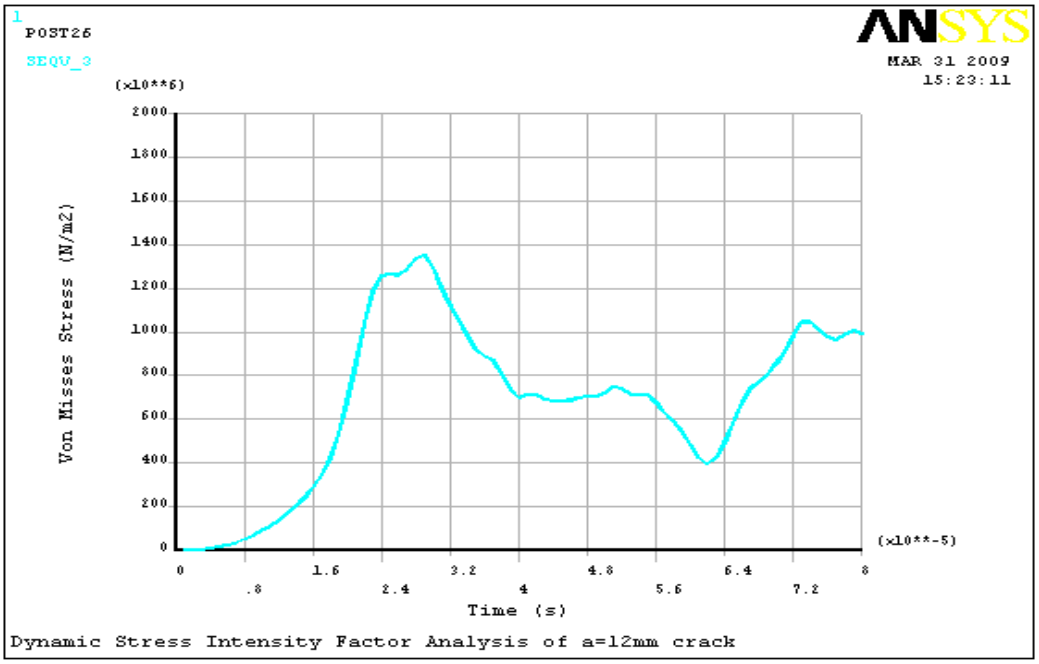

Figure 5.16 Dynamic von Misses stress time history graph for a=12mm

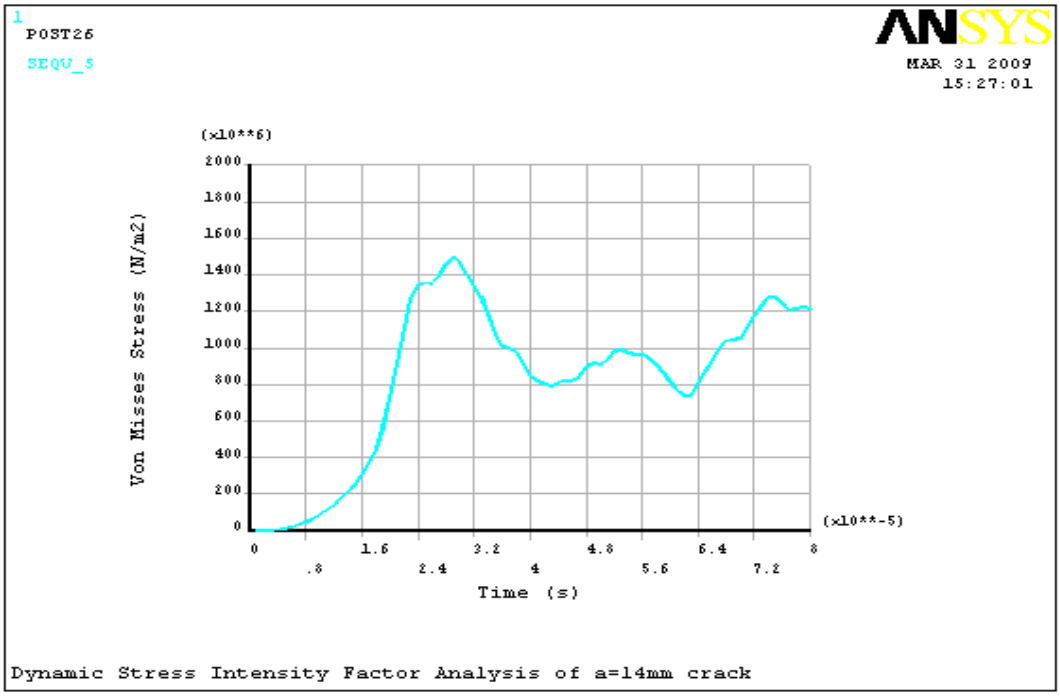

Figure 5.17 Dynamic von Misses stress time history graph for a=14mm

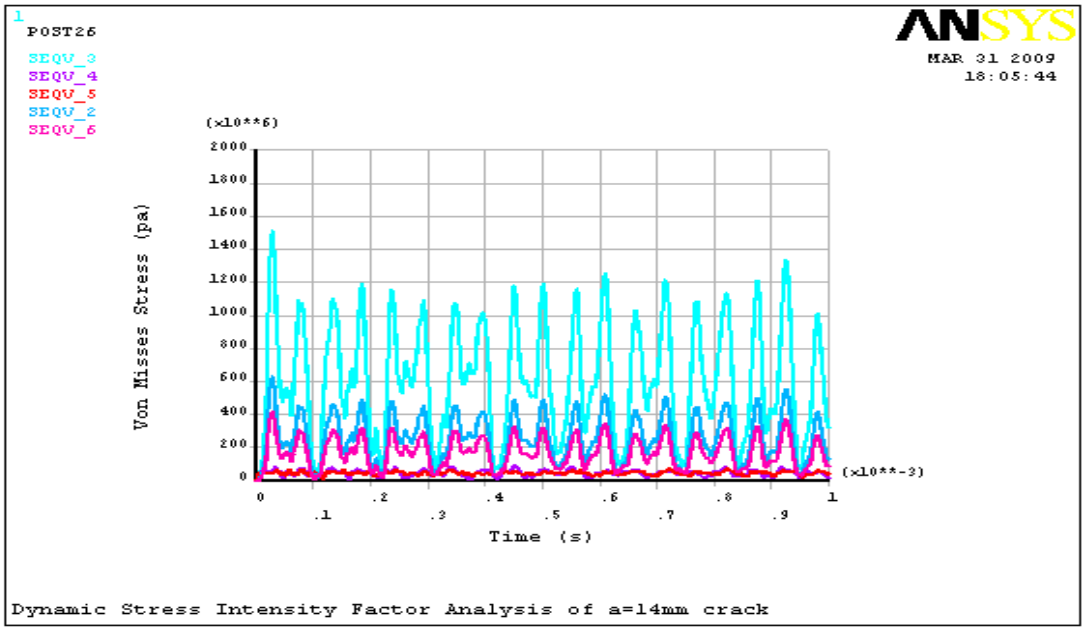

Figure 5.18 Dynamic von Misses stress time history graph at different points for 1000μs

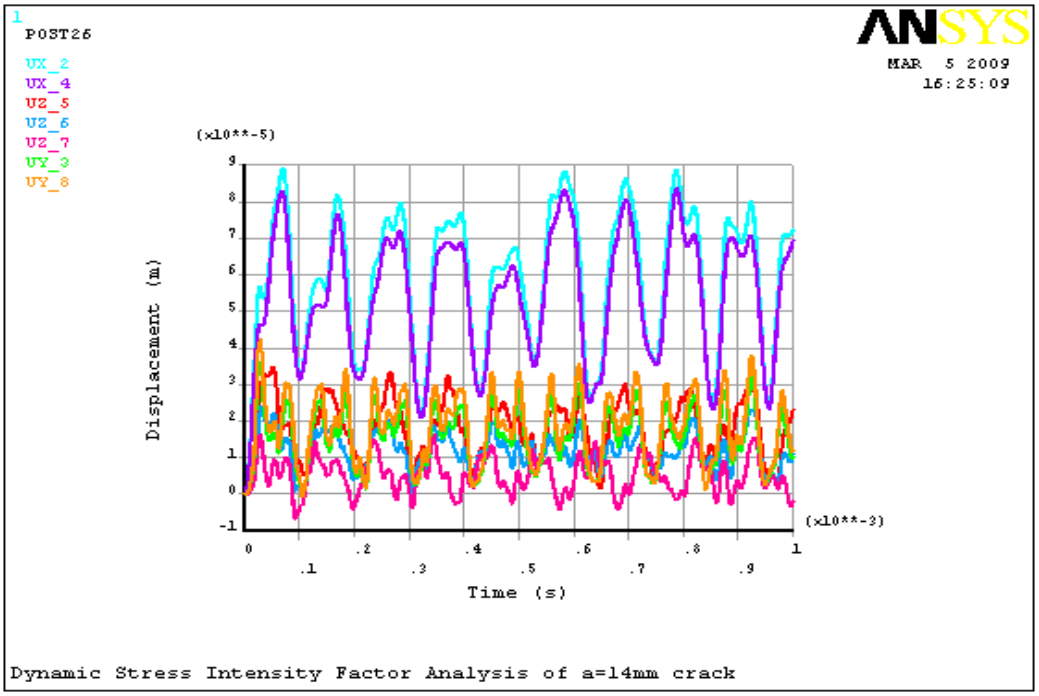

Figure 5.19 Displacement time history graph for 1000μs

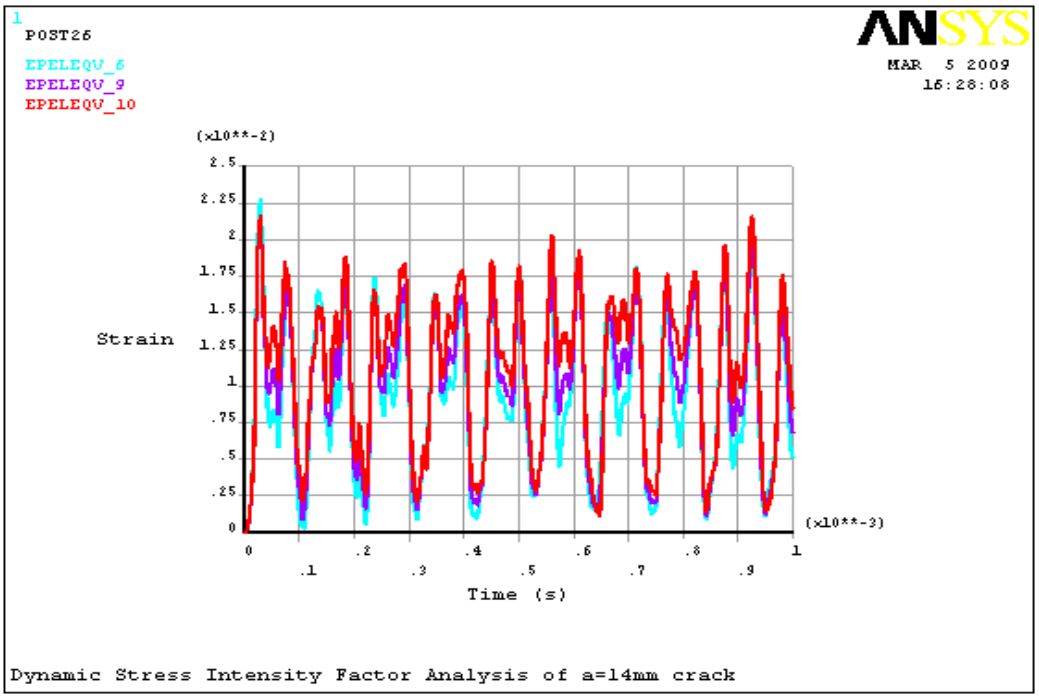

Figure 5.20 Dynamic von Misses strain time history graph for 1000μs

5.3.2 Dynamic Stress Intensity Factor for Longitudinal Crack

The dynamic stress intensity factor increases in similar manner with that of the dynamic Von Misses stress. Since dynamic stress intensity factor is main objective of this thesis, more diagrammatical elaboration is displayed. As mentioned earlier, the actual value is obtained from POST1 ANSYS. For all the three cases, the graph is obtained in their actual and its normalized value. The normalization is done using quasi-static stress intensity factor. Figures 5.20 and 5.21 are the results of dynamic stress intensity factor versus time graph in actual value and normalized form for a=10mm crack.

The dynamic stress intensity factor increases until the stress wave reaches at the crack surface and decreases after it passes the crack. This phenomenon is due to the tensile stress, and makes the crack faces move apart. The movement of the crack faces in the outward directions is due to the reflection and diffraction of the stress wave. The interaction of reflected and dilatational stress wave increases the stress intensity at the crack tip. After the stress wave passes the crack, the gap between cracks faces decreases due to compression. This causes the decline of the dynamic stress intensity factor. Similar phenomenon occurs for a=12 and 14mm cracks.

This analysis also shows how the dynamic stress intensity factor increases with crack length increment. As sown in figure 5.26 the dynamic stress intensity factor increases as the crack length increases. Tables 5.3 to 5.5 show the dynamic stress intensity factor with time for half of the loading cycle. Figures 26 and 27 are done by combining the values of tables 5.3 – 5.5. Figure 5.26 shows how the fracture parameter increases with the crack length.

Data of dynamic stress intensity factor for a=12mm crack

S.No.	DSIF	TIME	S.No.	DSIF	TIME
1	38244	1.00E-06	27	2.40E+07	2.70E-05
2	60045	2.00E-06	28	2.43E+07	2.80E-05
3	11310	3.00E-06	29	2.37E+07	2.90E-05
4	57048	4.00E-06	30	2.15E+07	3.00E-05
5	1.85E+05	5.00E-06	31	1.87E+07	3.10E-05
6	3.68E+05	6.00E-06	32	1.65E+07	3.20E-05
7	5.99E+05	7.00E-06	33	1.54E+07	3.30E-05
8	9.04E+05	8.00E-06	34	1.41E+07	3.40E-05
9	1.27E+06	9.00E-06	35	1.24E+07	3.50E-05
10	1.71E+06	1.00E-05	36	1.08E+07	3.60E-05
11	2.22E+06	1.10E-05	37	9.70E+06	3.70E-05
12	2.78E+06	1.20E-05	38	8.48E+06	3.80E-05
13	3.40E+06	1.30E-05	39	7.39E+06	3.90E-05
14	4.07E+06	1.40E-05	40	7.09E+06	4.00E-05
15	4.80E+06	1.50E-05	41	7.09E+06	4.10E-05
16	5.69E+06	1.60E-05	42	6.37E+06	4.20E-05
17	6.78E+06	1.70E-05	43	5.48E+06	4.30E-05
18	8.28E+06	1.80E-05	44	5.40E+06	4.40E-05
19	1.04E+07	1.90E-05	45	5.57E+06	4.50E-05
20	1.33E+07	2.00E-05	46	5.23E+06	4.60E-05
21	1.68E+07	2.10E-05	47	4.98E+06	4.70E-05
22	2.03E+07	2.20E-05	48	5.16E+06	4.80E-05
23	2.30E+07	2.30E-05	49	5.27E+06	4.90E-05
24	2.43E+07	2.40E-05	50	5.26E+06	5.00E-05
25	2.43E+07	2.50E-05	51	5.41E+06	5.10E-05
26	2.40E+07	2.60E-05	52	5.67E+06	5.20E-05

Table 5.2 Dynamic stress intensity factor a=10mm

Where DSIF = Dynamic Stress Intensity Factor

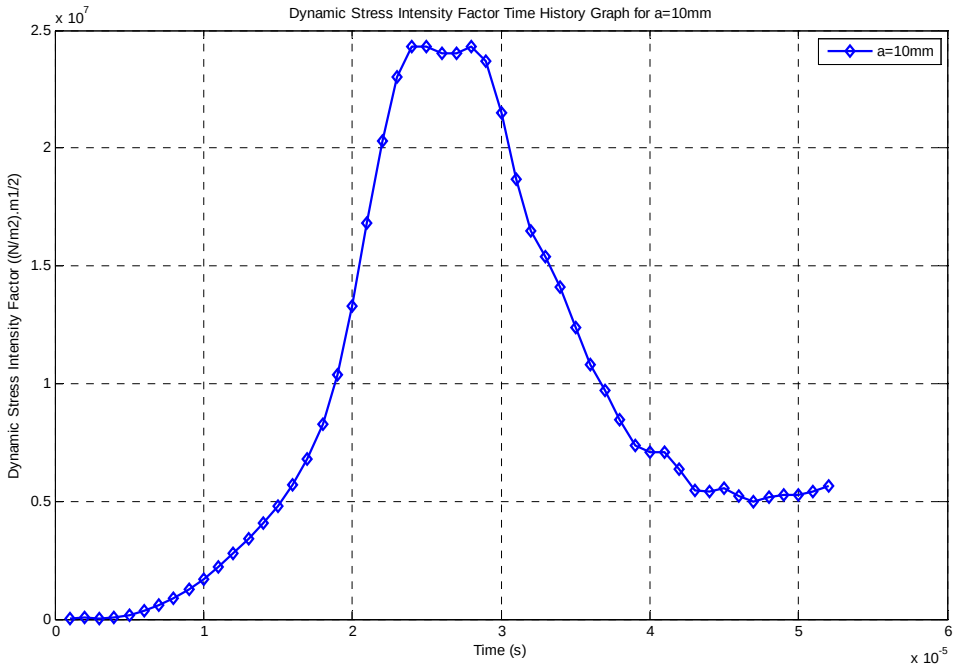

Figure 5.21 Dynamic stress intensity factor time history graph

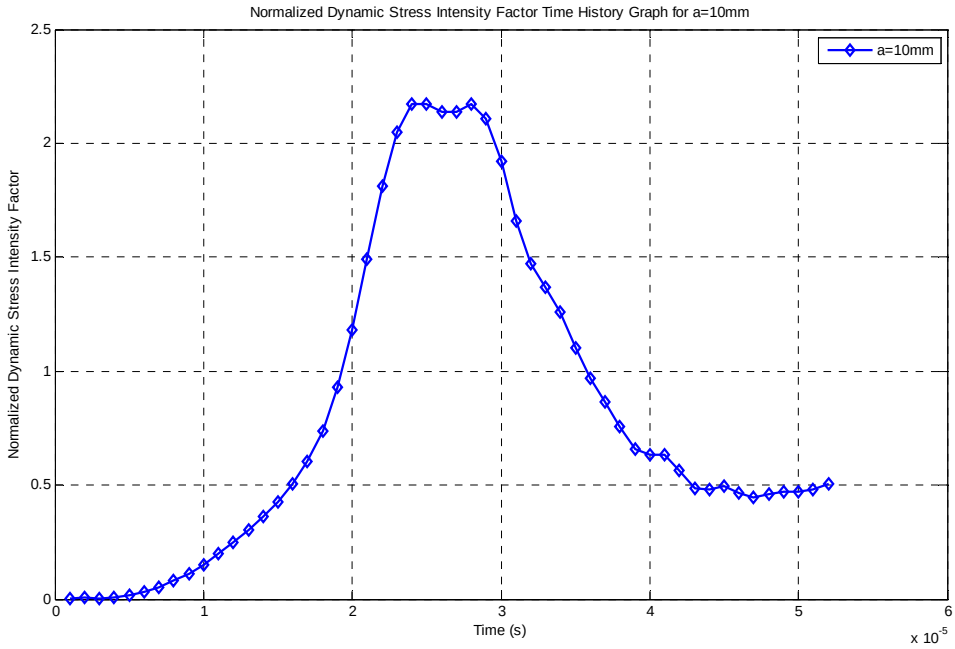

Figure 5.22 Dynamic stress intensity factor time history graph

Data of dynamic stress intensity factor for a=12mm crack

S.No.	DSIF	TIME	S.No.	DSIF	TIME
1	38682.0	1.00E-06	27	26140000.0	2.70E-05
2	57948.0	2.00E-06	28	27155000.0	2.80E-05
3	13551.0	3.00E-06	29	27411000.0	2.90E-05
4	58232.0	4.00E-06	30	26121000.0	3.00E-05
5	185830.0	5.00E-06	31	23909000.0	3.10E-05
6	364230.0	6.00E-06	32	21923000.0	3.20E-05
7	602840.0	7.00E-06	33	20265000.0	3.30E-05
8	897190.0	8.00E-06	34	18293000.0	3.40E-05
9	1262100.0	9.00E-06	35	16222000.0	3.50E-05
10	1694500.0	1.00E-05	36	14949000.0	3.60E-05
11	2204200.0	1.10E-05	37	14187000.0	3.70E-05
12	2791500.0	1.20E-05	38	12638000.0	3.80E-05
13	3438100.0	1.30E-05	39	10472000.0	3.90E-05
14	4158400.0	1.40E-05	40	9259500.0	4.00E-05
15	4950400.0	1.50E-05	41	9120200.0	4.10E-05
16	5889300.0	1.60E-05	42	8675000.0	4.20E-05
17	7069000.0	1.70E-05	43	7826700.0	4.30E-05
18	8661600.0	1.80E-05	44	7513400.0	4.40E-05
19	10893000.0	1.90E-05	45	7478400.0	4.50E-05
20	13875000.0	2.00E-05	46	7120400.0	4.60E-05
21	17469000.0	2.10E-05	47	7008300.0	4.70E-05
22	21119000.0	2.20E-05	48	7342500.0	4.80E-05
23	23970000.0	2.30E-05	49	7424600.0	4.90E-05
24	25413000.0	2.40E-05	50	7522100.0	5.00E-05
25	25616000.0	2.50E-05	51	8088300.0	5.10E-05
26	25555000.0	2.60E-05	52	8329800.0	5.20E-05

Table 5.3 Dynamic stress intensity factor for a=12mm

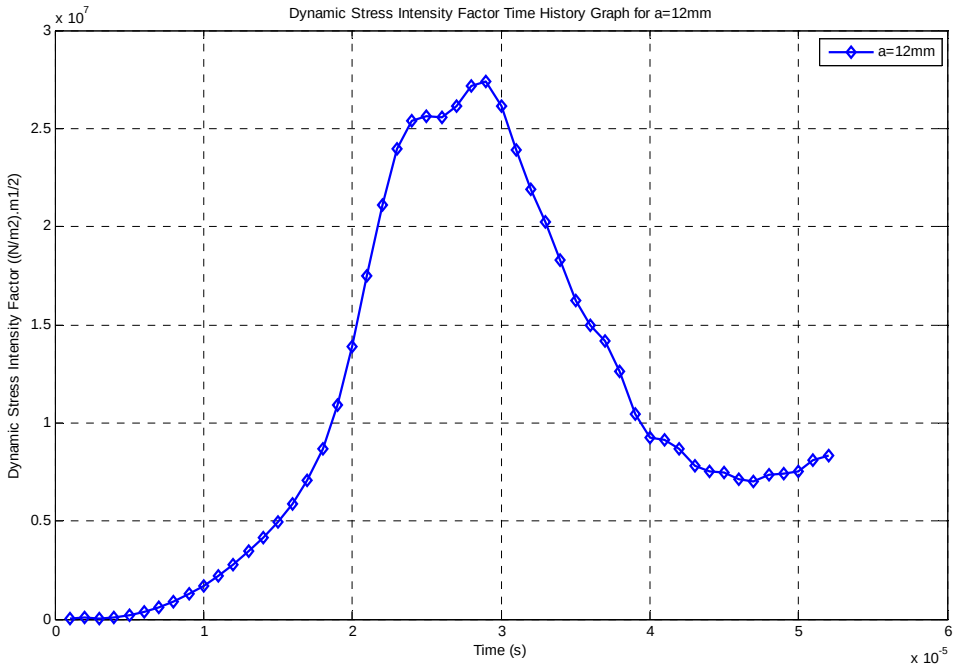

Figure 5.23 Dynamic stress intensity factor time history graph

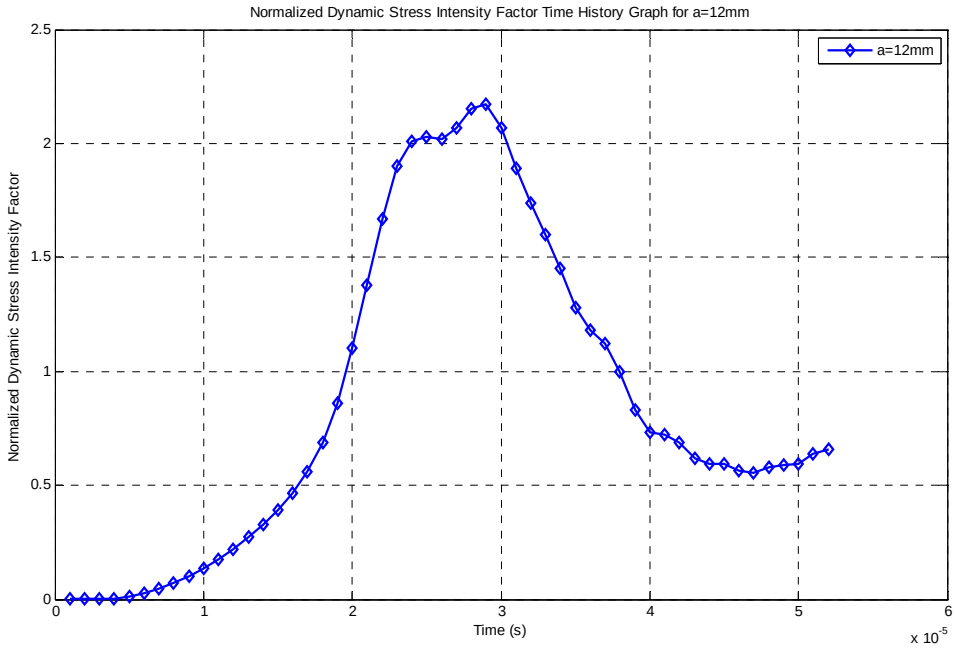

Figure 5.24 Dynamic stress intensity factor time history graph

Data of dynamic stress intensity factor for a=14mm crack

S.No.	DSIF	TIME	S.No.	DSIF	TIME
1	38702.0	1.00E-06	27	27377000.0	2.70E-05
2	57880.0	2.00E-06	28	28705000.0	2.80E-05
3	13435.0	3.00E-06	29	29526000.0	2.90E-05
4	58598.0	4.00E-06	30	29084000.0	3.00E-05
5	186300.0	5.00E-06	31	27827000.0	3.10E-05
6	364120.0	6.00E-06	32	26618000.0	3.20E-05
7	602290.0	7.00E-06	33	25320000.0	3.30E-05
8	897650.0	8.00E-06	34	23208000.0	3.40E-05
9	1261700.0	9.00E-06	35	20623000.0	3.50E-05
10	1688400.0	1.00E-05	36	18824000.0	3.60E-05
11	2191000.0	1.10E-05	37	18040000.0	3.70E-05
12	2772500.0	1.20E-05	38	17079000.0	3.80E-05
13	3425100.0	1.30E-05	39	15376000.0	3.90E-05
14	4171000.0	1.40E-05	40	13711000.0	4.00E-05
15	5001500.0	1.50E-05	41	12566000.0	4.10E-05
16	5985900.0	1.60E-05	42	11544000.0	4.20E-05
17	7214900.0	1.70E-05	43	10668000.0	4.30E-05
18	8866700.0	1.80E-05	44	10339000.0	4.40E-05
19	11173000.0	1.90E-05	45	10154000.0	4.50E-05
20	14240000.0	2.00E-05	46	9689500.0	4.60E-05
21	17922000.0	2.10E-05	47	9568500.0	4.70E-05
22	21670000.0	2.20E-05	48	10056000.0	4.80E-05
23	24633000.0	2.30E-05	49	10282000.0	4.90E-05
24	26197000.0	2.40E-05	50	10057000.0	5.00E-05
25	26523000.0	2.50E-05	51	10285000.0	5.10E-05
26	26603000.0	2.60E-05	52	10937000.0	5.20E-05

Table 5.4 Dynamic stress intensity factor for a=14mm

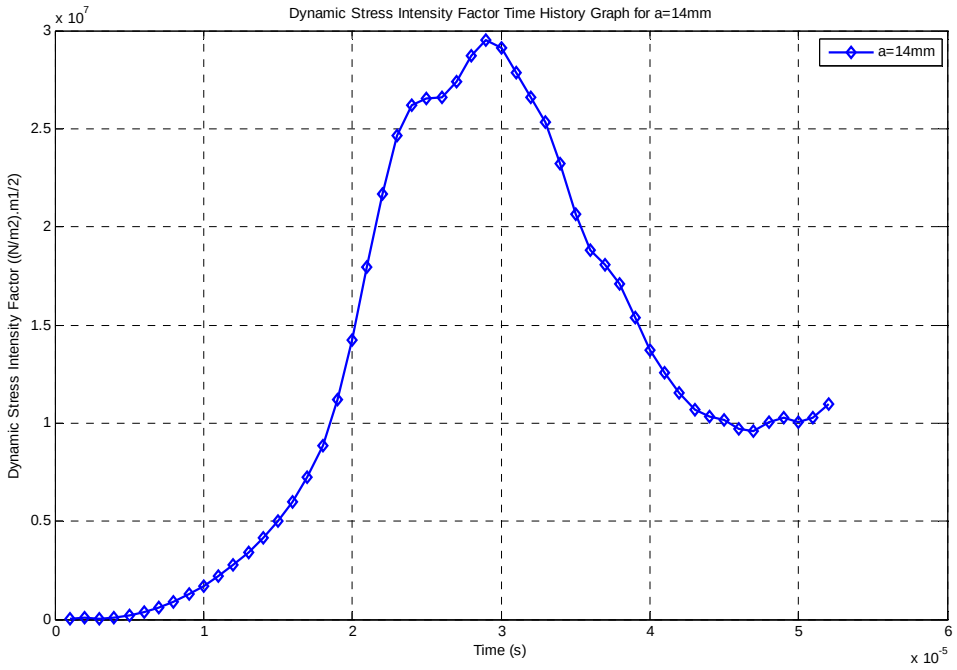

Figure 5.25 Dynamic stress intensity factor time history graph

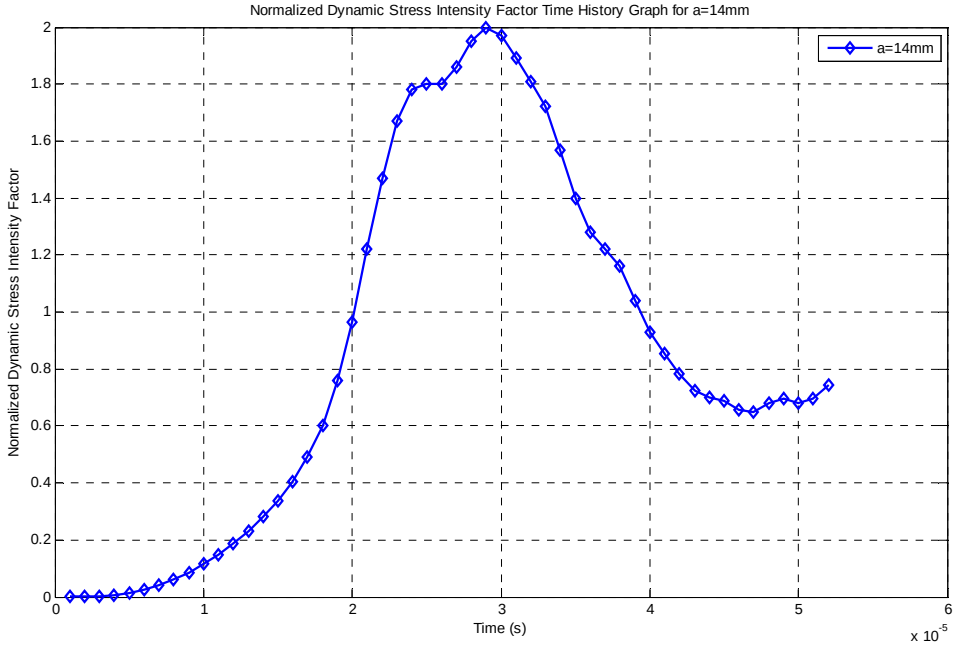

Figure 5.26 Dynamic stress intensity factor time history graph

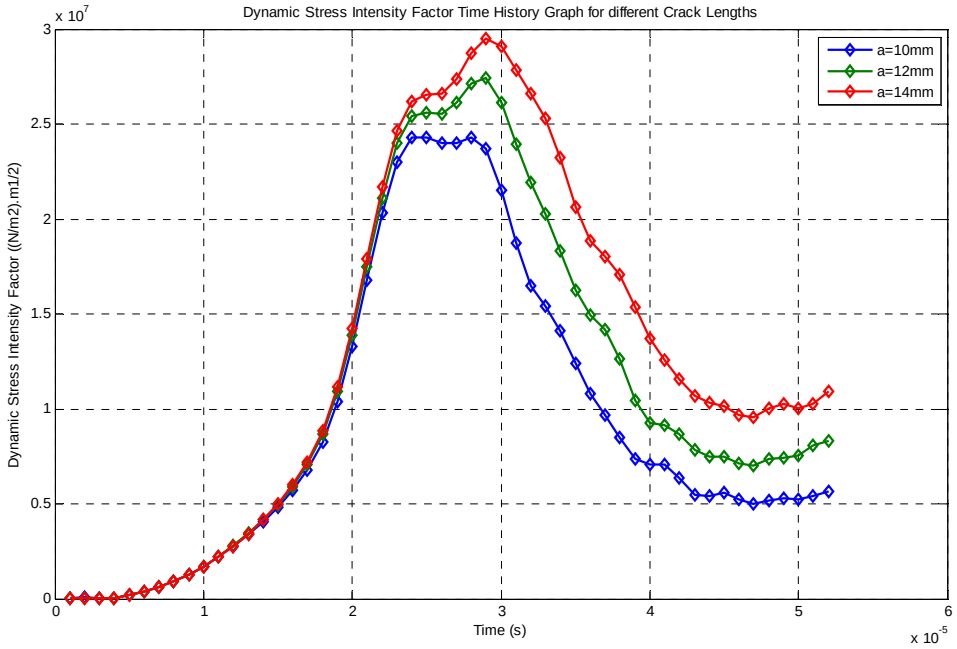

Figure 5.27 Dynamic stress intensity factor time history graph

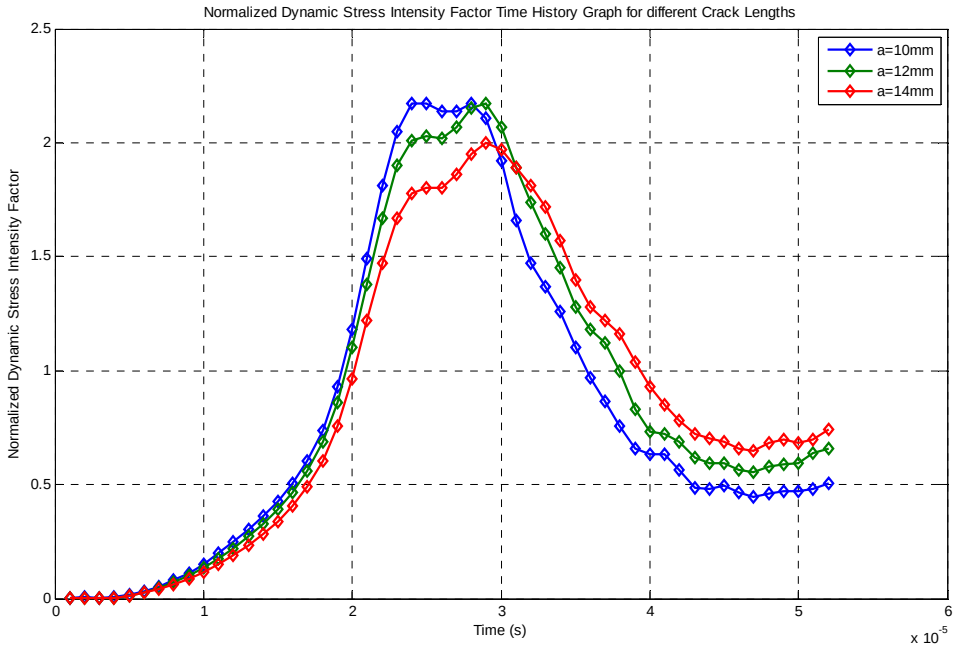

Figure 5.28 Dynamic stress intensity factor time history graph

5.3.3 Dynamic Stress Intensity Factor for Circumferential Crack

Dynamic fracture analysis of circumferential crack is done to make comparison the results with the longitudinal crack. The von Misses stress time history graph shows the conditions of the stress at the crack tip as shown in figure 5.29. Similarly, the dynamic stress intensity factor is displayed in figure 5.30.

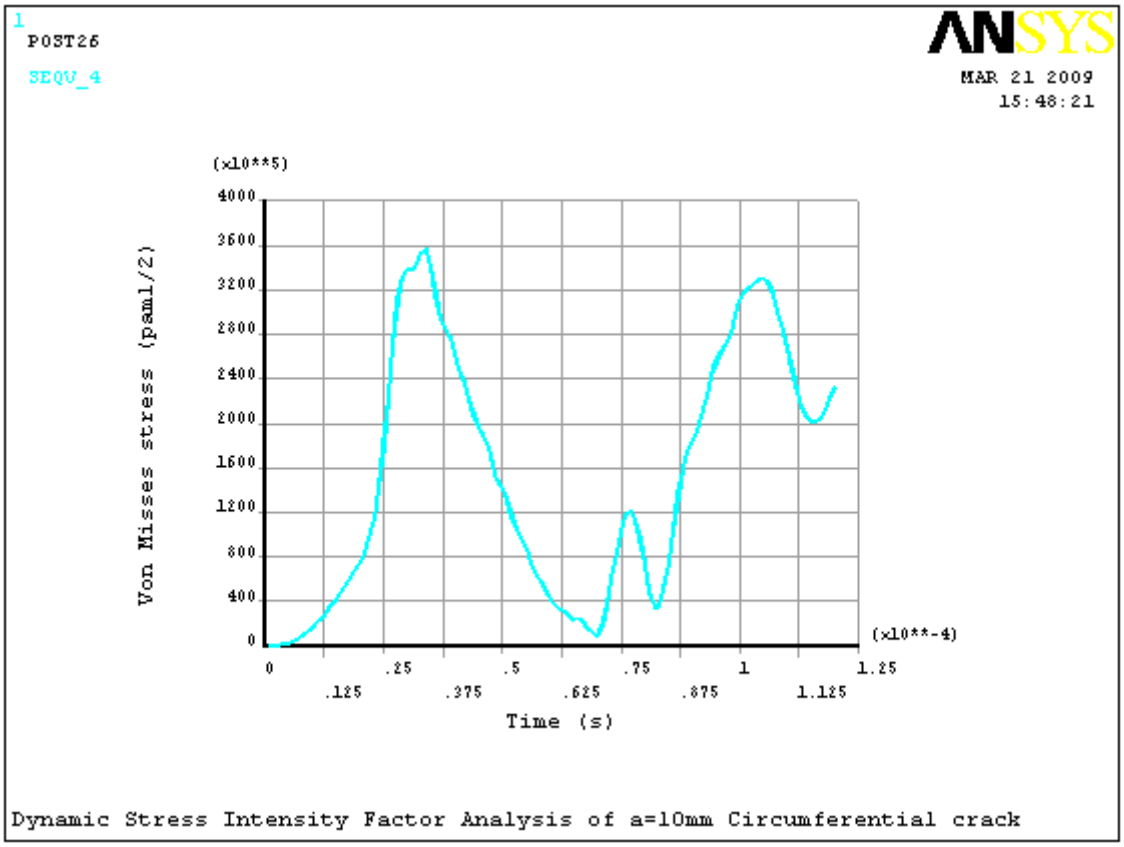

Figure 5.29 Dynamic von Misses stress time history graph for a=10mm crack

The fracture analysis of circumferential crack is done only for 20mm crack length. As shown from figure 5.14 and figure 5.29 the von Misses stress at the pick is much greater for longitudinal crack. The same phenomenon happens for the required fracture parameter, as can be compared figure 20 from to figure 30.

Data of stress intensity factor for circumferential crack

S.No.	Dynamic Stress Intensity factor ($pa(m)^{1/2}$)	Time (S)	S.No.	Dynamic Stress Intensity factor ($pa(m)^{1/2}$)	Time (S)
1	2916.624	1.00E-06	28	10507664	2.80E-05
2	5764.256	2.00E-06	29	11090009	2.90E-05
3	12735.15	3.00E-06	30	11269812	3.00E-05
4	18157.07	4.00E-06	31	11323093	3.10E-05
5	57946.41	5.00E-06	32	11598474	3.20E-05
6	102585.6	6.00E-06	33	11931988	3.30E-05
7	149615.4	7.00E-06	34	11925396	3.40E-05
8	250027.6	8.00E-06	35	11390107	3.50E-05
9	312223.4	9.00E-06	36	10571290	3.60E-05
10	452342.4	1.00E-05	37	9943995	3.70E-05
11	565126.6	1.10E-05	38	9545114	3.80E-05
12	717606.5	1.20E-05	39	9156670	3.90E-05
13	883147.8	1.30E-05	40	8662368	4.00E-05
14	1029115	1.40E-05	41	8223591	4.10E-05
15	1231952	1.50E-05	42	7821689	4.20E-05
16	1401190	1.60E-05	43	7296517	4.30E-05
17	1610929	1.70E-05	44	6713732	4.40E-05
18	1811706	1.80E-05	45	6375146	4.50E-05
19	2032440	1.90E-05	46	6172465	4.60E-05
20	2297668	2.00E-05	47	5796344	4.70E-05
21	2630560	2.10E-05	48	5243743	4.80E-05
22	3098880	2.20E-05	49	4815420	4.90E-05
23	3819126	2.30E-05	50	4541862	5.00E-05
24	4830663	2.40E-05	51	4136225	5.10E-05
25	6202942	2.50E-05	52	3728245	5.20E-05
26	7786315	2.60E-05	53	3376641	5.30E-05
27	9321185	2.70E-05	54	3077659	5.40E-05

Table 5. 5 Dynamic stress intensity factor time history graph for circumferential through crack

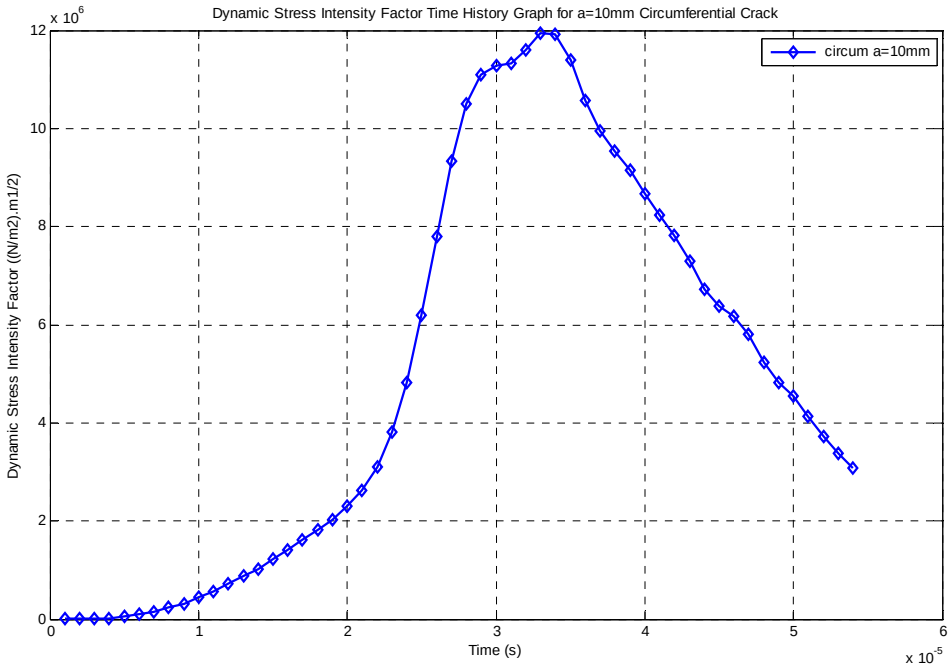

Figure 5.30 Dynamic stress intensity factor time history graph

5.4 Coupled Dynamic Stress and Stress Intensity Factor

The thermal shock result is obtained due to sudden cooling. If the period of the shock duration is small enough compared to the first natural frequency, the dynamic thermo elasticity is very important [41]. As we mentioned earlier, the infinite strip is taken. It is assumed that the pressure vessel has uniform temperature 303K, and suddenly cooled by conduction to 273K for the analysis of stationary crack. The sudden cooling process creates thermal shock. This thermal shock propagates to the tip of the crack and affects the stress condition. The von Misses stress with time shown in figure 5.31, higher temperature change analysis is taken having uniform temperature 561K and cooled to 394K as shown in figure 5.32.

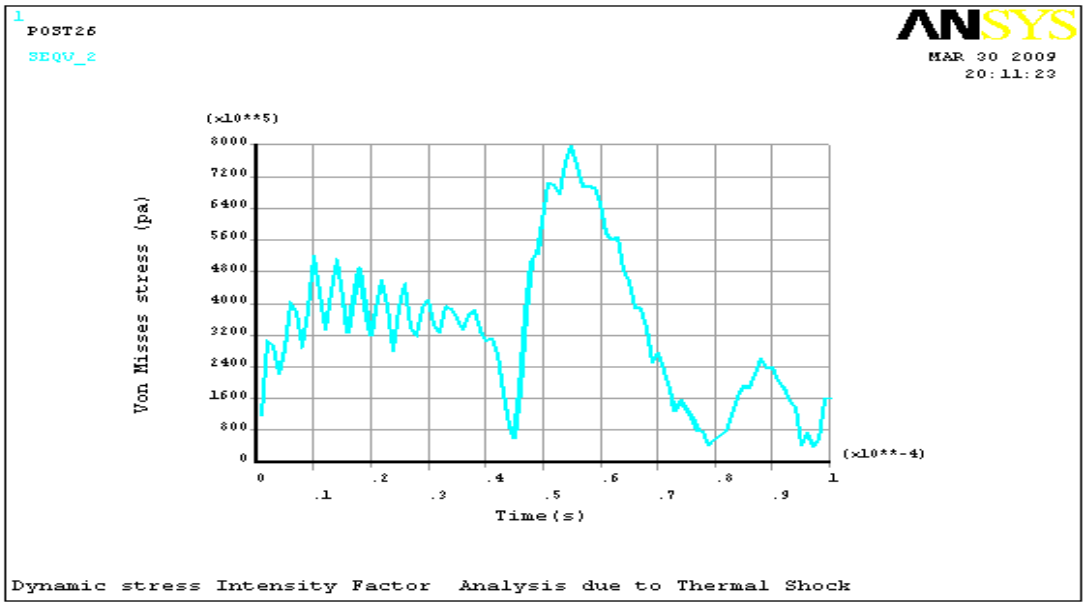

Figure 5. 31 Dynamic Von Misses stress time history graph for circumferential crack

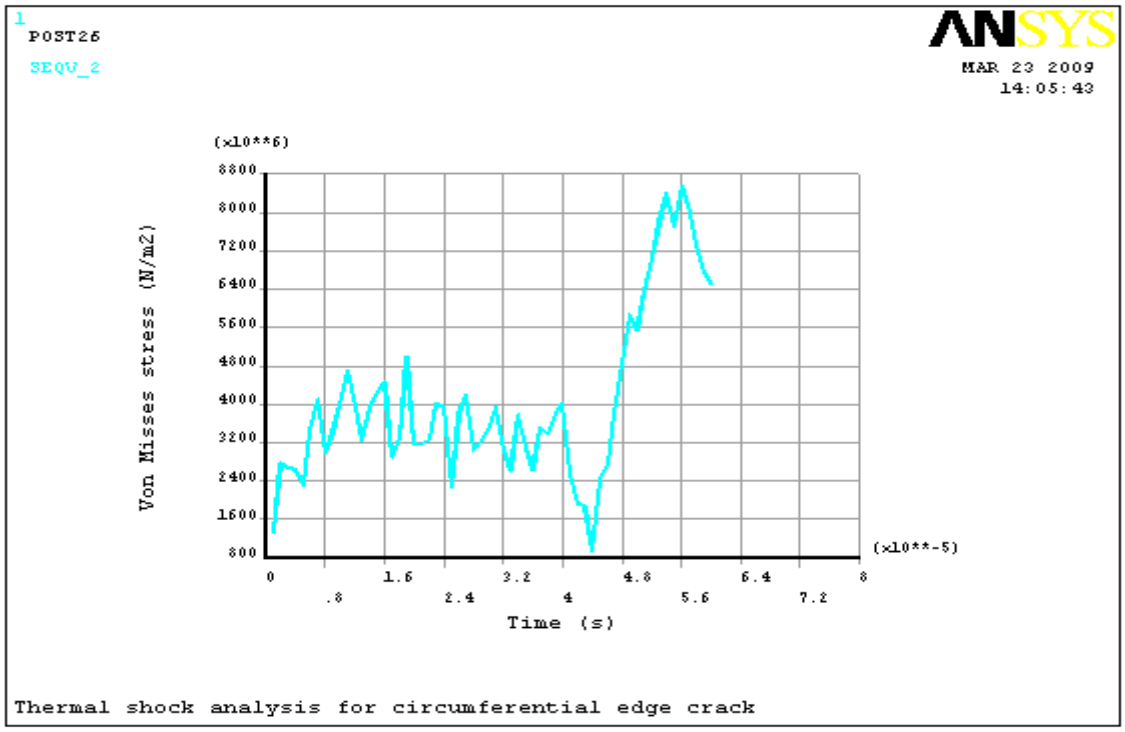

Figure 5. 32 Dynamic Von Misses stress time history graph for circumferential crack

The dynamic stress intensity factor created by this thermal shock is presented in figure 5.32.the dynamic stress intensity factor the thermo elastic waves reaches at the crack front/tip of the crack. The cold shock produces tensile stress in the y-direction, and compressive stress produces in the x direction. The same phenomenon as that of dynamic fracture analysis occurs.

Data of stress intensity factor due to thermal shock for stationary crack

S.No.	Dynamic Stress Intensity factor ($pa(m)^{1/2}$)	Time (S)	S.No.	Dynamic Stress Intensity factor ($pa(m)^{1/2}$)	Time (S)
1	7.22E+06	1.00E-06	35	1.61E+07	3.50E-05
2	1.18E+07	2.00E-06	36	1.39E+07	3.60E-05
3	9.88E+06	3.00E-06	37	1.69E+07	3.70E-05
4	1.25E+07	4.00E-06	38	1.83E+07	3.80E-05
5	1.57E+07	5.00E-06	39	1.37E+07	3.90E-05
6	1.65E+07	6.00E-06	40	1.10E+07	4.00E-05
7	1.40E+07	7.00E-06	41	1.19E+07	4.10E-05
8	1.53E+07	8.00E-06	42	9.90E+06	4.20E-05
9	2.17E+07	9.00E-06	43	2.23E+06	4.30E-05
10	2.07E+07	1.00E-05	44	4.97E+06	4.40E-05
11	1.66E+07	1.10E-05	45	7.06E+06	4.50E-05
12	1.93E+07	1.20E-05	46	1.42E+07	4.60E-05
13	2.14E+07	1.30E-05	47	2.46E+07	4.70E-05
14	2.01E+07	1.40E-05	48	2.65E+07	4.80E-05
15	1.84E+07	1.50E-05	49	2.67E+07	4.90E-05
16	1.78E+07	1.60E-05	50	3.09E+07	5.00E-05
17	1.94E+07	1.70E-05	51	3.41E+07	5.10E-05
18	1.97E+07	1.80E-05	52	3.35E+07	5.20E-05
19	1.85E+07	1.90E-05	53	3.25E+07	5.30E-05
20	1.72E+07	2.00E-05	54	3.58E+07	5.40E-05
21	1.58E+07	2.10E-05	55	3.71E+07	5.50E-05
22	1.95E+07	2.20E-05	56	3.32E+07	5.60E-05
23	1.37E+07	2.30E-05	57	3.05E+07	5.70E-05
24	1.66E+07	2.40E-05	58	3.12E+07	5.80E-05
25	1.94E+07	2.50E-05	59	3.22E+07	5.90E-05
26	1.77E+07	2.60E-05	60	2.73E+07	6.00E-05
27	1.53E+07	2.70E-05	61	2.38E+07	6.10E-05
28	1.53E+07	2.80E-05	62	2.55E+07	6.20E-05
29	1.87E+07	2.90E-05	63	2.51E+07	6.30E-05
30	1.77E+07	3.00E-05	64	2.03E+07	6.40E-05
31	1.59E+07	3.10E-05	65	1.61E+07	6.50E-05
32	1.54E+07	3.20E-05	66	1.80E+07	6.60E-05
33	1.70E+07	3.30E-05	67	1.23E+07	6.70E-05
34	1.90E+07	3.40E-05	68	1.04E+07	6.80E-05

Table 5. 6 Dynamic stress intensity factor time history graph for circumferential edge crack

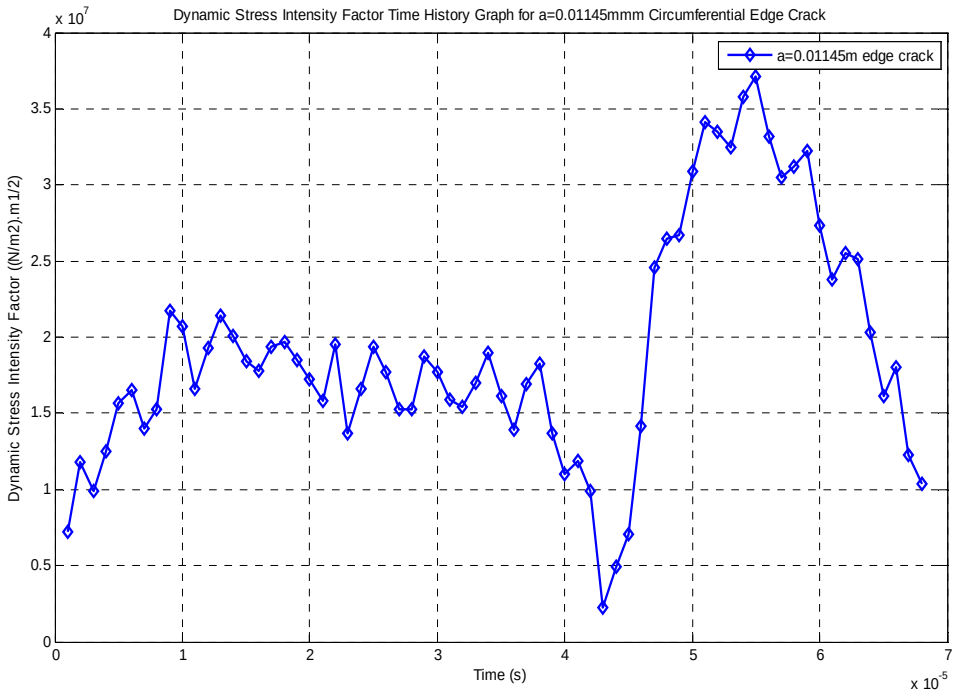

Figure 5. 33 Dynamic stress intensity factor time history graph for circumferential stationary edge crack

The fracture toughness of the material as mentioned in section 4.4.3 is 50Mpa (m) $^{1/2}$, the maximum dynamic stress intensity factor result found from figure 5.33 below the toughness value. This indicates that the crack does not grow by the stress of figure 5.31, which is created due to thermal shock. To compare the result of figure 5.33, a cooling temperature change of 167K is taken as shown in figure 5.34. Unlikely, in figure 5.34, the value of the dynamic stress intensity factor is greater than the toughness value; this shows the crack behavior in general.

Data of stress intensity factor due to thermal shock

S.No.	Dynamic Stress Intensity factor ($pa(m)^{1/2}$)	Time (S)	S.No.	Dynamic Stress Intensity factor ($pa(m)^{1/2}$)	Time (S)
1	5.71E+07	1.00E-06	28	1.33E+08	2.80E-05
2	1.08E+08	2.00E-06	29	1.44E+08	2.90E-05
3	1.13E+08	3.00E-06	30	1.38E+08	3.00E-05
4	1.05E+08	4.00E-06	31	1.68E+08	3.10E-05
5	1.05E+08	5.00E-06	32	1.26E+08	3.20E-05
6	1.48E+08	6.00E-06	33	1.12E+08	3.30E-05
7	1.53E+08	7.00E-06	34	1.63E+08	3.40E-05
8	1.40E+08	8.00E-06	35	1.23E+08	3.50E-05
9	1.39E+08	9.00E-06	36	1.11E+08	3.60E-05
10	1.74E+08	1.00E-05	37	1.43E+08	3.70E-05
11	1.90E+08	1.10E-05	38	1.44E+08	3.80E-05
12	1.59E+08	1.20E-05	39	1.60E+08	3.90E-05
13	1.59E+08	1.30E-05	40	1.68E+08	4.00E-05
14	1.55E+08	1.40E-05	41	1.04E+08	4.10E-05
15	1.76E+08	1.50E-05	42	8.55E+07	4.20E-05
16	1.87E+08	1.60E-05	43	6.55E+07	4.30E-05
17	1.26E+08	1.70E-05	44	4.35E+07	4.40E-05
18	1.46E+08	1.80E-05	45	9.90E+07	4.50E-05
19	1.84E+08	1.90E-05	46	1.25E+08	4.60E-05
20	1.45E+08	2.00E-05	47	1.57E+08	4.70E-05
21	1.34E+08	2.10E-05	48	2.19E+08	4.80E-05
22	1.38E+08	2.20E-05	49	2.48E+08	4.90E-05
23	1.64E+08	2.30E-05	50	2.44E+08	5.00E-05
24	1.56E+08	2.40E-05	51	2.73E+08	5.10E-05
25	1.10E+08	2.50E-05	52	3.01E+08	5.20E-05
26	1.59E+08	2.60E-05	53	3.50E+08	5.30E-05
27	1.61E+08	2.70E-05	54	3.49E+08	5.40E-05

Table 5. 7 Dynamic stress intensity factor time history graph for circumferential edge crack

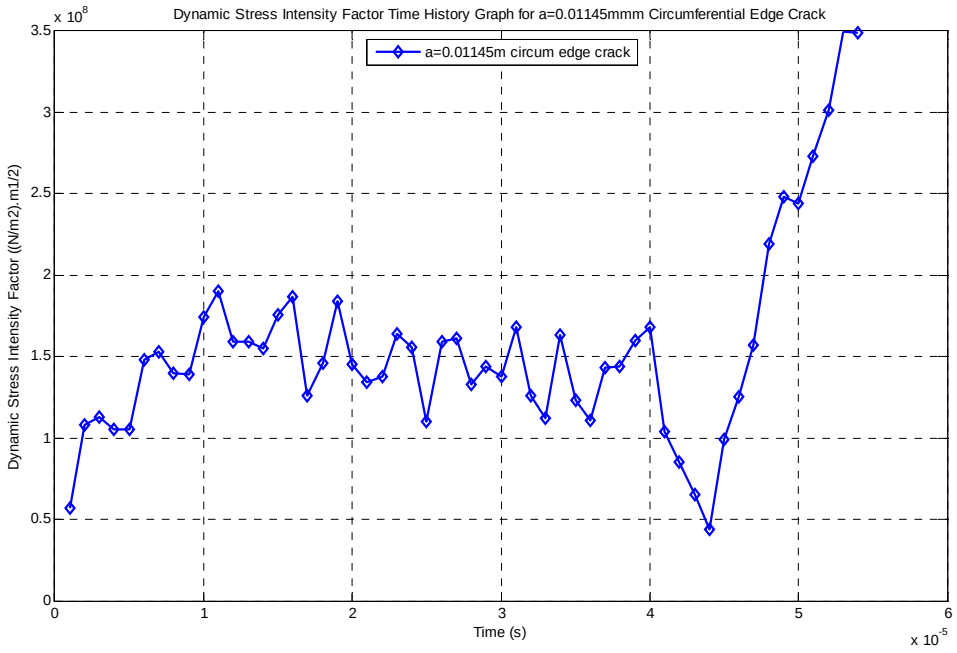

Figure 5. 34 Dynamic stress intensity factor time history graph for circumferential edge crack

When the dynamic stress intensity factor is below the fracture toughness, the crack becomes stable until it reaches the critical value (figure 5.33). On the other hand, as the dynamic stress intensity factor increases above the fracture toughness of material value, the crack may grow by constant speed or may create inertia effect (figure5.34).

Chapter Six

6 Conclusion and Recommendation

6.1 Conclusion

From the literature and background of this thesis, the general idea shows that when dynamic loading is applied on the fractured body, the fracture analysis is treated as dynamic fracture mechanics. The fracture analysis is parameterized by dynamic stress intensity factor for elastic body.

The analysis of this thesis shows four squeezed important points

1. For longitudinal crack of pressure vessels as the crack, length increases the fracture parameter, stress intensity factor, increases. This shows that the probability of failures increases as the crack length increases for stationary crack. More over this, the thesis shows that the stress intensity factor of longitudinal crack is greater than the circumferential crack for the same crack length and geometry. It also confirms the theoretical singularity at the crack tip.
2. When the load is rapidly applied on a cracked body, the stress wave travels to the crack face, this traveling stress wave reflected and diffracted from the crack faces toward the body because of media change. The refracted and reflected wave interacts with the dilatational wave; this interaction creates high stress magnitude at the crack tip.
3. The phenomenon of dynamic loading creates higher stress intensity factor from normal operating pressure or static operation. The dynamic stress intensity factor increases until the stress wave reaches to the crack front and decline when the stress wave moves onwards for the first load cycle and the stress wave decreases as the time increases. It also fulfills the conclusion mentioned in point 2. The value of dynamic stress intensity factor increases as the crack length increases for the same vessel dimension and crack orientation. It also tells us higher magnitude of dynamic stress intensity factor is obtained for longitudinal crack when we compare with the same circumferential crack length
4. Lastly, we obtained that the thermal shock creates dynamic stress intensity factor, which sever the body if there is sudden cooling of temperature. The analysis

resulted that the dynamic stress intensity factor increases as the load cycle increase for the load creates above fracture toughness and similar situation obtained as point 3 for stationary crack.

Those points show us how loading conditions varies fracture analysis. This helps us how we should treat crack behaviors during design. It also helps to determine crack dimension and orientation during design, crack investigation after manufacturing and during maintenance to investigate crack-arresting mechanisms.

6.2 Recommendations of Future Work

As mentioned before, the goal of this dissertation research was the determination dynamic fracture parameter. This thesis determined the behavior of dynamic fracture parameter for circumferential and longitudinal cracks of mode I case. However, it is easy to conclude the results of the angular orientation of a crack between axial and circumferential direction, mixed mode fracture criterion can be evaluated. However; number suggestion can be made, the following future works can be the initial of similar kinds of research:

1. Dynamic fracture analysis of surface crack for elastic body of pressure vessel
2. Dynamic fracture analysis of through, and surface cracks for time dependent materials
3. Dynamic fracture analysis of different crack types and orientation for growing crack
4. Dynamic fracture analysis of growing crack for suddenly applied loading
5. Dynamic fracture analysis of growing crack for time dependent materials
6. Dynamic fracture analysis of time dependent materials for suddenly applied loading
7. Stress wave reflection, diffraction and interaction at the crack tip for different crack orientation of pressure vessel
8. Fracture analysis of pressure vessel due to thermal shock for longitudinal surface crack

References

1. Anderson, Robert B. and Sullivan, Timothy L., "Fracture mechanics of through–cracked cylindrical pressure vessels", *National Aeronautics and Space Administration*, Washington D.C, NASA TN D-3252, 1966.
2. Sullivan, Timothy L. and Pierce, William S. , " Effect of radius an Bulging and Fracture of Through Cracked Cylindrical Pressure Vessels at Cryogenic Temperatures", *National Aeronautics and Space Administration*, Washington D.C., NASA TN D- 4951 , 1968
3. Newman, J.C " Fracture Analysis of Surface and Through Cracks in Cylindrical Pressure Vessels", *National Aeronautics and Space Administration*, Washington D.C, NASA TN.D-8325, 1976
4. Prause, R.H, " Dynamic Modeling of Pressure Vessels and Piping Systems", *The Shock and Vibration Digest* 2.13, SAGE Publications, 1977
5. Young, Richard D., Rose, Cheryl A. and Starnes, James H., "Nonlinear Local Bending Response and Bulging Factors for Longitudinal and Circumferential Cracks in Pressured Cylindrical Shells", *National Aeronautics and Space Administration*, NASA-99, 1999
6. Choa, Tong Wa and Shepherd, E. Joseph , " Fracture response of Externally Flawed Cylindrical Shells to Internal Gaseous Detonation Loading", *International Journal of Fracture*, Vol. 134, No. 1, pp. 59-90(32), Springer,2005
7. Chao, Tong Wa and Shepherd, E Joseph , "Comparison of Fracture Response of pre Flawed Tubes Under Internal Static and Detention Loading", *Journal of Pressure Vessel Technology*, 2004
8. Gning, P.B , Tarfaui, M., Collombet, F. and Davis, P., " Prediction of Damage in Composite cylinders after impact", *Journal of Composite Materials,* SAGE Publications, 39;917, 2005
9. Health and Safety Executive, "Fluid Structure Interaction Effects on and Dynamic Response of Pressure Vessels and Tanks Subjected to Dynamic Loading", Health and Safety Executive, Crown, 2007.

10. Gonclaves, Paulo B., Da silva, Fredrico M.A. and Del prado, Zenon J.G.N, "Transient Stability of Empty and Fluid Filled Cylindrical Shells", *J. of the Braz. Soc. Of mech. Sci. and Eng.* , 2006
11. Bogy, D.B., Green –berg, H.J and Talke, F.E, "Steady Solution for Circumferential Moving Loads on Cylindrical Shells", *IBM Journal of Research and Development*, Vol.18, No. 5, 1974
12. Orange, Thomas W., Sullivan, Timothy L. and Calfo, Fredrick D., "Fracture of Thin Sections Containing Through and Part–through Cracks", N*ational Aeronautics and Space Administration*, Washington D. C ,NASA TN D-6305, 1971.
13. Annaratane, Donatello, *Pressure Vessel Design*, Springer, Millano, 2007
14. Zeman, Josef L., *Pressure Vessel Design the Direct Route*, Elsevier Ltd. London, 2006
15. Rodriguez – Caste llanos, A, Rodriguez – Sanchez, J.E, *Nunez –Farfan J., and Olivera – Villasenor, R.E, Revista Mexicana de Fisica* 52 (2) 104 – 110, 2005
16. kiciak, A., Glinka, G. and Burns, D. J., " Calculation of Stress Intensity Factors and Crack Opening Displacements for Cracks Subjected to Complex Stress Fields", *Journal of Pressure Vessel Technolog*y, Volume 125, PP 260 – 266, 2003
17. Anthony Lawrence Kohan, *Pressure Vessel Systems: A User's Guide to Safe Operation and Maintenance*, McGraw – Hill, 1987.
18. Ngo, T., Mends, P., Gupta, A. and Ramsay, J., "Blast Loading and Blast Effects on Structure: An Overview", *EISE special issue*, 2007.
19. Broek, David, *Elementary Engineering Fracture Mechanics*, *3rd revised ed*., Martinus Nijhoff Publisher, 3300 A H Dordrecht, 1984.
20. Raju, J.S and Newman, J.C, "Stress intensity Factor for Internal and External Surface Cracks in Cylindrical Shell", *Journal of Pressure Vessel Technology*, V-104, pp 293, 1982.
21. Nishioka, T. and Atluri, S. N, "Analysis of Surface Flaw in Pressure Vessels", *Journal of Pressure Vessel Technology*, V-104, pp 299, 1982

22. Bass, B.R., Bryanm, R.H, Bryson, J.W., and Merkle,J.G, "Application of Energy Release Rate Techniques to Part-through Cracks in Experimental Pressure Vessels", *Journal of Pressure Vessel Technology*, V – 104, pp-308, 1983
23. Jung, J. and Kanninen, M.F., "Analysis of Dynamic Crack Propagation and Arrest in Nuclear Pressure Vessels Under Thermal Shock Conditions", *Journal pressure vessel technology*, V-105 pp- 111, 1983
24. Lee, P.S and Raymund, M., "Stress Intensity Factor Solutions for Internal longitudinal Semi – Circulars Surface Flaws in Cylinder Under Arbitrary Loadings", *Journal of Pressure Vessel Technology*, V-105, pp – 309, 1983
25. Haraun, M.A., "Hydrodynamic Pressure and Tanks by Momentum Balance", *Journal of Pressure Vessel Technology*, V-108 pp 413, 1986
26. Leishear, Robert A., "Stress in Cylinder Subjected to an Internal Shock", *Journal of Pressure Vessel Technology*, V-129 pp 372, 2007.
27. Ray Xu, L. and Ping Wang, "Dynamic Fracture Mechanics Analysis of Failure Mode Transitions Along Weekend Interfaces in Elastic Solid", *Engineering Fracture Mechanics,* vol.73, 2006
28. Papaspyrou, S., Valougeorgis, D., and Karamanos, S. A., "Sloshing Effects in Half-Full Horizontal Cylindrical Vessels under Longitudinal Excitation", *Journal of Applied Mechanics Vol. 71/255*, 2004.
29. Timoshinko, S. P. and Goodier, J. N., *Theory of Elasticity*, 3rd ed., McGraw Hill, 1970
30. Ragab, Abdel – Rah man A.F and Ayoumi, Salah Eldin A.B, *Engineering Solid Mechanics: Fundamental and Application*, CRC press, Baca Raton, 1999
31 Harvey, John F., *Theory and Design of Pressure Vessels*, 2nd ed., Chapman and Hall, London, 1991
32 Freund, L.B, *Dynamic Fracture Mechanics*, Cambridge university press, New York, 1998
33 Owen, D.R.J and Luxmoore, A.R., *Numerical Methods in Fracture Mechanics*, Pine ridge press, Swansea, 1980
34 Anderson, T.L, *Fracture mechanics: Fundamentals and application*, 3rd ed., CRC press, Boca Raton, 2005

35 Kwan, Young W. and Hyochoong Bang, *The Finite Element Methods Using Matlab*, 2nd ed., CRC press, Boca Raton, 2000

36 Kare Hellan, *Introduction to Fracture Mechanics*, McGraw – Hill, 1984

37 Sanford, R.J., *Principles of Fracture Mechanics*, Pearson Education, Upper saddle river, 2003

38 Gdoutus, E.E., *Fracture Mechanics: An Introduction*, 2nd ed, Springer, 3300 AA Dordercht, 2005

39 Arun Shukla, *Practical Fracture Mechanics in Design*, 2nd ed., Marcel Dekker, New York, 2005

40 Harrison, H.R and Nettleton, T., *Advanced Engineering dynamics*, John willy and Sons, London, 1997

41 P. Hosseini-Tehrani, M. R. Eslami and H. R. Daghynai, " Dynamic Crack Analysis Under Coupled Thermoelastic Assumption", *Journal of Applied Mechanics*, volume 68, 2001.

42 ANSYS, *Release 10.0 Documentation for ANSYS*

43 William F. Carroll, *A Primer for Finite Element in Elastic Structure*, John Willey and Sons,1998

44 Richard B. Hetnorski, *Volume 1 Thermal Stress,* Elsevier Science Publisher, Netherlands, 1986

Appendix

Appendix A

Frequency analysis

As previously defined, the frequency analysis helps to determine the time integration step numerically. The time integration step is above the high pick of the frequency. The time integration step 1e-6s is, agree with this analysis

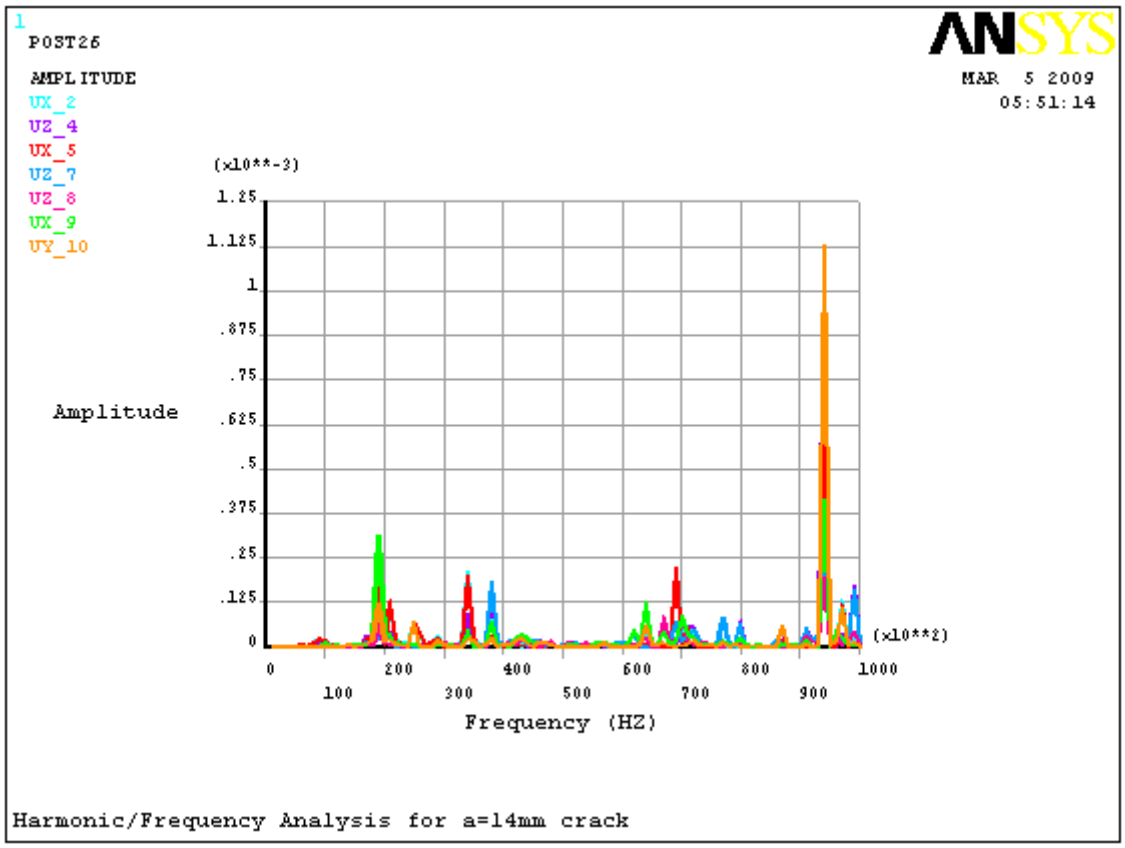

Appendix B

Nomenclature and abbreviation

DSIF= Dynamic Stress Intensity Factor

FEA = Finite Element Analysis

FEM = Finite Element Method

ITS= Integration Time Step

POST1 =First post processing of ANSYS

POST2= Second post processing of ANSYS

ux-2= displacement at crack tip

ux-4= displacement at crack tip

uz-5= displacement away from crack tip

uz-6= displacement away from crack tip

uz-7= displacement far away crack tip

uy-3= displacement away from crack tip

uy-8= displacement away from crack tip

EPLEQV-10= average von Misses strain at crack tip

EPLEQV-9= average von Misses strain at crack edge

EPLEQV-6 =average von Misses strain at crack tip

SEQV-3= average von Misses stress at the crack tip

SEQV-4 = average von Misses stress away from crack tip

SEQV-5 =average von Misses stress away from the crack tip

SEQV-2 =average von Misses stress away from the crack tip

SEQV-6 =average von Misses stress away from the crack tip

Appendix C

Stress Intensity Factor Parameters

Stress intensity factors and correction factor of fracture problems of pressure vessels

For longitudinal through crack of thin walled pressure vessels, the through crack parameter is

$$\lambda_t = \frac{a}{\sqrt{Rt}} \tag{A.1}$$

where λ_t=through crack parameter

R=radius of pressure vessel

t=thickness of the vessel

a= half crack length

The factor, F that governs stress intensity factor is

$$F = \left(1 + 0.5\lambda_t + 1.29\lambda_t^{\,2} + -0.074\lambda_t^{\,3}\right)^{\frac{1}{2}} \tag{A.2}$$

The applied stress of pressure vessel is calculated as

$$\sigma^* = \frac{PR}{t}, \text{ for circumferential stress} \tag{A.3}$$

$$\sigma^* = \frac{PR}{2t}, \text{ for axial stress} \tag{A.4}$$

where P pressure

Appendix D

Crack Orientation and Singular Element Configuration

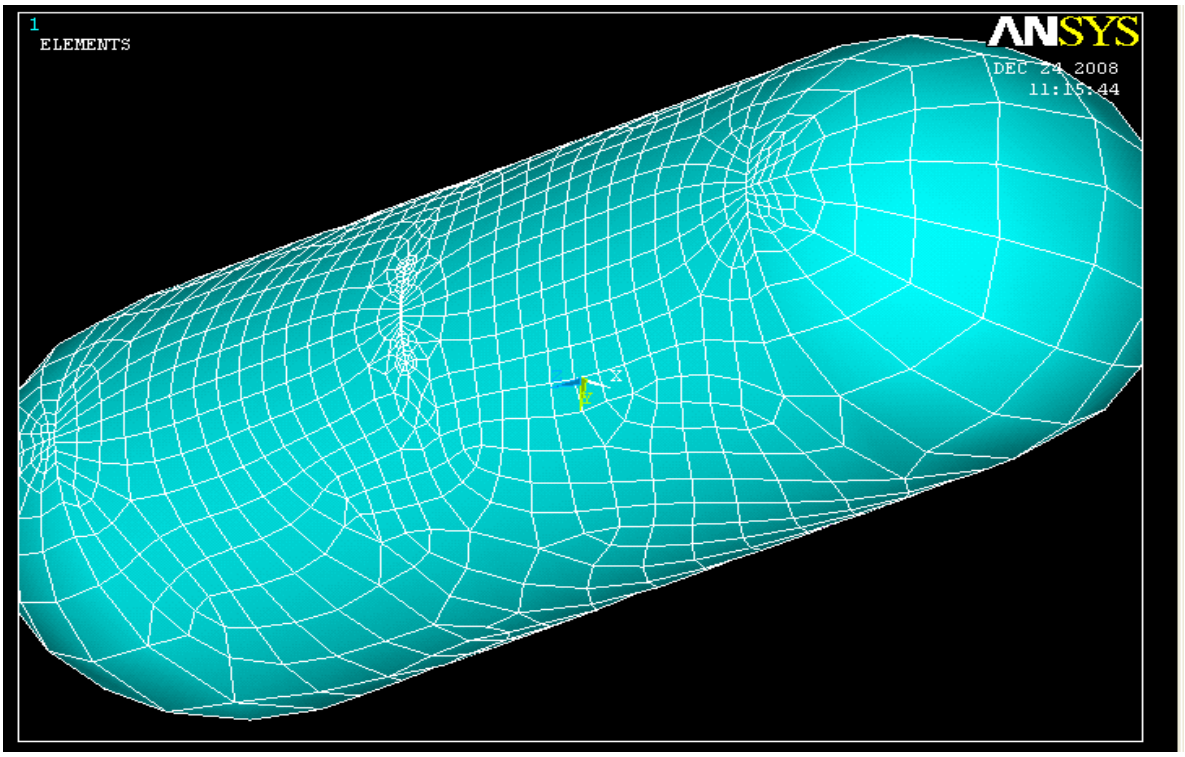

Fiure A .1 circumferential crack

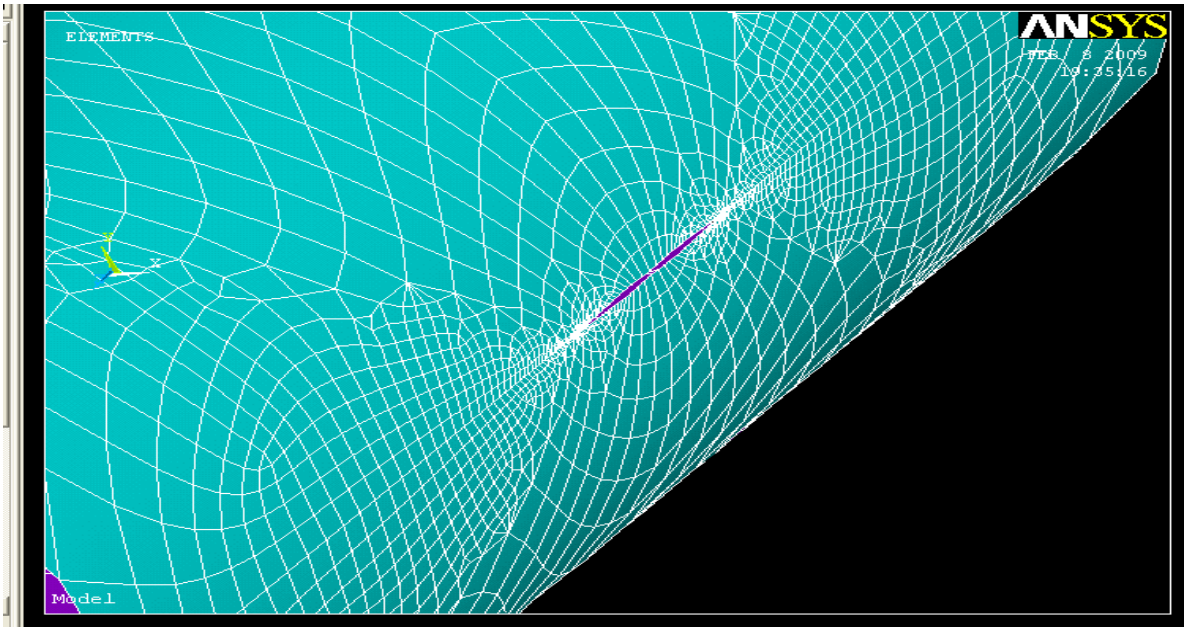

Figure A.2 longitudinal crack

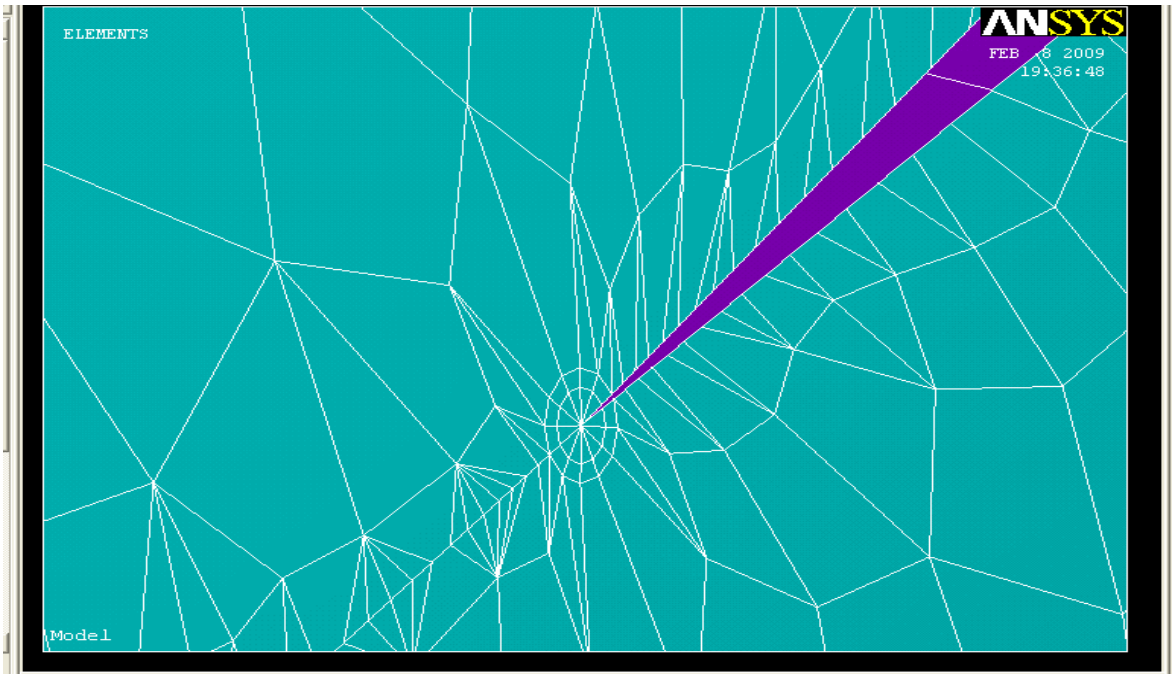

Figure A.3 Longitudinal crack and singular elements

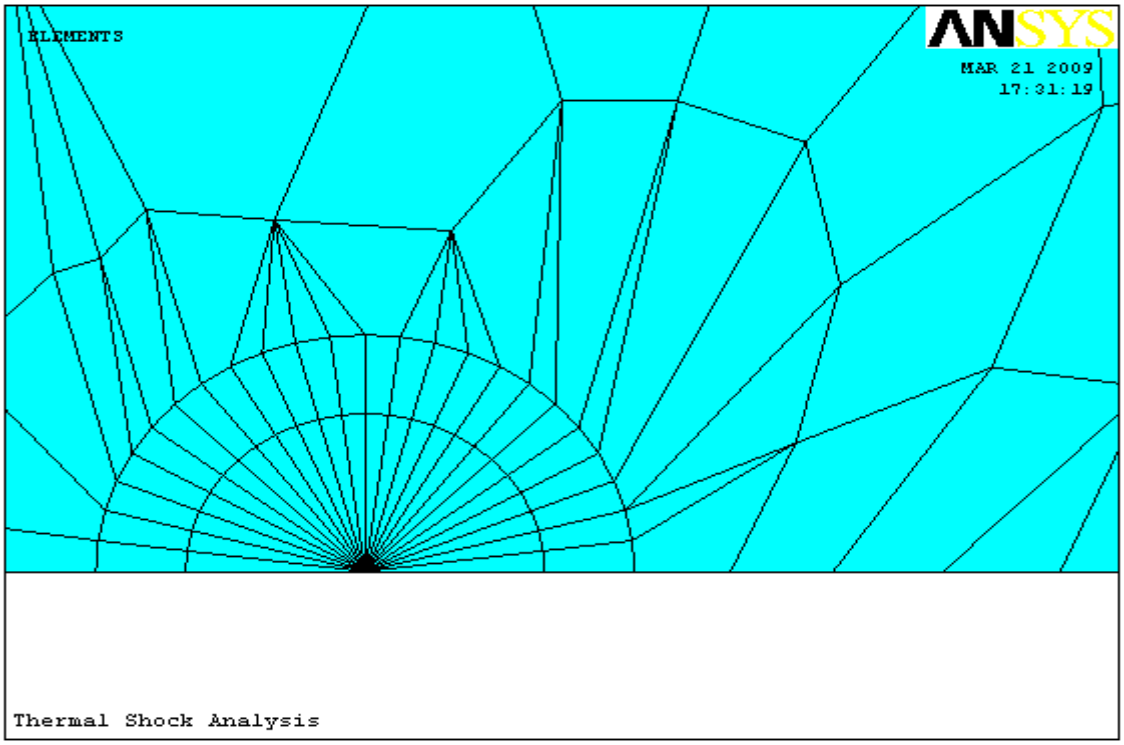

Figure A.4 singular elements of edge crack

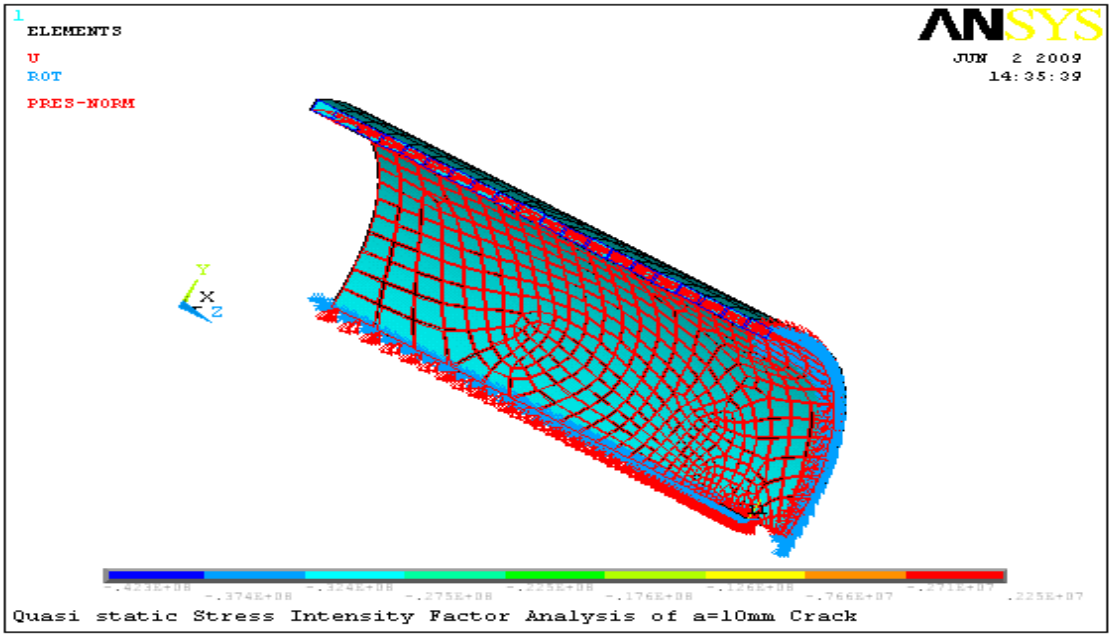

Figure A.5 Boundary Condition

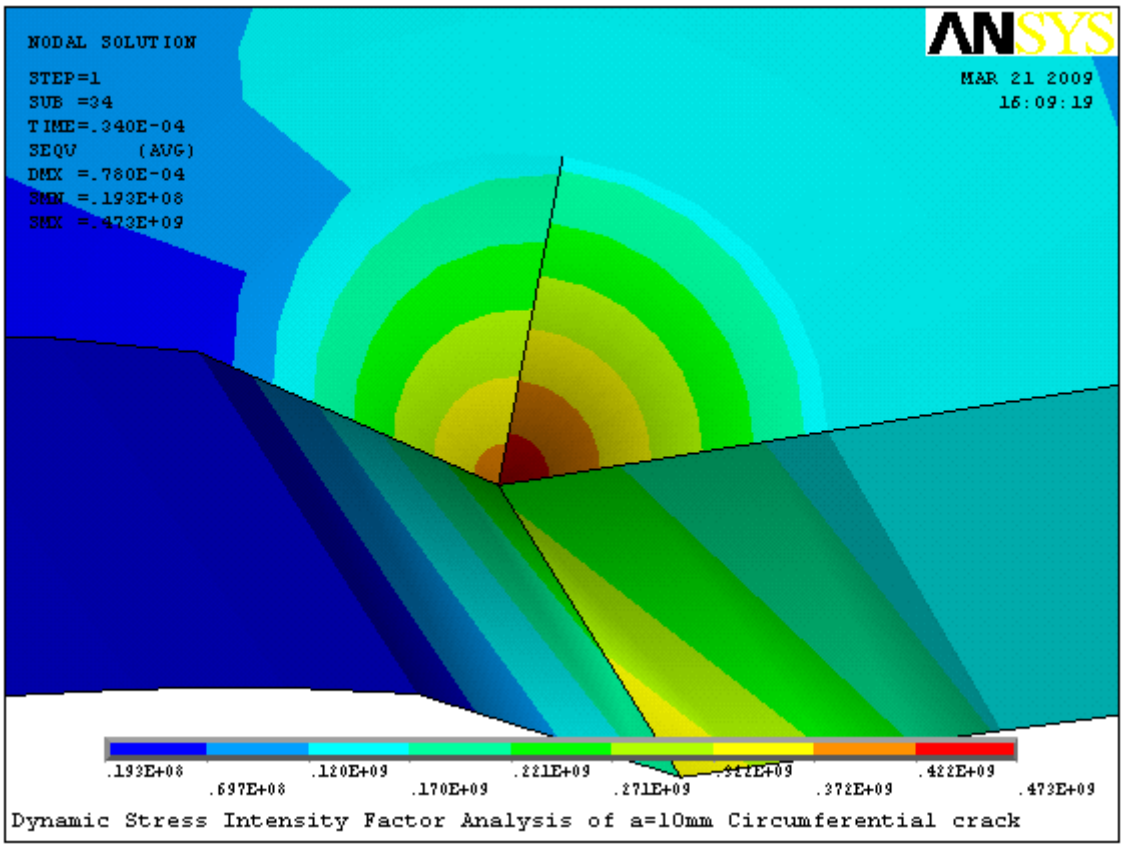

Figure A.6 stress distribution of crack tip

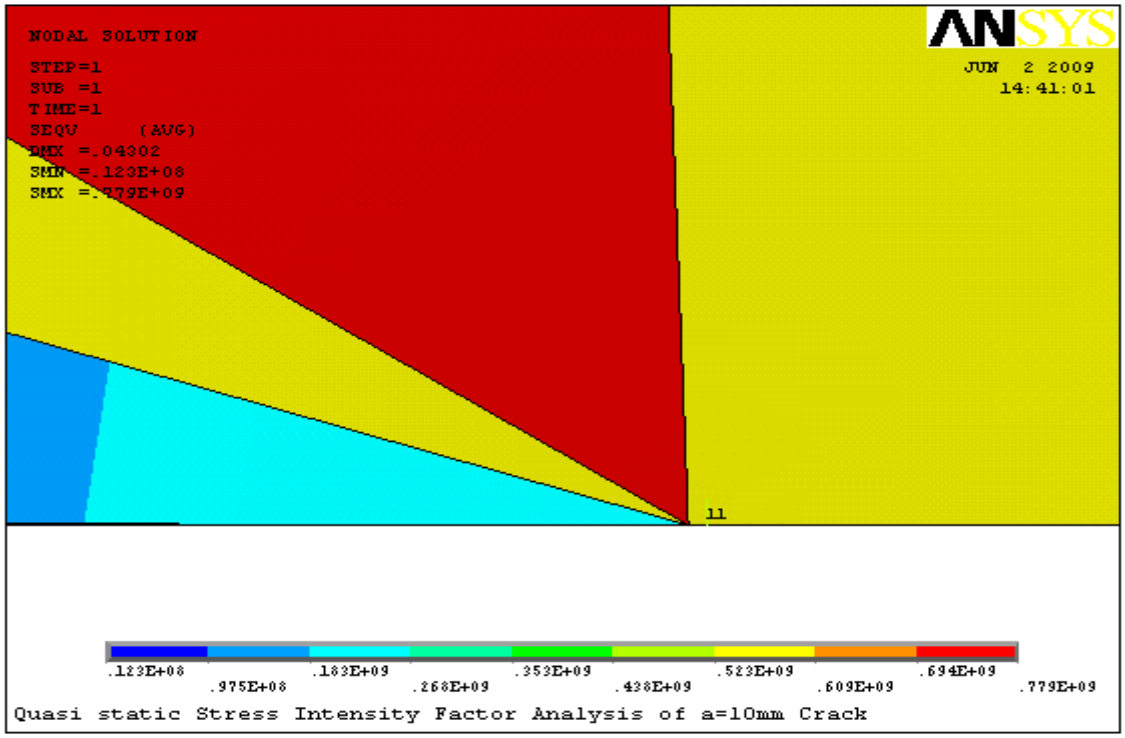
NODAL SOLUTION
STEP=1
SUB =1
TIME=1
SEQV (AVG)
DMX =.04302
SMN =.123E+08
SMX =.779E+09
ANSYS
JUN 2 2009
14:41:01
11
.123E+08
.975E+08
.183E+09
.268E+09
.353E+09
.438E+09
.523E+09
.609E+09
.694E+09
.779E+09
Quasi static Stress Intensity Factor Analysis of a=10mm Crack

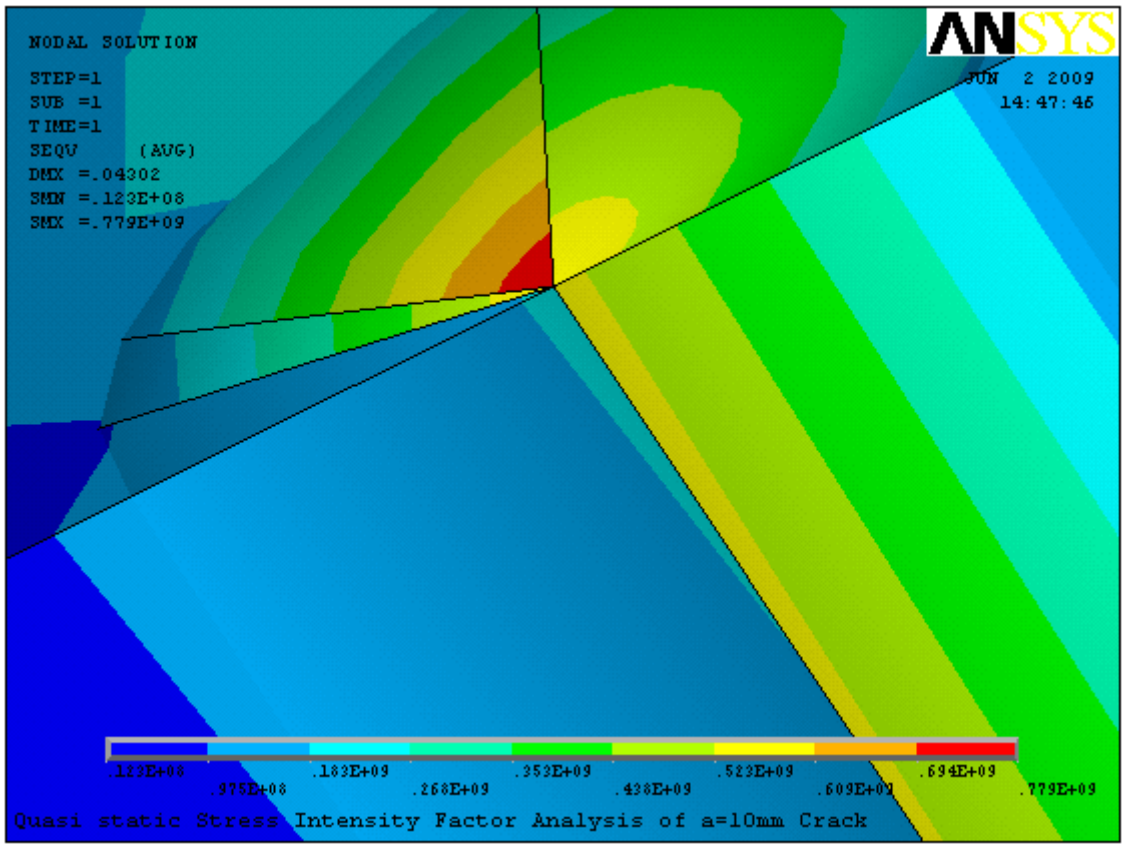
NODAL SOLUTION
STEP=1
SUB =1
TIME=1
SEQV (AVG)
DMX =.04302
SMN =.123E+08
SMX =.779E+09
ANSYS
JUN 2 2009
14:47:46
.123E+08
.975E+08
.183E+09
.268E+09
.353E+09
.438E+09
.523E+09
.609E+09
.694E+09
.779E+09
Quasi static Stress Intensity Factor Analysis of a=10mm Crack

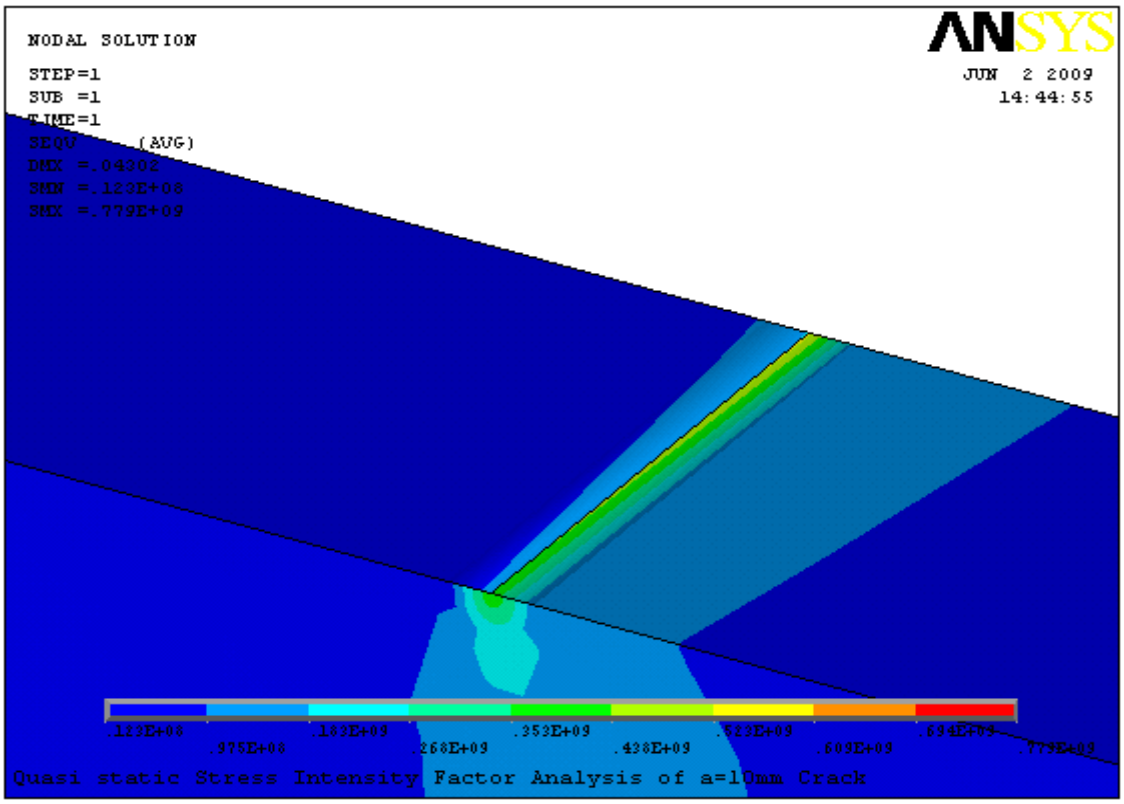
NODAL SOLUTION
STEP=1
SUB =1
TIME=1
SEQV (AVG)
DMX =.04302
SMN =.123E+08
SMX =.779E+09
ANSYS
JUN 2 2009
14:44:55
.123E+08
.975E+08
.183E+09
.268E+09
.353E+09
.438E+09
.523E+09
.609E+09
.694E+09
.779E+09
Quasi static Stress Intensity Factor Analysis of a=10mm Crack

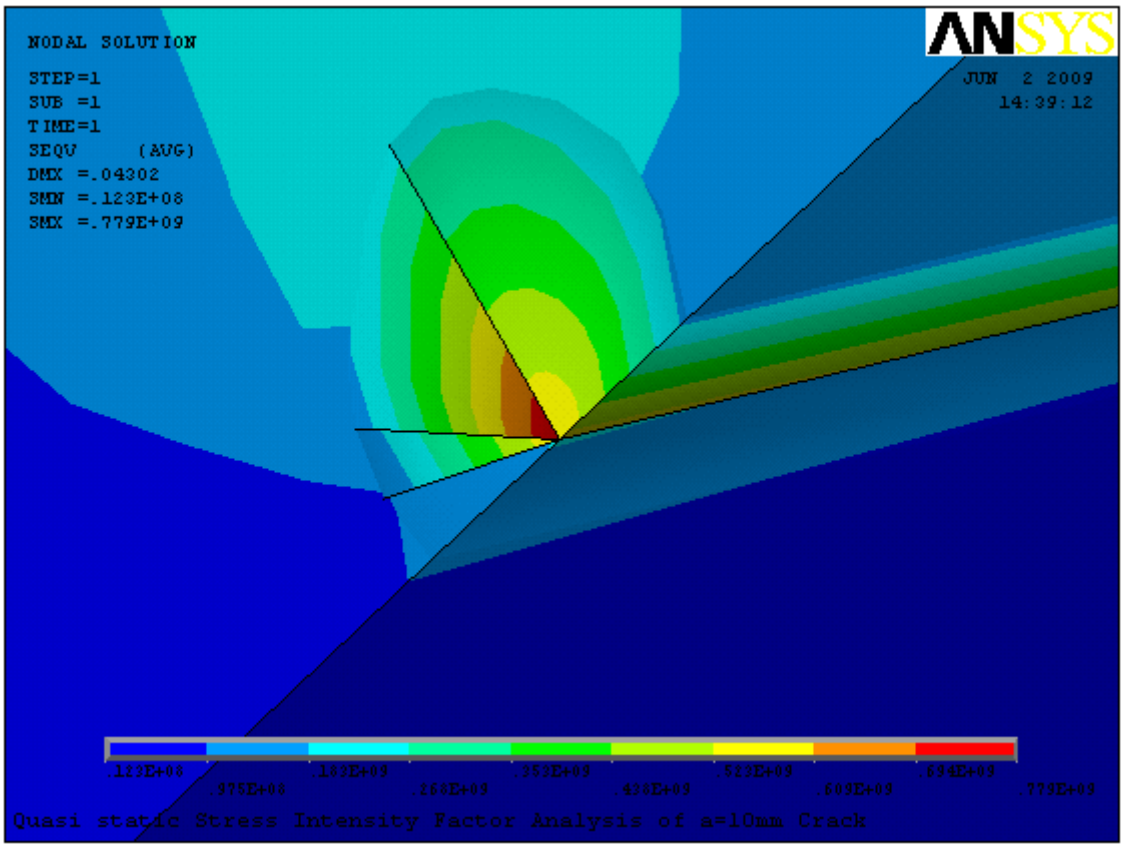
NODAL SOLUTION
STEP=1
SUB =1
TIME=1
SEQV (AVG)
DMX =.04302
SMN =.123E+08
SMX =.779E+09
ANSYS
JUN 2 2009
14:39:12
.123E+08
.975E+08
.183E+09
.268E+09
.353E+09
.438E+09
.523E+09
.609E+09
.694E+09
.779E+09
Quasi static Stress Intensity Factor Analysis of a=10mm Crack

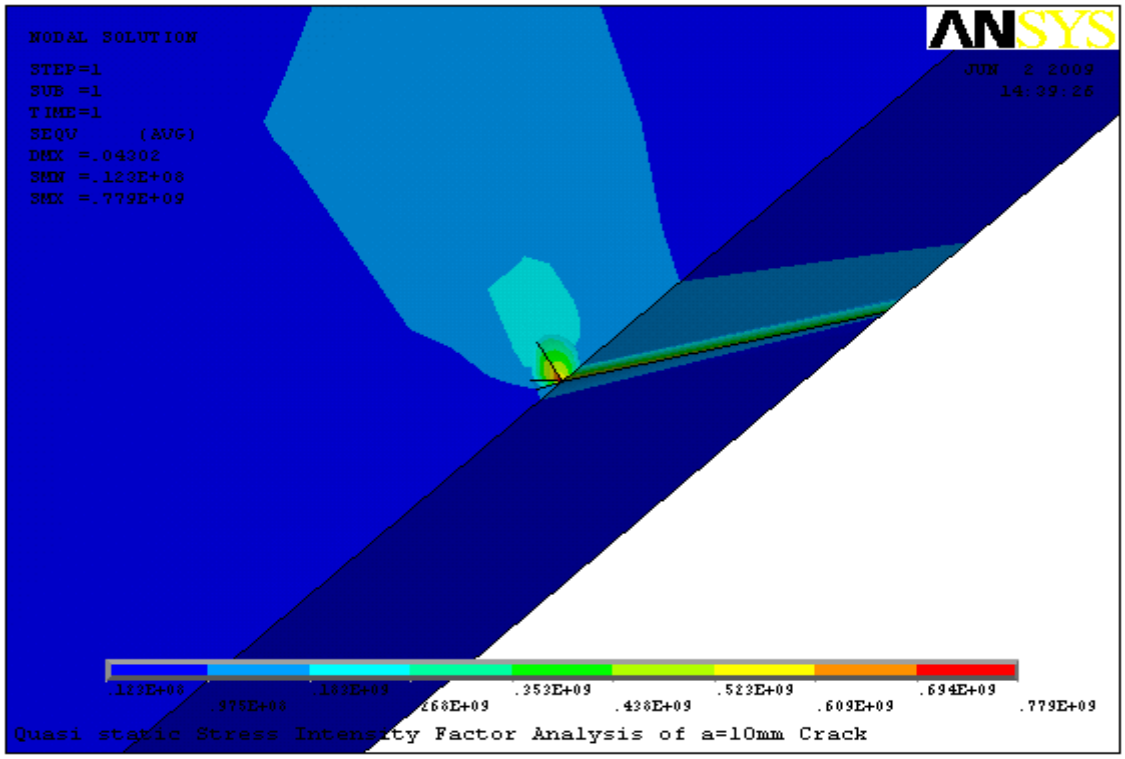
NODAL SOLUTION
STEP=1
SUB =1
TIME=1
SEQV (AVG)
DMX =.04302
SMN =.123E+08
SMX =.779E+09
ANSYS
JUN 2 2009
14:39:26
.123E+08
.975E+08
.183E+09
.268E+09
.353E+09
.438E+09
.523E+09
.609E+09
.694E+09
.779E+09
Quasi static Stress Intensity Factor Analysis of a=10mm Crack

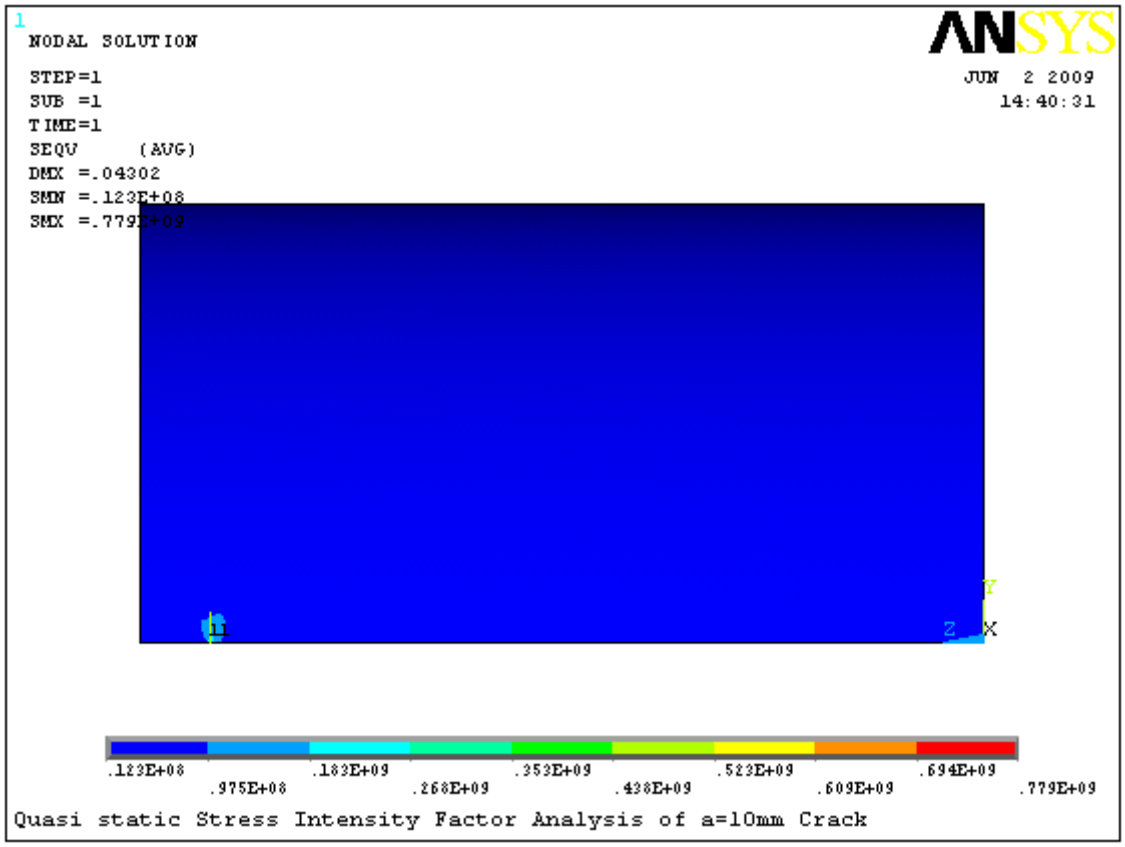
1
NODAL SOLUTION
STEP=1
SUB =1
TIME=1
SEQV (AVG)
DMX =.04302
SMN =.123E+08
SMX =.779E+09
ANSYS
JUN 2 2009
14:40:31
Y
Z
X
.123E+08
.975E+08
.183E+09
.268E+09
.353E+09
.438E+09
.523E+09
.609E+09
.694E+09
.779E+09
Quasi static Stress Intensity Factor Analysis of a=10mm Crack